# Étude et optimisation des procédés et des matériaux pérovskites par recuit photonique pour l'électronique hybride

par

Moulay Ahmed SLIMANI

THÈSE PAR ARTICLES PRÉSENTÉE À L'ÉCOLE DE TECHNOLOGIE SUPÉRIEURE COMME EXIGENCE PARTIELLE À L'OBTENTION DU DOCTORAT EN GÉNIE
Ph.D.

MONTRÉAL, LE 30 MAI, 2025

ÉCOLE DE TECHNOLOGIE SUPÉRIEURE
UNIVERSITÉ DU QUÉBEC

**PRÉSENTATION DU JURY**

CETTE THÈSE A ÉTÉ ÉVALUÉE

PAR UN JURY COMPOSÉ DE:

M. Ricardo Izquierdo, directeur de thèse
Département de génie électrique à l'École de Technologie Supérieure

M. Sylvain G. Cloutier, co-directeur
Département de génie électrique à l'École de Technologie Supérieure

M. Ricardo Zednik, président du jury
Département de génie mécanique à l'École de Technologie Supérieure

M. Martin Bolduc, membre du jury
Département de génie électrique à UQTR

M. Andy Shih, membre du jury
Département de génie électrique à l'École de Technologie Supérieure

M. Joshua Byers, examinateur externe
Département de chimie à Université du Québec à Montréal

ELLE A FAIT L'OBJET D'UNE SOUTENANCE DEVANT JURY ET PUBLIC

LE 30 AVRIL, 2025

À L'ÉCOLE DE TECHNOLOGIE SUPÉRIEURE

## REMERCIEMENTS

En entreprenant ce projet de doctorat, j'ai rapidement compris qu'il s'agissait de bien plus qu'un effort individuel. En réalité, c'est un travail véritablement collectif. Sans le soutien de nombreuses personnes, cette thèse n'aurait jamais pu aboutir. Leur aide précieuse m'a permis d'apprendre et de progresser tout au long de ce parcours.

Ce travail est dédié à la mémoire de mon père, qui a toujours nourri en moi le goût de l'apprentissage, et à ma mère, dont le sacrifice et l'amour inconditionnel ont soutenu mes frères et moi. Je leur en suis profondément reconnaissant. À ma femme Meriem, pour son amour, son soutien et sa confiance en moi durant toutes ces années de mariage, et à mes enfants, Amira, Malik et Jinane, à qui j'espère transmettre le flambeau de l'apprentissage. Mes frères Sidi Mohamed et Moulay Ali ainsi que tous mes neveux.

Je voudrais tout d'abord adresser mes sincères remerciements à mes directeurs Ricardo Izquierdo et Sylvain G. Cloutier pour leurs soutiens financiers, leurs conseils durant cette thèse. Merci une autre fois pour la liberté que vous m'avez donné dans la direction de mon projet de recherche, et de me donner l'opportunité de développer mes compétences et mon savoir-faire.

Je remercie Mohammad Saadati pour son professionnalisme et ses compétences d'analyse. Son aide, et la grande qualité de son travail ont eu un impact positif sur mes propres travaux. Je remercie également les personnes de l'ETS, en particulier Mathieu Gratuze, pour son soutien exceptionnel tout au long de ce projet, ainsi que Normand et Ismail. Un grand merci également aux personnes de l'UQAM : Gwenail, Galina, Daphné, Mohsen et Ahmed, pour leur aide.

Finalement, je tiens à exprimer toute ma gratitude envers mes collègues : Abhiroop, Alexandre, Arjun, Astrid, Debika, Émilie, Fabrice, Fatemeh, Felipe, François-Xavier, Jaime, Julie, Kevie, Krunal, Mohammad, Shayan, Xiaohang et Yin. Merci pour votre aide, votre présence et votre soutien. Je suis reconnaissant d'avoir eu l'opportunité de vous connaître, ainsi que pour les grandes discussions, contributions et collaborations scientifiques partagées avec chacun d'entre vous.

**Étude et optimisation des procédés et des matériaux pérovskites par recuit photonique pour l'électronique hybride**

Moulay Ahmed SLIMANI

## RÉSUMÉ

La sensibilité croissante aux enjeux environnementaux et la demande grandissante en énergie font de l'énergie solaire une solution propre et indispensable pour une transition énergétique vers la décarbonation. L'émergence de la technologie photovoltaïque, et le potentiel des matériaux de type pérovskite, qui possèdent des propriétés optiques et électriques remarquables, positionnent les cellules solaires à base de pérovskites comme une solution prometteuse pour l'avenir. Les pérovskites hybrides offrent de nombreux avantages tels qu'une efficacité élevée, un coût de production réduit, ainsi qu'une synthèse et un processus de fabrication simplifiés.

À ce jour, la fabrication des cellules à base de pérovskites repose sur des traitements thermiques conventionnels, avec des temps de recuit relativement longs (de 15 minutes à 1 heure), ce qui limite leur application à grande échelle ou dans des procédés en continu (R2R).

Les travaux de cette thèse visent à répondre à cette problématique. L'objectif principal est d'intégrer le procédé de recuit photonique dans la fabrication des cellules solaires pérovskites pour remplacer le recuit thermique traditionnel. Cette technique sera appliquée aux couches de transport d'électrons et à la couche active de pérovskite. Dans un premier temps, il s'agira de développer un procédé de recuit photonique pour les films de $\mathrm{SnO_2}$ déposés sur des substrats en verre, afin d'améliorer leurs propriétés électriques. Dans un second temps, la cristallisation des films de pérovskites sera optimisée pour produire des cellules entièrement traitées par recuit photonique, comparables en performance à celles fabriquées par recuit thermique.

Notre procédé de recuit photonique sera optimisé à l'aide de différentes techniques de caractérisation et validé à travers des dispositifs solaires fonctionnels comparables à ceux produits par recuit thermique.

**Mots-clés:** Recuit photonique, perovskite, $\mathrm{SnO_2}$, cellule solaire perovskite

**Study and Optimization of Processes and Perovskite Materials Using Photonic Annealing for Hybrid Electronics**

Moulay Ahmed SLIMANI

## ABSTRACT

The growing sensitivity to environmental issues and the increasing demand for energy make solar energy a clean and essential solution for a transition toward decarbonized energy. The emergence of photovoltaic technology, coupled with the potential of perovskite materials, which have remarkable optical and electrical properties, positions perovskite-based solar cells as a promising solution for the future. Hybrid perovskites offer numerous advantages, such as high efficiency, low production costs, and simplified synthesis and manufacturing processes.

Currently, the production of perovskite-based cells relies on conventional thermal treatments, with relatively long annealing times (from 15 minutes to 1 hour), which limits their large-scale or roll-to-roll (R2R) application.

The aim of this thesis is to address this issue. The primary objective is to integrate photonic curing into the manufacturing process of perovskite solar cells as a replacement for traditional thermal annealing. This technique will be applied to the electron transport layers as well as the active perovskite layer. The first step will involve developing a photonic curing process for $SnO_2$ films deposited on glass substrates to enhance their electrical properties. The second step will focus on optimizing the crystallization of perovskite films to produce fully photonically cured cells with performance comparable to those manufactured using standard annealing.

Our photonic curing process will be optimized using various characterization techniques and validated through functional solar devices comparable to those produced by thermal annealing.

**Keywords:** Photonic curing, perovskite, $SnO_2$, perovskite solar cell

## TABLE DES MATIÈRES

Page

## LISTE DES TABLEAUX

## LISTE DES FIGURES

Page

## LISTE DES ABRÉVIATIONS, SIGLES ET ACRONYMES

| | |
|---|---|
| A | Absorbance |
| AFM | (anglais, Atomic force microscopy) |
| Ag | Argent |
| Al | Aluminium |
| Au | Or |
| B | Induction magnétique |
| Bi | Bismuth |
| CA | courant alternatif |
| $CaTiO_3$ | Titanate de calcium |
| CC | Courant continu |
| $Ch_3NH_3PbI_3$ | (anglais, Methylammonium lead iodide, MAPI) |
| DEE | (anglais, Diethyl ether) |
| DMSO | (anglais, Dimethyl sulfoxide) |
| E | Champ électrique |
| ETL | (anglais, Electron transport layer) |
| ETS | École de Technologie Supérieure |
| FA | Formamidinium |
| FIRA | (anglais, Flash infrared annealing) |
| FTO | (anglais, Fluorine-doped Tin Oxide) |
| FWHM | (anglais, Full width at half maximum) |
| Ge | Gérmanium |
| GIXRD | (anglais, Grazing incident X-Ray Diffraction) |
| HTL | (anglais, Hole transport layer) |
| I | Faisceau incident |
| $I_0$ | Faisceau transmis |

| | |
|---|---|
| In | Indium |
| IR | Infra-rouge |
| ITO | (anglais, indium-doped Tin Oxide) |
| MA | Méthylammonium |
| MDPI | (anglais, Multidisciplinary Digital Publishing Institute) |
| NiO | (anglais, Nickel oxide) |
| n-i-p | (anglais, Regular negative-intrinsic-positive) |
| Pb | Plomb |
| $PbI_2$ | Iodure de plomb (II) |
| PC | (anglais, Photonic curing) |
| p-i-n | (anglais, Inverted positive-intrinsic-nagative) |
| R2R | (anglais, Roll-to-roll) |
| $R_H$ | (anglais, Hall constant) |
| Sb | Antimoine |
| SEM | (anglais, Scanning electron microscopy ) |
| Sn | Étain |
| $SnO_2$ | Dioxide d'étain |
| t | (anglais, thickness) |
| T | Transmittane |
| TA | (anglais, Thermal annealing) |
| $TiO_2$ | Dioxide de titane |
| UV | Ultra-violet |
| X | Anion |
| XRD | (anglais, X-Ray Diffraction) |

## LISTE DES SYMBOLES ET UNITÉS DE MESURE

| | |
|---|---|
| Ω | Ohm |
| A | Ampère |
| E | Champs électrique |
| B | Induction magnétique |
| Hz | Hertz |
| m | Mètre |
| k | Constante de Scherrer |
| s | Seconde |
| V | Volt |
| W | Watt |
| R | Résistance |
| K | Kelvin |
| t | Facteur de tolerence |
| F | Faraday |
| W | Watt |
| ci | Capacité thermique |
| Ki | Conductivité thermique |
| $\rho$ | Densité |
| $\epsilon$ | Déformation |
| $\lambda$ | Longueur d'onde |
| $\theta$ | Angle de diffraction |
| $\psi$ | Angle d'inclinaison |
| $\mu$ | Mobilité de porteurs de charges |
| $R_{CT}$ | Résistance de transfert de charges |
| $\tau$ | Temps de réponse |
| $\delta$ | Différence de chemin optique |

# INTRODUCTION

## Contexte énergétique mondiale

L'évolution rapide des besoins énergétiques mondiaux et la sensibilisation croissante à l'environnement font de l'énergie solaire une solution essentielle pour une transition énergétique durable. Cette vision de décarbonisation exige l'utilisation des énergies propres, notamment l'énergie solaire, qui est une source d'énergie propre et abondante sur Terre Touzani (2023), avec une attractivité qui évolue constamment. Les prévisions de la consommation énergétique mondiale montrent une chute de la production d'électricité à partir des énergies fossiles Nijsse, Mercure, Ameli, Larosa, Kothari, Rickman, Vercoulen & Pollitt (2023), passant de 62 % à 21 % (Figure 0.1a) entre 2020 et 2050. Cependant, l'énergie solaire sera responsable de 56 % de la production Nijsse *et al.* (2023). Cette évolution est due à l'émergence de la technologie photovoltaïque, dont le rythme de développement technologique extraordinaire a permis une diminution moyenne de 20.2 % du prix des modules solaires pour chaque doublement de capacité installée ( Figure 0.1b).

## L'énergie photovoltaïque

Le soleil est une source d'énergie propre et abondante sur terre (885 000 000 TWh/an) Shih, Zhang, Li & Bai (2018). La quantité d'énergie reçue par terre pendant une heure est équivalente à la consommation annuelle mondiale Hadouchi (2017). Actuellement, en se sert de plusieurs familles de cellules photovoltaïques pour convertir l'énergie solaire en électricité Fraas & O'Neill (2023). Ce phénomène a été découvert pour la première fois en 1839 par le physicien Alexandre Edmond Becquerel Gable (2022). L'industrialisation des cellules PV ont commencé à partir des années 70, et depuis cette technologie n'a pas cessez de se développer. Le développement de la technologie photovoltaïque pourrait jouer un rôle important dans la transition énergétique mondiale Gielen, Boshell, Saygin, Bazilian, Wagner & Gorini (2019), comme le confirme les

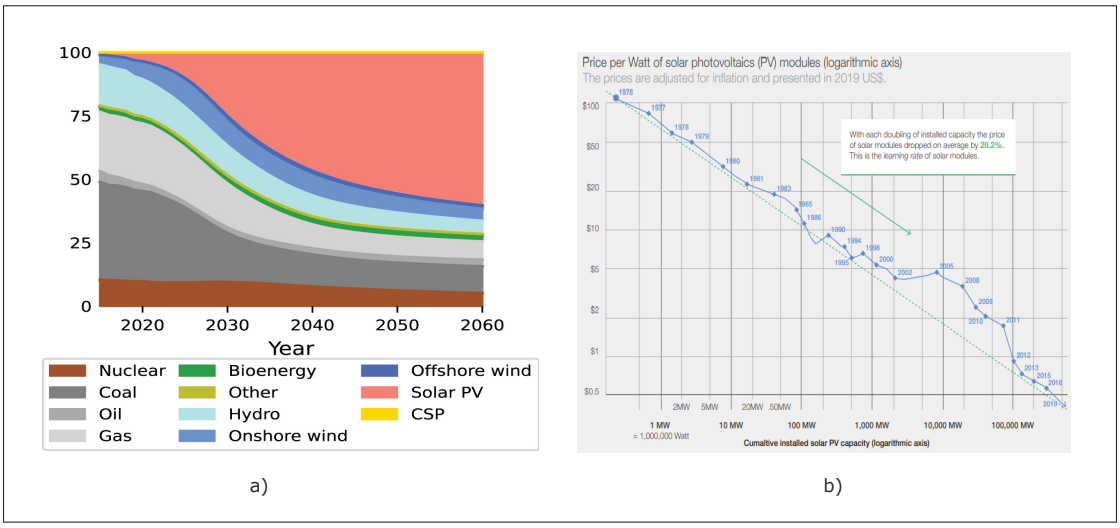


FIGURE 0.1 a) Part mondiale dans la production d'électricité de diverses technologies Nijsse *et al.* (2023). b) diminution de prix du module solaire de 99.6 % depuis 1976 Word (2024)

prévisions de la production énergétique mondiale associé à chaque technologie (Figure 0.1a). Il existe actuellement 3 filières qui dominent le marché de la technologie photovoltaïque Benetti (2019) :

- silicium : (silicium monocristallins, polycristallins).
- couches minces : cellules de tellurure de cadmium (CdTe), diséléniure de cuivre indium gallium (CIGS) et silicium amorphe.
- troisième génération : les cellules photovoltaïques organiques (OPV), les cellules solaires à colorants (DSSCs) et les cellules solaires pérovskite (PSCs).

La technologie de la filière silicium a profité de plusieurs années de développement ce qui a rendu sa technologie fiable, durable et performante. La technologie couche mince a permet d'avoir des performances comparables à celle de la famille silicium et son coût de développement ne cesse de diminuer. Cependant, pour la filière de la troisième génération et particulièrement pour

les cellules pérovskites nous pouvons constater qu'ils ont atteint des rendements de conversion énergétique impressionnants (Figure 0.2), rivalisant avec les technologies photovoltaïques établies en seulement une décennie de développement NREL (2024). L'amélioration de ces performances ont été basé sur des stratégies notamment, l'optimisation des matériaux Shrivastav, Madan & Pandey (2024), l'ingénierie des couches actives et l'utilisation de nouveaux concepts tels que les cellules tandem Cheng & Ding (2021a); Mahapatra, Parikh, Kumar, Kumar, Prochowicz, Kalam, Tavakoli & Yadav (2020).

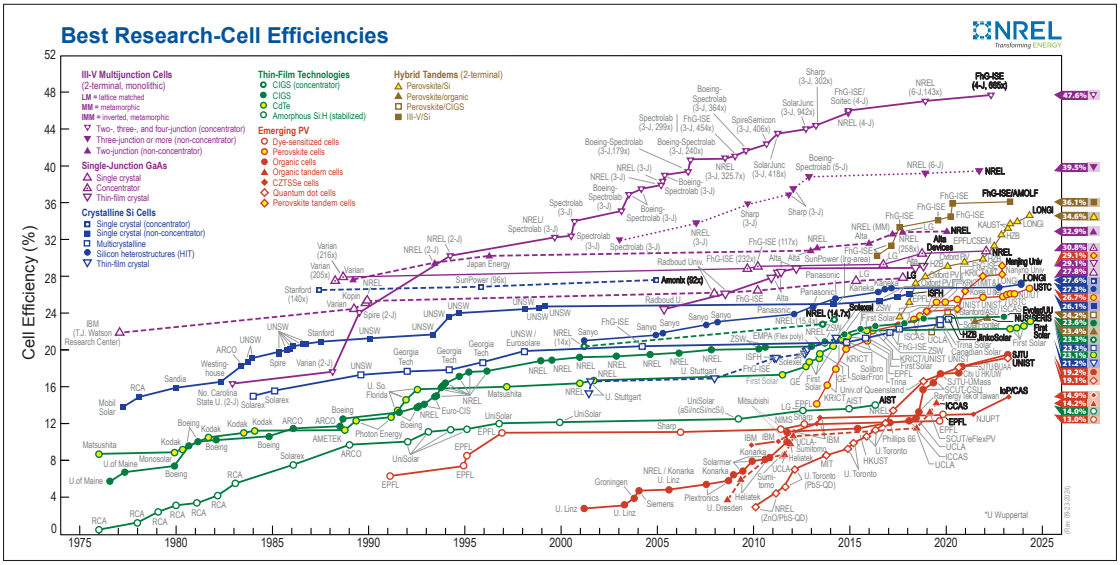


FIGURE 0.2 Rendement de conversion de cellules solaires réalisés par diverses technologies. Publiée par le Laboratoire National de l'Énergie Renouvelable (NREL) NREL (2024)

**Problématique et objectifs de la recherche**

Dans le contexte de cette révolution énergétique, les cellules solaires pérovskites (PSC) hybrides ont retenu l'attention des chercheurs en raison de leur rendement de conversion élevé, de leur coût de fabrication potentiellement faible et de leur souplesse de conception. Cependant, même avec ces avantages, des défis subsistent, notamment en ce qui concerne la durabilité à long terme et la production à grande échelle. Les (PSC) sont généralement constituées d'un

empilement de couches : la couche Electron Transport Layer (ETL), la couche active, la couche Hole Transport Layer (HTL), et les électrodes. Les PSC sont souvent fabriquées par recuit thermique, un processus impliquant le chauffage des matériaux à des températures élevées afin d'améliorer leurs propriétés cristallines et optoélectroniques. Cependant, le recuit thermique des couches HTL, ETL et pérovskites requiert fréquemment des températures élevées et des temps de traitement prolongés. Cette méthode peut ainsi engendrer plusieurs inconvénients :

- dégradation des matériaux : Une exposition prolongée à des températures élevées peut provoquer la dégradation des matériaux, affectant ainsi la performance et la durabilité des cellules solaires.
- complexité du processus : Le besoin de contrôler précisément la température et la durée du recuit, combiné à la sensibilité de certains substrats (comme les plastiques) aux hautes températures, ajoute de la complexité au processus de fabrication.
- consommation d'énergie : Les températures élevées augmentent la consommation d'énergie, ce qui rend le processus moins écologique et plus coûteux.

Les travaux présentés dans cette thèse de doctorat s'inscrivent pleinement dans cette problématique. L'objectif principal est de développer une alternative au recuit des cellules pérovskites, capable de contourner les limites du recuit thermique traditionnel, notamment les températures élevées et l'exposition prolongée aux conditions environnementales. Ces recherches se concentrent sur l'intégration du procédé de recuit photonique dans la fabrication des cellules pérovskites, ainsi que son impact sur l'amélioration de la granularité, de la microstructure, et des propriétés optiques et électriques.

**Structure de la thèse**

Pour exposer les motivations de ces travaux de recherche, leur déroulement, les résultats obtenus ainsi que les perspectives futures, les chapitres suivants ont été élaborés :

- le CHAPITRE 1 est une revue de la littérature qui porte sur les cellules solaires à base de pérovskites hybrides, en retraçant l'évolution de leur développement jusqu'aux performances record actuelles. Elle examine en détail les propriétés des matériaux pérovskites et analyse l'impact des facteurs environnementaux sur ces dispositifs. De plus, Elle offre une vue d'ensemble de l'art du recuit photonique des couches HTL, ETL et pérovskites, couvrant les travaux récents qui n'ont pas été inclus dans notre premier article, correspondant au chapitre 3.
- le CHAPITRE 2 couvre la méthodologie expérimentale et met en évidence toutes les techniques de caractérisation utilisées tout au long de ce projet.
- le CHAPITRE 3 est un article publié dans la revue MDPI nanomaterials qui propose l'état de l'art du recuit photonique. Son objectif principal est de fournir un aperçu global de la technique de recuit photonique et de son potentiel dans la fabrication de couches ETL, HTL, et pérovskites, en vue d'améliorer les performances des cellules pérovskites.
- le CHAPITRE 4 est un article publié dans la revue MDPI nanomaterials, il examine comment les déformations résiduelles dans les films de pérovskite affectent leurs propriétés physiques, optiques et électriques, en se concentrant particulièrement sur la mobilité et la stabilité des porteurs. L'étude confirme que la relaxation des contraintes résiduelles par la température peut améliorer de manière significative le transport des porteurs de charge et la stabilité des films. Cette compréhension pourrait permettre d'améliorer les performances et la longévité des dispositifs à base de pérovskite.
- le CHAPITRE 5 est un article publié dans la revue MDPI nanomaterials. L'article explore l'amélioration des performances du $SnO_2$ nanocristallin, utilisé comme couche ETL dans

les cellules solaires pérovskites, grâce au recuit photonique. L'étude utilise la spectroscopie d'impédance pour analyser l'impact de ce traitement sur les propriétés électriques du $SnO_2$. Elle confirme une amélioration signifiante des performances des couches traitées par recuit photonique par rapport au recuit thermique.

- le CHAPITRE 6 est un articlé publié dans la revue MDPI Nanomaterials, explore l'utilisation du recuit photonique pour optimiser les performances des films minces de pérovskite MAPI. Cette technique permet d'améliorer de manière significative la qualité des films, notamment en augmentant la taille des grains, qui devient presque six fois supérieure à celle obtenue avec un recuit thermique. Cette augmentation de la taille des grains explique les performances comparables des cellules pérovskites traitées par recuit photonique, en comparaison avec celles recuites thermiquement.

Enfin, ce manuscrit se termine par une conclusion portant sur l'ensemble de cette thèse. IL permettra une discussion des résultats présentés dans ce travail, ainsi qu'un résumé des perspectives d'évolution permises par les résultats obtenus lors de ce doctorat.

# CHAPITRE 1

# REVUE DE LITTÉRATURE

## 1.1 Introduction

Les cellules solaires à pérovskite hybrides se sont imposées comme l'une des technologies les plus prometteuses pour la conversion photovoltaïque de l'énergie solaire au cours de la dernière décennie Tu, Wu, Xu, Yang, Cai, Gong, Zhu & Huang (2021). Ce succès s'explique par la structure cristalline unique des matériaux pérovskites, qui leur confère des propriétés optoélectroniques remarquables. Parmi celles-ci, on note une excellente absorption de la lumière, une diffusion efficace des porteurs de charge, une bande interdite ajustable, ainsi qu'un faible coût de fabrication. Ces caractéristiques offrent de nombreux avantages en termes de performances et de compétitivité par rapport aux technologies photovoltaïques traditionnelles, telles que les cellules à base de silicium Wang, Hou, Zhang, Yang, Xu, Ao, Kang, Pan & Mao (2021b). De plus, la flexibilité des pérovskites en matière de fabrication permet de les intégrer sur divers types de substrats, y compris les surfaces flexibles, ouvrant ainsi la voie à des applications innovantes, comme les dispositifs photovoltaïques portables ou intégrés dans des textiles intelligents. La possibilité de fabriquer ces cellules à basse température et avec des méthodes de dépôt peu coûteuses, telles que l'impression par sérigraphie, slot die, ou jet d'encre, rend leur production à grande échelle plus accessible, réduisant potentiellement les coûts de fabrication à long terme. L'intérêt croissant des chercheurs pour ces matériaux est également alimenté par la possibilité d'intégrer des nouvelles technologies comme le recuit photonique, ayant le potentiel d'améliorer la qualité des films et par suite le rendement de conversion Ghahremani, Martin, Ankireddy & Druffel (2019). Grâce à ces avancées, les cellules solaires à pérovskite continuent de susciter un intérêt grandissant dans la quête de sources d'énergie renouvelable plus efficaces et économiques.

### 1.1.1 Structure de la pérovskite

La structure cristalline de type pérovskite, caractérisée par un arrangement cubique de cations métalliques dans une matrice d'anions, a été initialement découverte en 1831 par le minéralogiste Russe L.A Perovski en découvrant le minéral $CaTiO_3$ Hadouchi (2017) ; Wang (2024), cette structure de forme $ABX_3$ comme le montre la figure 1.1 ou A et B sont des cations occupant respectivement les sommets d'un cube et le centre d'un octaèdre formé par 6 anions $(BX_6)^{4-}$ Wang (2024), tandis que le X est un ion négatif ou anion (fréquemment un oxyde) qui se lie au deux cations Hadouchi (2017) ; Sum & Mathews (2014). On peut retrouver les pérovskites sous deux formes principales : sous forme d'oxyde (inorganique) ou halogéné (inorganique ou organique-inorganique) Hadouchi (2017) ; Salek Esfahani (2022). Quand l'élément A est une molécule organique tel que ($CH_3NH_3I$ = MA) ou le formamidinium ($HC(NH_2)^2$ = FA) la pérovskite est dite hybride Nayak, Akthar, Guchhait & Saha (2021), cette configuration a été testé pour la première fois par Weber Weber (1978) et depuis les pérovskites hybrides présentent un grand intérêt pour les scientifiques. Toutefois, cette structure n'a été exploitée que récemment pour des applications photovoltaïques. Les pérovskites à halogénures organiques, notamment le triiodure de plomb méthylammonium ($CH_3NH_3PbI_3$), sont les plus étudiées en raison de leur large plage d'absorption, de leur mobilité élevée des porteurs de charge et de leur facilité de fabrication Guo, Dahal, Thapa, Poudel, Liu & Li (2021) ; Jassim, Bakr & Mustafa (2020) ; Nandigana, Saminathan, Sriram, Sujatha, Subramanian & Panda (2024).

### 1.1.2 Propriétés et stabilité de la pérovskite

Les pérovskites hybrides offrent des avantages significatifs en combinant des composés organiques et inorganiques pour créer des matériaux dotés de propriétés optiques et de transport de charge remarquables. Cette hybridation permet d'exploiter les meilleures caractéristiques des semi-conducteurs organiques et inorganiques tout en réduisant les coûts de fabrication grâce à des processus de production moins complexes. En résulte une classe de matériaux hautement performants, facilement élaborables et économiquement attrayants, dotés d'un rendement quantique externe élevé, d'un excellent coefficient d'absorption de la lumière et d'une longue

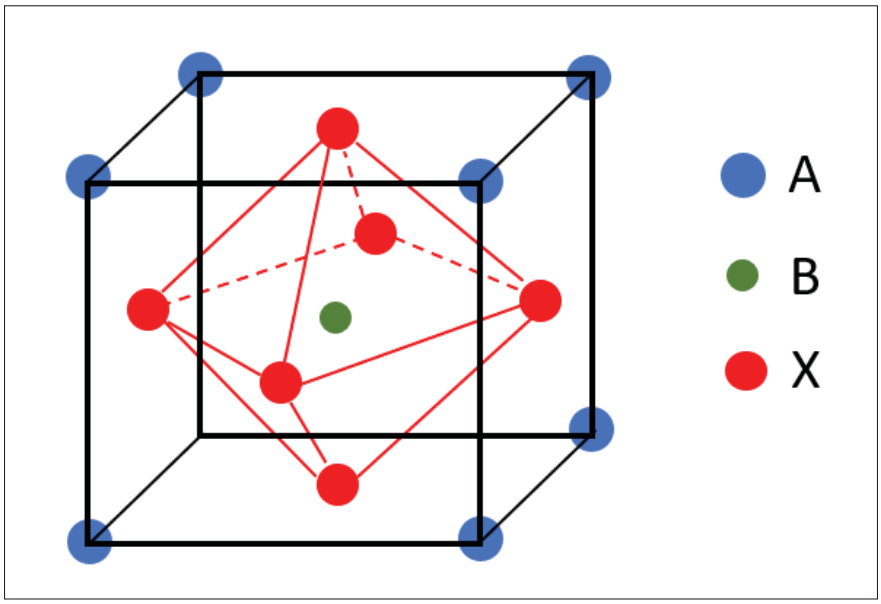


FIGURE 1.1 La structure cubique 3D de la pérovskite, avec la formule générale $ABX_3$

durée de vie Liang, Gu, Xia, Mei, Pang, Zhang, Guo, Guo, Shen & Yang (2022) ; Xu, Yuan, Zeng & Song (2019). Malgré ces avantages, les cellules à base de pérovskite souffrent d'une stabilité à long terme, ce qui constitue un défi majeur pour la commercialisation des dispositifs pérovskites. L'évaluation de la stabilité et de la distorsion des cellules à base de pérovskite peut être réalisée au moyen de diverses techniques expérimentales et de modélisation. Parmi celles-ci figurent le test de vieillissement, la caractérisation spectroscopique, la microscopie électronique à balayage (MEB) et la modélisation informatique. Ces différentes approches aident les chercheurs à obtenir une évaluation complète de la stabilité et de la distorsion des cellules à base de pérovskite, ce qui est essentiel pour le développement de cette technologie en vue d'applications commerciales à grande échelle. Les paramètres utiliser pour cette évaluation sont le facteur de tolérance t et le facteur octhaédral $\mu$ définis respectivement par Spalla (2019) :

$$t = \frac{R_A + R_X}{\sqrt{2}(R_B + R_X)} \tag{1.1}$$

$$\mu = \frac{R_B}{R_X} \tag{1.2}$$

Avec :

$0.81 < t < 1.11$

$0.44 < \mu < 0.90$

Et $R_A$, $R_B$ et $R_X$ représentent les rayons ioniques de A, B et X.

Dépendamment de la valeur de t la configuration de la structure pérovskite change en conséquence, il possède une symétrie cubique pour t=1, cependant quand le t s'écarte de 1, il y a distorsion de l'octaèdre $[BX_6]$ et la structure pérovskite devient orthorhombique ou tétragonale Park (2013) ; Zhou (2020). À température ambiante, les structures orthorhombiques et tétragonales sont favorisées pour certaines pérovskites. Cependant, lorsque la température augmente et se rapproche de 327 K (environ 54 °C), la structure cristalline peut subir une transition vers une structure cubique Hoque, Islam, Zhu & Fan (2017) ; Patru, Khassaf, Pasuk, Botea, Trupina, Ganea, Pintilie & Pintilie (2021) [20, 21]. Cette transition de phase est une caractéristique intéressante des matériaux cristallins et peut avoir un impact significatif sur leurs propriétés physiques et chimique. Elle pourrait-être due à divers mécanismes, tels que des changements dans les interactions entre les atomes ou la mobilité des ions à l'intérieur de la structure cristalline. Comprendre ces transitions de phase est crucial pour exploiter les propriétés des pérovskites dans diverses applications, notamment en électronique, en énergie solaire et en catalyse, où ces matériaux sont largement étudiés pour leurs performances exceptionnelles. La sensibilité aux facteurs environnementaux tels que l'humidité, la chaleur et la lumière a conduit à des recherches intensives sur le développement de revêtements protecteurs, de structures pérovskites alternatives et de techniques de passivation de surface. En combinant ces approches, les chercheurs espèrent surmonter les défis liés à la stabilité à long terme des cellules solaires à base de pérovskite et rendre cette technologie plus viable sur le plan commercial. Les facteurs ayant un grand impact

sur la stabilité des cellules solaires pérovskites sont classés selon 2 catégories : les facteurs de dégradation intrinsèque et extrinsèque Cheng & Ding (2021b) ; Spalla (2019).

1. Facteurs extrinsèques : Ce sont des éléments extérieurs tels que l'humidité, l'oxygène. Les matériaux pérovskites y sont particulièrement sensibles, ce qui entraîne une dégradation rapide et réduit la durée de vie des cellules solaires. Toutefois, des techniques avancées d'encapsulation permettent de limiter les effets de ces facteurs externes ;
2. Facteurs intrinsèques : Ils sont liés à la composition et à la dégradation interne des cellules, représentant les phénomènes d'instabilité les plus complexes à maîtriser par l'ingénierie des dispositifs. Cette instabilité intrinsèque est due aux propriétés des matériaux pérovskites, tel que la migration des ions, aux réactions entre les métaux et la pérovskite, ainsi qu'aux contraintes résiduelles Cheng & Ding (2021b) ; Wang, Wang, Chen, Yin, Mei, Zhong, Yao, Li, Wang & Song (2021a).

Un autre facteur préoccupant s'ajoute à ces causes de dégradation : la présence de plomb (Pb) dans les cellules solaires pérovskites. De nombreuses pérovskites à haute performance contiennent du plomb, ce qui soulève des inquiétudes quant à une possible contamination de l'environnement si les cellules se brisent ou se dégradent, générant des déchets dangereux. Bien que des éléments comme le bismuth (Bi), le germanium (Ge), l'antimoine (Sb), l'indium (In), l'argent (Ag), le tellure (Te) et surtout l'étain (Sn), qui présentent des similitudes chimiques et physiques avec le plomb, aient été étudiés pour remplacer ce dernier, ces alternatives restent limitées. Selon des recherches récentes, le rendement de conversion de puissance (PCE) des cellules solaires à pérovskite sans plomb se situe autour de 14 à 15 % Nishimura, Kamarudin, Hirotani, Hamada, Shen, Iikubo, Minemoto, Yoshino & Hayase (2020) ; Schileo & Grancini (2021) un chiffre nettement inférieur aux pérovskites à base de plomb, qui ont atteint un PCE supérieur à 25 % Sharif, Khalid, Ahmad, Rehman, Qutab, Akhtar, Mahmood, Afzal & Saleem (2023). Les pérovskites à base d'étain montrent un potentiel prometteur, mais il demeure difficile d'atteindre une grande stabilité et un rendement élevé, principalement en raison de l'oxydation spontanée de l'étain en Sn(IV) Schileo & Grancini (2021) ; Shao, Li, Shi, Ma, Wang, Liu, Jiang,

Hao, Zhang & Liu (2023) À l'heure actuelle, les cellules solaires sans plomb ne peuvent rivaliser avec celles à base de plomb en termes d'efficacité. Cependant, la quantité de plomb utilisée dans les dispositifs est très faible, et un conditionnement bien contrôlé pour limiter les fuites de plomb, ainsi qu'un recyclage facilité par l'utilisation de solvants à basse température, pourraient revitaliser cette technologie en équilibrant ses avantages et les risques associés.

### 1.1.3 Méthodes de fabrication et applications potentielles

La fabrication des cellules solaires à pérovskite a connu une évolution significative. Les méthodes traditionnelles, telles que le dépôt par spin-coating, ont été les premières à être utilisées, mais des techniques plus avancées sont apparues, notamment le dépôt par évaporation de couches minces, la cristallisation en solution, l'électrodéposition, slot die et, plus récemment, l'utilisation du jet d'encre Al-Katrib, Perrin, Flandin & Planes (2023) ; Lee, Kim, Park, Lee & Kim (2023) ; Liu, Shi, Khan, Chu, Huang, Shi, Sun, Li, Zhou & Xiao (2024). Ces progrès visent à améliorer la reproductibilité et l'extensibilité de la fabrication. En raison de leur flexibilité, de leur légèreté et de leur coût potentiellement faible, les cellules solaires pérovskites ont suscité un intérêt croissant pour toute une série d'applications, allant des appareils portables aux intégrations architecturales, ouvrant la voie à des solutions innovantes dans le domaine de l'énergie solaire. Malgré les difficultés persistantes, les cellules solaires pérovskites représentent une voie passionnante dans le domaine de l'énergie photovoltaïque. Les cellules solaires à pérovskite peuvent être configurées de différentes manières, principalement en fonction de la disposition des couches de matériaux. Les deux configurations courantes sont les structures n-i-p et p-i-n comme illustré à la figure 1.2. Elles comprennent généralement un substrat, souvent en verre ou en plastique, sur lequel se trouvent plusieurs couches : une couche de transport de trous (HTL), représentant le matériau de type p, comme le PEDOT ou le NiO, suivie de la couche active en pérovskite, puis d'une couche de transport d'électrons (ETL), constituée de matériaux de type n tels que le $\mathrm{TiO_2}$, le $\mathrm{SnO_2}$ ou le PCBM Barbé, Tietze, Neophytou, Murali, Alarousu, Labban, Abulikemu, Yue, Mohammed & McCulloch (2017) ; Hu, Zhang, She, Wu, Zhou, Li, Wang, Miao, Mi & Chen (2020a) ; Li, Yan, Ai, Jiang, Lin, Shou, Yan, Sheng & Ye (2020) ; Song, Kang, Pyeon, Lim, Lee,

Park & Choi (2017) ; Tavakoli, Yadav, Tavakoli & Kong (2018). Cet empilement de couches est encapsulé entre deux électrodes. L'une d'elles est généralement transparente, faite d'oxyde d'indium-étain (ITO) ou d'oxyde de fluorure d'étain (FTO), tandis que l'autre peut être un métal tel que l'argent (Ag), l'aluminium (Al) ou l'or (Au).

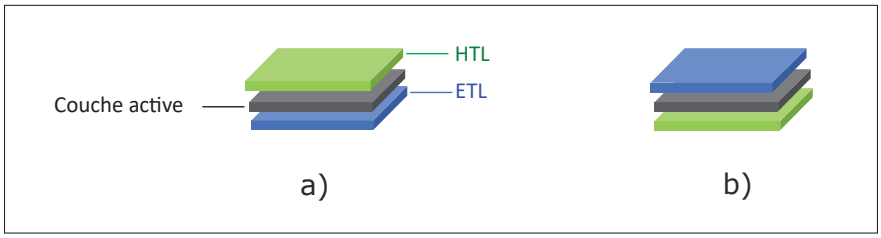


FIGURE 1.2 Configurations cellule solaire pérovskite n-ip et p-i-n

En laboratoire, les matériaux pérovskites ainsi que les couches ETL et HTL sont généralement recuits à l'aide de techniques standards pour améliorer leur conductivité électrique, essentielle au transport efficace des porteurs de charge (électrons et trous). Ce recuit permet également de favoriser la formation de structures cristallines optimales, ce qui améliore significativement la qualité des couches et, par conséquent, l'efficacité des cellules solaires. Cependant, ce processus exige des températures élevées et des durées de traitement relativement longues, ce qui représente un obstacle pour la fabrication à haut débit ou en rouleau-à-rouleau (R2R). Pour surmonter cette limitation, le recuit photonique émerge comme une technique prometteuse, offrant des perspectives intéressantes pour l'avenir des cellules à pérovskite.

## 1.2 Principe du recuit photonique

Dans ce projet, nous allons étudier le recuit photonique, une technique relativement nouvelle qui peut répondre aux problématiques du recuit thermique en offrant une méthode plus précise et moins contraignante pour modifier les matériaux. Le recuit photonique (PC) est une technique principalement employée dans l'électronique imprimée et les revêtements, destinée à sécher et polymériser des encres et matériaux grâce à de puissantes impulsions lumineuses. Ce procédé utilise divers spectres lumineux, notamment les UV, l'infrarouge (IR) et la lumière blanche

flash. Son principe repose sur les éléments suivants Garlapati, Marques, Gebauer, Dehm, Bruns, Winterer, Tahoori, Aghassi-Hagmann, Hahn & Dasgupta (2018) ; Hilt, Hovish, Rolston, Brüning, Tassone & Dauskardt (2018) :

- Utilisation de la lumière : Le recuit photonique utilise des impulsions lumineuses intenses pour chauffer rapidement le matériau Kim, Kwon & Yu (2022) ;
- Chauffage rapide : Contrairement aux méthodes de recuit traditionnelles qui utilisent des fours ou des plaques chauffantes nécessitant des temps de traitement plus longs, le recuit photonique offre un chauffage et un refroidissement très rapides de Boode, Phillips, Lau, Adomkevicius, McGettrick & Deganello (2022) ; Troughton, Charbonneau, Carnie, Davies, Worsley & Watson (2015) ;
- Contrôle précis : La durée et l'intensité des impulsions lumineuses sont contrôlées avec une grande précision, permettant un traitement spécifique et adapté à chaque matériau Troughton, Carnie, Davies, Charbonneau, Jewell, Worsley & Watson (2016).

Principalement employé pour fritter des films minces à base de nanoparticules, le PC comprend trois étapes clés : préparation de l'encre ou pâte, séchage pour éliminer les solvants, puis exposition à une lumière intense pour former un film dense Slimani, Cloutier & Izquierdo (2024b). Contrairement au recuit thermique, le recuit photonique utilise des impulsions lumineuses pour chauffer et modifier rapidement la surface d'un matériau dans les conditions ambiantes empêchant son oxydation. Ce procédé est particulièrement utile pour :

1. Traiter des couches minces et des films sur des substrats sensibles à la chaleur Hsu & Piper (2024) ;
2. Réduire les temps de traitement grâce à un chauffage et un refroidissement rapide Wijesinghe, Tetlow, Maiello, Fleck, O'Dowd, Beattie, Longo & Hutter (2024) ;
3. Améliorer les propriétés optiques et électriques des matériaux semi-conducteurs Slimani *et al.* (2024b) ;

4. Mieux adapté à la production à haut débit et à faible coût, ainsi qu'à la fabrication roll-to-roll (R2R) Hsu (2021).

### 1.2.1 Mécanismes du recuit photonique

Le principe du recuit photonique repose sur l'absorption de l'intensité lumineuse par les nanoparticules présentes dans l'encre, qui la transforment en énergie thermique. Cette lumière est produite par des lampes flash au xénon, couvrant une plage spectrale allant de 200 à 1200 nm. La majorité de cette lumière, soit plus de 60 %, se situe dans le spectre visible. Le mécanisme du recuit photonique se décompose en plusieurs étapes clés :

1. Absorption de la lumière : Les photons sont absorbés par le matériau, ce qui augmente son énergie interne et provoque une montée rapide de la température Xu, Daunis, Piper & Hsu (2020a) ;
2. Diffusion thermique : La chaleur générée par l'absorption des photons se propage à travers le matériau, entraînant des modifications dans sa structure cristalline ou amorphe ;
3. Réduction des défauts : Le recuit photonique contribue à diminuer les défauts présents dans les films minces, tels que les dislocations et les imperfections de surface, ce qui améliore les propriétés électriques et optiques du matériau Yarali, Koutsiaki, Faber, Tetzner, Yengel, Patsalas, Kalfagiannis, Koutsogeorgis & Anthopoulos (2020) ;
4. Activation des dopants : Dans les semi-conducteurs, le recuit photonique permet d'activer les dopants, en les intégrant dans le réseau cristallin du matériau, renforçant ainsi ses propriétés conductrices Xu, Piper, Zheng, Malko & Hsu (2022).

Une analyse détaillée du mécanisme de recuit photonique appliqué aux couches minces est illustrée à la figure 1.3. Dans cette illustration, e représente l'épaisseur de l'encre, T la température, $t_p$ le temps d'impulsion, et $\tau$ le temps d'équilibre thermique, il est propre à chaque matériau, est décrit par l'expression suivante Schroder (2011) :

$$\tau_i = \frac{C_i \cdot \rho_i \cdot e_i^2}{4K_i} \tag{1.3}$$

Ou $C_i$ est la capacité thermique spécifique $J.K^{-1}.Kg^{-1}$, $\rho$ la densité volumétrique $Kg.m^{-3}$, $K_i$ la conductivité thermique $W.m^{-1}.K^{-1}$ et e l'épaisseur. Une brève impulsion de lumière intense d'une durée tp chauffe la couche mince à la température $T_{pic}$.

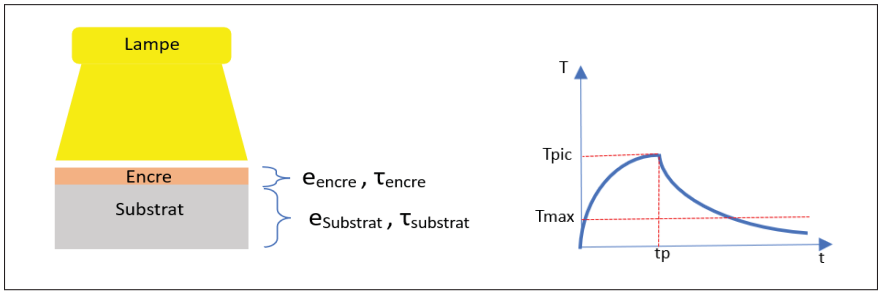


FIGURE 1.3 Principe de recuit photonique

L'absorption de l'impulsion lumineuse par la couche mince permet un chauffage rapide. Ce processus transitoire crée un gradient de température entre la surface de la couche mince d'encre et le substrat Schroder (2011). Ce durcissement transitoire ne peut être optimal que si les conditions suivantes sont établies : Le film doit être beaucoup plus mince que le substrat, afin que la masse thermique de ce dernier puisse le refroidir par conduction. Si le film n'est pas refroidi assez rapidement, des températures de traitement plus basses sont nécessaires pour éviter d'endommager le substrat. Le chauffage doit être suffisamment rapide pour empêcher l'énergie de chauffer l'ensemble du substrat, ce qui limiterait le refroidissement. Une courte impulsion nécessite une puissance élevée pour traiter efficacement le film mince, mais les films imprimés, en raison de porosités et de solvants résiduels, prennent plus de temps à chauffer et à atteindre une température de traitement adéquate.

### 1.2.2 Recuit photonique des couches HTL, ETL et pérovskites

Le chapitre à venir propose une analyse exhaustive des progrès récents dans l'utilisation du durcissement photonique pour les matériaux HTL, ETL, ainsi que pour les couches de pérovskite Ghahremani, Martin, Gupta, Bahadur, Ankireddy & Druffel (2020) ; Zhu, Liu, Ke, Clark, Secor, Song, Kanatzidis, Li & Hersam (2017), avec pour objectif d'améliorer les performances des cellules solaires à pérovskite. Le durcissement photonique, en tant que technique prometteuse, permet d'optimiser les propriétés électriques et structurales de ces matériaux, favorisant ainsi une meilleure efficacité énergétique et une stabilité accrue des dispositifs. Toutefois, dans cette section spécifique, l'accent est mis sur les avancées les plus récentes, réalisées au cours des dernières années, portant sur le recuit photonique de ces matériaux. Cette mise à jour se concentre sur les innovations techniques, les résultats expérimentaux et les défis encore à surmonter pour exploiter pleinement le potentiel de cette technologie dans le développement de cellules solaires à haute performance.

#### 1.2.2.1 Matériaux HTL

De nombreux matériaux de transport de trous nécessitent un recuit photonique et peuvent être utilisés dans les configurations de cellules solaires à pérovskite. Parmi ces matériaux, on peut citer l'oxyde de nickel (NiOx), l'oxyde de cuivre (CuOx) Makenali, Kazeminezhad, Ahmadi & Roghabadi (2021), le poly(bis(4-phényl)(2,4,6-triméthylphényl)amine) (PTAA) Wang, Duan, Zhang, Hameiri, Liu, Bai & Hao (2022c), Poly(3,4-ethylenedioxythiophene) polystyrene sulfonate (PEDOT :PSS), et le thiocyanate de cuivre (CuSCN) Nizamuddin, Arith, Rong, Zaim, Rahimi & Saat (2021) [41]. Les études montrent que le recuit thermique de ces matériaux améliore souvent leurs propriétés de transport de trous et leur transparence. Cependant, dans la littérature, seul le matériau NiOx a été soumis à un recuit photonique dans le cadre d'une configuration de cellule solaire à pérovskite Piper, Daunis, Xu, Schroder & Hsu (2021). La plupart de ces matériaux sont hautement transparents, ce qui pose des défis techniques. Cela nécessite le développement de processus spécifiques pour faciliter leur compatibilité avec la technique du recuit photonique. Des recherches récentes ont montré que le durcissement rapide

des films de PEDOT à l'aide de rayonnements proche infrarouge (NIR) peut considérablement améliorer leur conductivité électrique, les rendant ainsi plus efficaces pour diverses applications électroniques Wang, Feng, Sun, Chai, Mai, Li, Chen, Zhao & Zhang (2024). Toutefois, cette méthode n'a pas encore été appliquée dans une configuration de cellule solaire à pérovskite. Le processus de traitement par rayonnement NIR consiste à chauffer rapidement les films, ce qui permet d'éliminer les solvants résiduels et d'améliorer la morphologie des films. En conséquence, les performances des films sont significativement améliorées par rapport aux méthodes de durcissement traditionnelles. Si ce procédé était adapté et optimisé pour les cellules solaires à pérovskite, il pourrait offrir des avantages substantiels en termes de rapidité de traitement, d'efficacité et de stabilité des matériaux de transport de trous, contribuant ainsi à l'essor de cette technologie photovoltaïque.

#### 1.2.2.2 Matériaux ETL

Contrairement aux matériaux HTL, beaucoup de matériaux ETL a été traité photoniquement tel que le dioxyde de titane ($TiO_2$), le dioxyde d'étain ($SnO_2$) et l'oxyde de zinc (ZnO), ce nouveau traitement a montré de meilleur performance optique et électrique par rapport au recuit thermique. En outre, il a pu régler les limitations causées par l'utilisation des hautes températures que nécessitent la cristallisation de ces matériaux. Les travaux de Sarda et al présente le durcissement photonique (PC) comme une méthode innovante pour fabriquer des films d'oxyde d'étain ($SnO_2$), utilisés dans les cellules solaires à pérovskite (PSC) Sarda, Vidhan, Basak, Hazra, Behera, Ghosh, Choudhary, Chowdhury & Sarkar (2023). Contrairement au traitement thermique traditionnel, le PC frit rapidement les films avec des impulsions lumineuses à haute énergie, réduisant le temps de traitement et la chaleur appliquée aux substrats, ce qui est idéal pour les matériaux sensibles et flexibles. Le PC améliore la qualité des films en augmentant leur cristallinité et en réduisant la rugosité de surface, ce qui optimise les performances électroniques. Cette technique permet d'obtenir des PSC plus efficaces, stables, et mieux adaptées à une production à grande échelle, ouvrant des perspectives prometteuses pour la commercialisation de cette technologie. Dans le contexte du ZnO, le durcissement photonique peut être utilisé pour fritter des nanofeuillets ou des

nanoparticules de ZnO, améliorant ainsi leurs propriétés électriques et optiques. Des recherches ont montré que le frittage photonique de nanofeuillets de ZnO, à l'aide d'une lumière blanche intense combinée à une irradiation UV profonde, peut être réalisé dans des conditions ambiantes et à des vitesses ultra-rapides Patil, Hwang, Yu, Shrestha & Kim (2017). Cette méthode présente l'avantage de permettre le traitement rapide du ZnO sans recourir à des fours à haute température, la rendant adaptée à l'électronique flexible et à d'autres applications où la sensibilité thermique pose problème. Un autre travail examine l'impact de la température de recuit photonique sur les propriétés structurelles et optiques des films de ZnO, synthétisés par pulvérisation assistée par double magnétron Zaitsev, Vaschilin, Kolesnik, Limarenko, Prokhorenkov & Evtushenko (2019). Ce travail montre que le recuit photonique, permet un traitement rapide des films sans nécessiter de chauffage prolongé, améliorant ainsi leur qualité. Les films de ZnO ont été exposés à diverses températures de recuit pour évaluer les changements dans la cristallinité, la morphologie de surface et les propriétés optiques. Les résultats montrent que des températures de recuit plus élevées augmentent la taille des grains cristallins et améliorent la cristallinité des films, ce qui se traduit par une qualité supérieure. Optiquement, les films traités à des températures élevées présentent une meilleure transmission dans le visible et une bande interdite optique optimisée, ce qui est essentiel pour les dispositifs optoélectroniques comme les cellules solaires et les diodes électroluminescentes. La morphologie de surface s'améliore également, avec une réduction de la rugosité, favorisant des performances optimales dans les applications.

#### 1.2.2.3 Matériaux pérovskites

Récemment plusieurs travaux ont abordé l'effet du durcissement photonique sur les matériaux pérovskites. Ces travaux révèlent une amélioration de la qualité et de la cristallisation de ces films ce qui pourrait accroître les performances des cellules pérovskites. Xu et al examine l'impact des résidus d'adduit de DMSO (diméthylsulfoxyde) sur les cellules solaires $\mathrm{MAPbI_3}$ (méthylammonium plomb iodure) durcies par photonic curing Xu, Bonner, Piper & Hsu (2023b). Le DMSO est souvent utilisé comme solvant dans la préparation des solutions de pérovskite, et sa présence résiduelle peut influencer les propriétés et les performances des cellules solaires.

L'étude vise à comprendre comment ces résidus affectent la structure, la morphologie et l'efficacité des cellules solaires $MAPbI_3$ après un durcissement photonique. Des cellules solaires contenant différents niveaux de DMSO résiduel ont été comparé, évaluant leur cristallinité, leur morphologie et leurs performances optiques et électriques. Les résultats montrent que des niveaux appropriés de DMSO résiduel peuvent améliorer la formation de la pérovskite, favorisant une cristallinité accrue et une meilleure uniformité des films, ce qui conduit à des performances optimisées. Cependant, un excès de DMSO peut entraîner des défauts de surface, une dégradation de la qualité du film et une diminution de l'efficacité de conversion énergétique. L'étude met également en lumière les mécanismes par lesquels le DMSO résiduel influence la formation de la pérovskite et la qualité des cellules. Les films avec un contrôle optimal de la quantité de DMSO présentent des rendements de conversion d'énergie plus élevés, tandis que les films avec trop de résidus souffrent de performances réduites.

Les techniques conventionnelles telles que le spin-coating et le recuit thermique ne sont pas adaptées à une production à grande échelle en raison de leur durée de traitement et de l'utilisation de solvants nocifs pour l'environnement. Le recuit infrarouge éclair (FIRA) répond à ces limitations en utilisant un réseau de lampes halogènes dans le proche infrarouge pour chauffer indirectement le substrat, ce qui évapore le solvant et recuit le film de pérovskite en moins de 2 secondes. Le procédé FIRA est une technique innovante de traitement des cellules solaires en pérovskite, qui offre une alternative rapide, efficace et évolutive aux méthodes traditionnelles. Dans Le processus FIRA, les substrats sont exposés à un rayonnement proche de l'infrarouge, qui est absorbé par la couche de l'oxyde transparent (FTO, ITO) Ling, Hagfeldt & Sanchez (2021). Ce chauffage rapide provoque l'évaporation du solvant et la cristallisation de la pérovskite, formant un film cristallin très uniforme. Une étude de comparaison entre l'utilisation d'un antisolvant avec recuit thermique conventionnel et la technique FIRA sans antivolant, a montré un PCE supérieurs à 20 % utilisant la technique FIRA. Les avantages environnementaux de la FIRA sont également remarquables. Les méthodes traditionnelles de fabrication de cellules solaires pérovskites impliquent souvent l'utilisation de solvants toxiques et nécessitent un recuit à haute température, qui consomme beaucoup d'énergie et présente des risques pour l'environnement.

En revanche, la FIRA est un procédé sans solvant qui fonctionne à des températures plus basses et dans des délais plus courts. Cette méthode élimine la nécessité d'utiliser des antisolvants et de longs temps de recuit, ce qui la rend adaptée au traitement en continu et aux substrats flexibles. Le recuit infrarouge éclair FIRA est une technique novatrice de traitement des cellules solaires en pérovskite, offrant une alternative rapide, efficace et évolutive aux méthodes traditionnelles. Lors du processus FIRA, les substrats sont exposés à un rayonnement proche de l'infrarouge, absorbé par la couche d'oxyde transparent (FTO, ITO). Ce chauffage rapide entraîne l'évaporation du solvant et la cristallisation de la pérovskite, formant un film cristallin très homogène. Une étude comparative entre l'utilisation d'un antisolvant avec recuit thermique conventionnel et la technique FIRA sans antisolvant a révélé un rendement de conversion (PCE) supérieur à 20 % avec la méthode FIRA. Les avantages environnementaux de cette technique sont également remarquables. Les méthodes traditionnelles de fabrication des cellules solaires en pérovskite impliquent souvent des solvants toxiques et nécessitent un recuit à haute température, énergivore et potentiellement nocif pour l'environnement. À l'inverse, la FIRA est un procédé sans solvant, fonctionnant à des températures plus basses et sur des durées plus courtes. Ce procédé élimine la nécessité d'utiliser des antisolvants et de longs temps de recuit, le rendant ainsi adapté au traitement en continu et à l'utilisation sur des substrats flexibles.

## 1.3 Conclusion

Dans ce chapitre, nous avons présenté l'état de l'art du recuit photonique appliqué aux matériaux de transport des électrons et des trous, ainsi qu'aux matériaux photoactifs tels que les pérovskites. Cette section complète le chapitre suivant, qui est dédié aux récents progrès du durcissement photonique des couches HTL, ETL et des couches de pérovskite, visant à améliorer les performances des cellules solaires en pérovskite. Elle aborde également les défis pratiques à relever pour rendre viable la commercialisation de ces cellules, notamment la dégradation de la pérovskite due à l'humidité, à la chaleur et à l'oxygène, qui impacte fortement la stabilité des dispositifs. L'optimisation adéquate des paramètres de ce traitement ultrarapide, avec sa nature transitoire, permet d'atteindre des températures plus élevées en un temps très court, favorisant

la cristallisation de la pérovskite sans endommager les substrats sensibles à la chaleur. Cela constitue un avantage majeur pour le traitement de grandes surfaces à moindre coût.

# CHAPITRE 2

# MÉTHODOLOGIES EXPÉRIMENTALES

## 2.1 Introduction

Les techniques de caractérisation jouent un rôle essentiel dans la science et l'ingénierie des matériaux. Elles sont indispensables pour comprendre et maîtriser les propriétés des matériaux, qu'il s'agisse de la recherche fondamentale ou des applications industrielles. Ces techniques permettent de sonder la structure interne, d'analyser la composition chimique, et d'évaluer les propriétés physiques et mécaniques des matériaux. Grâce à elles, il est possible d'adapter et de perfectionner les matériaux pour répondre aux exigences des secteurs tels que l'électronique, l'aérospatiale, l'énergie, et bien d'autres. En particulier, dans le cadre des dispositifs solaires à base de pérovskites, les techniques de caractérisation sont cruciales pour le développement de nouveaux matériaux plus performants et stables. Elles permettent d'optimiser les performances des cellules solaires tout en garantissant leur fiabilité à long terme. Dans ce chapitre, nous allons présenter les outils de caractérisation utilisés dans ce projet pour analyser, comprendre, et optimiser les processus de synthèse et de recuit des dispositifs solaires à base de pérovskites. Le but est d'explorer les moyens d'améliorer la cristallisation et la stabilité des couches de pérovskites, ainsi que d'optimiser leur fabrication en utilisant des techniques avancées telles que le recuit photonique.

## 2.2 Diffraction des rayons X (XRD)

La diffraction des rayons X est une technique d'analyse non destructive utilisée pour étudier les phases cristallines sous l'effet d'une onde électromagnétique. Elle permet, entre autres, d'identifier les phases, de déterminer l'orientation des cristaux et d'analyser la composition chimique. Cette méthode fournit également des informations sur la cristallinité, la taille moyenne des grains, les contraintes, ainsi que les défauts présents dans les cristaux Slimani (2019). Lorsque les rayons X d'un faisceau incident interagissent avec les plans atomiques d'un cristal,

des interférences se produisent ce qui génère le phénomène de diffraction des rayons X (figure 2.1). Les interférences constructives obéissent à la loi de Bragg (équation 2.3), la différence de marche optique entre deux rayons incidents est donnée par la somme des chemins AB et BC.

$$\delta = n \cdot \lambda \tag{2.1}$$

$$A + B = n \cdot \lambda \tag{2.2}$$

$$2d \cdot sin\theta = n \cdot \lambda \tag{2.3}$$

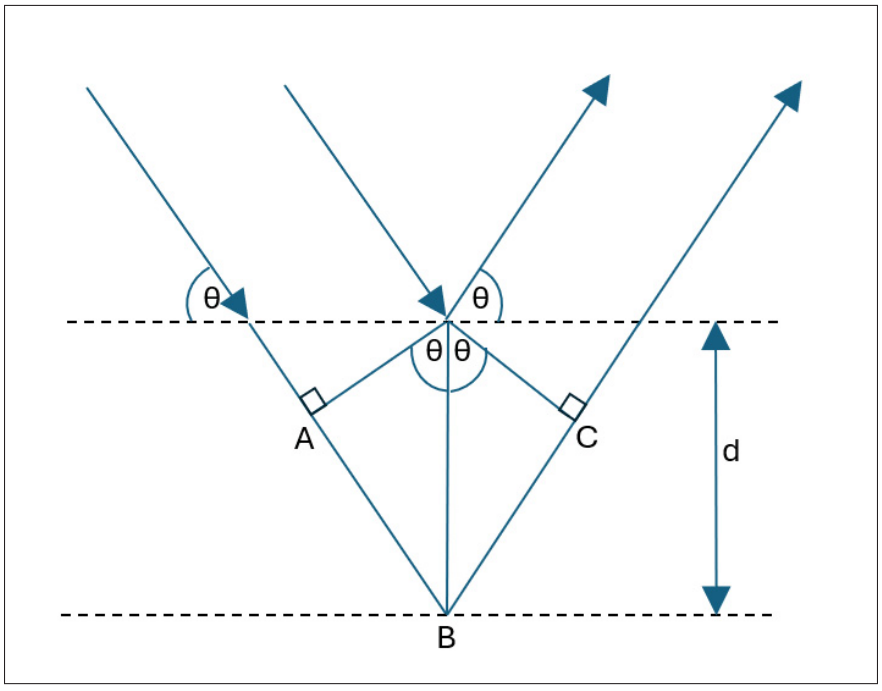


FIGURE 2.1 Illustration diffraction des rayons X

## 2.3 Williamson-Hall

Contrairement à la méthode de Scherrer qui tient compte seulement de l'élargissement dû à la taille des cristallites, la technique Williamson -Hall tient compte repose sur l'analyse de l'élargissement des pics de diffraction, qui peut être dû à la fois à la taille des cristallites et aux déformations du réseau cristallin dues aux les imperfections structurelles telles que les dislocations, les lacunes et les défauts d'empilement Hall (1949) ; Mote, Purushotham & Dole (2012). La contrainte déduite de l'équation suivante Gordillo, Torres, Abella, Peña & Virguez (2020) :

$$\beta_{hkl} \cdot cos\Theta_{hkl} = k\frac{\lambda}{D} + 4\varepsilon \cdot sin\Theta_{hkl} \tag{2.4}$$

ou $\beta_{hkl}$ est la largeur à mi-maximum (FWHM), k est la constante de Scherrer égale 0.94, $\lambda$ est la longueur d'onde de la source de rayons X, D est la taille des cristallites, $\theta_{hkl}$ est la position du pic (°) et $\epsilon$ est la déformation.

## 2.4 Diffraction à incidence rasante des rayons X (GIXRD)

C'est une technique non destructive largement utilisée pour analyser les propriétés cristallographiques des couches superficielles des matériaux. Elle est particulièrement adaptée à l'étude des couches minces, des interfaces, et des surfaces nanostructurées, rendant possible l'examen détaillé des matériaux sur des échelles de quelques nanomètres d'épaisseur.

- Principe de fonctionnement Un faisceau de rayons X est dirigé sur la surface de l'échantillon avec un angle d'incidence très faible, généralement inférieur à 1 degré Yang, Yang & Feng (2020). Cette incidence rasante permet aux rayons X d'interagir principalement avec la fine couche supérieure du matériau, tout en minimisant la pénétration dans le volume sous-jacent. Afin d'éviter le contraste avec la diffraction des rayons X classique.

- Sensibilité aux propriétés de surface Grâce à son faible angle d'incidence, GIXRD est très sensible aux couches superficielles des matériaux, ce qui la rend idéale pour étudier les structures nanométriques comme les films minces et les revêtements, où les propriétés de surface sont cruciales pour les applications technologiques.

La GIXRD est une technique essentielle pour analyser les propriétés cristallographiques des surfaces et films minces à l'échelle nanométrique. Non destructive, elle est particulièrement utile en microélectronique, nanotechnologie et pour les nouveaux revêtements. Cependant, elle nécessite une expertise spécialisée pour l'interprétation des résultats et peut être limitée par la faible intensité des signaux et nécessite des revêtements et des substrats plats Rodriguez, Babuska, Curry, Griego, Dugger, Larson & Mings (2024).

## 2.5 Spectroscopie d'absorption UV-Visible

Cette méthode mesure l'absorption de la lumière dans les domaines de l'ultraviolet (UV) et du visible. L'énergie lumineuse du faisceau traversant l'échantillon est absorbée par les molécules, provoquant des transitions électroniques entre différents niveaux d'énergie. La spectroscopie d'absorption UV-visible est une technique puissante utilisée pour identifier et quantifier les composés chimiques dans un échantillon. Elle repose sur la loi de Beer-Lambert (équation 2.5), qui décrit la relation entre l'absorption de la lumière, la concentration des composés dans l'échantillon et son épaisseur :

$$A = -log\left(\frac{I}{I_0}\right) = -log\,(T) \tag{2.5}$$

Avec Avec $I_0$ faisceau incident, $I$ faisceau transmis et $T$ la transmittance en (%).

Pour les matériaux à base de pérovskites, cette technique permet de sonder les transitions optiques ainsi que de détecter les résidus de $\mathrm{PbI_2}$, fournissant ainsi des informations précieuses pour la caractérisation et l'évaluation de la stabilité de ces matériaux.

## 2.6 Spectroscopie infrarouge à transformée de Fourier (FTIR)

C'est une technique puissante utilisée dans à un large champs d'application pour obtenir un spectre infrarouge d'absorption ou d'émission d'un échantillon solide, liquide ou gazeux Tkachenko & Niedzielski (2022). Chaque type de liaison chimique dans un matériau vibre à des fréquences spécifiques lorsqu'il est exposé à une radiation infrarouge selon les deux modes d'étirement ou de flexion Guerrero-Pérez & Patience (2020). En mesurant ces vibrations, la FTIR permet d'identifier les groupes fonctionnels présents, de détecter des impuretés, et d'étudier les interactions chimiques dans un échantillon. Pour les matériaux à base de pérovskites, la FTIR permet d'étudier la structure chimique et d'identifier les groupes fonctionnels liés à la stabilité, la dégradation, et les performances optiques et électroniques. Elle aide également à analyser les modifications structurelles et les produits de décomposition, tels que $\mathrm{PbI_2}$, formés lors des processus de synthèse, de recuit, ou de vieillissement.

## 2.7 Microscopie électronique à balayage (SEM)

Est une technique d'imagerie puissante qui utilise un faisceau d'électrons pour balayer la surface d'un échantillon à fort grossissement, produisant des images détaillées de sa topographie et de sa composition. Le faisceau d'électrons est dirigé vers l'échantillon et interagit avec les atomes de sa surface, générant divers signaux Mohammed & Abdullah (2018). Ces interactions sont ensuite détectées par un capteur, permettant ainsi de créer une image précise de la surface. Pour les échantillons non conducteurs, il est souvent nécessaire de les recouvrir d'une fine couche conductrice afin d'optimiser la caractérisation. Le SEM permet d'analyser la composition chimique et les propriétés des matériaux, tels que les métaux, les polymères et les semi-conducteurs, avec une résolution spatiale pouvant aller de l'échelle nanométrique à micrométrique, jusqu'à environ 1 nm Akhtar, Khan, Khan & Asiri (2018). Il offre également une grande profondeur de champ, permettant une observation détaillée des surfaces en trois dimensions.

## 2.8 Microscopie à force atomique (AFM)

C'est est une technique d'imagerie qui utilise une sonde extrêmement fine pour balayer la surface d'un échantillon. Contrairement à la microscopie électronique à balayage (MEB), l'AFM n'emploie pas de faisceau d'électrons, mais utilise une pointe nanométrique. Lors du balayage, les forces d'interaction entre la pointe et la surface de l'échantillon sont mesurées, permettant de produire une image topographique en trois dimensions avec une résolution atomique. L'AFM est couramment utilisé pour analyser les surfaces à l'échelle nanométrique, sans nécessiter de préparation conductrice préalable de l'échantillon. AFM opère selon 3 modes Joshua, Cheng & Lau (2023) ; Schwartz, Jakob & Centrone (2022) :

- Modes contact : pointe est en contact avec la surface (applicable pour les matériaux robustes),
- Modes sans contact : la pointe oscille à proximité de la surface pour éviter d'endommager la surface (matériaux sensibles),
- Modes tapping : la pointe est en contact intermittent.

L'AFM présente des avantages tel que : une résolution verticale de 0.1 nm et latérale de 2-3 nm Umeda, McArthur & Kodera (2023). il peut imager dans des interface air liquides sans avoir besoin d'un traitement de surface spécifique Buchoux (2011). Il est capable de mesurer des propriétés mécaniques, électriques, magnétiques, chimiques à l'échelle nanométrique, et produire des images 3D de haute résolution.

## 2.9 Spectroscopie Raman

La spectroscopie Raman est une technique d'analyse avancée permettant de déterminer la composition chimique et la structure moléculaire des matériaux. Elle tire son nom de l'effet Raman, découvert en 1928 par le physicien indien C.V. Raman Raman (1928), qui a reçu le prix Nobel de physique pour cette découverte. Cette méthode repose sur la diffusion inélastique de la

lumière, qui fournit des informations précieuses sur les vibrations moléculaires et les interactions chimiques au sein d'un échantillon. Son principe de fonctionnement repose sur plusieurs étapes :

- Illumination : l'échantillon est irradié par une lumière chromatique d'une source laser Agarwal & Atalla (2020) ;
- Diffusion de la lumière : l'interaction de la lumière avec l'échantillon produit une diffusion inélastique Orlando, Franceschini, Muscas, Pidkova, Bartoli, Rovere & Tagliaferro (2021) ;
- Analyse du spectre ; les photons diffusés sont collectés et analysés et révèlent le spectre Raman qui résulte du décalage fréquentiel correspondant aux énergies des vibrations moléculaires spécifiques du matériau.

La spectroscopie Raman est une technique analytique puissante, largement utilisée dans des domaines variés. Contrairement à d'autres techniques similaires, comme la spectroscopie infrarouge, le signal collecté est moins sensible à la présence d'eau Orlando *et al.* (2021). Cependant, ses limitations en termes de sensibilité et d'interférences lumineuses doivent être prises en compte lors de son utilisation Jones, Hooper, Zhang, Wolverson & Valev (2019a) ; Zhao, Liu, Sui, Xu & Tong (2021).

## 2.10 Spectroscopie d'impédance électrochimique

La spectroscopie d'impédance (IS), est une technique analytique puissante utilisée pour mesurer l'impédance d'un système sur une gamme de fréquences. Cette méthode est particulièrement utile pour étudier les propriétés électriques des matériaux et des interfaces, comme celles que l'on trouve dans les batteries, les piles à combustible et les études sur la corrosion. IS est une technique utiliser pour étudier les processus cinétiques dans les systèmes électrochimiques Magar, Hassan & Mulchandani (2021). Lors de la mesure, un petit signal de courant alternatif (CA) est superposé à une tension de courant continu (CC) et appliqué à l'appareil. La différence de phase entre la tension continue et le courant alternatif est mesurée sur une large gamme de fréquences, permettant d'identifier les différents phénomènes physiques au sein du dispositif.

Ainsi, les mesures IS peuvent analyser les processus physiques et chimiques dans divers types de dispositifs, y compris les dispositifs optoélectroniques, les piles à combustible et les batteries à l'état solide Sinclair (1995). De plus, l'IS est une méthode non destructive. Généralement, les mesures IS présentent deux arcs correspondant aux réponses basse fréquence (LF) et haute fréquence (HF), respectivement Suo, Xiao, Li, Liu, Xin, Meng, Liang, Kan, Yao, Li & others (2023). A partir du circuit équivalent les réponses HF et LF permettent de déterminer la résistance série (Rs), la résistance de transfert de charge ($R_{CT}$) et la capacité parallèle.

## 2.11 Effet Hall

L'effet Hall, découvert par Edwin Hall en 1879, se produit lorsqu'un conducteur ou un semi-conducteur traversé par un courant est placé perpendiculairement à un champ magnétique, générant une tension à angle droit par rapport au courant. L'effet Hall est plus prononcé dans les semi-conducteurs que dans les métaux en raison de la présence de porteurs de charges (électrons et trous). Cela permet de mesurer la tension de Hall et de déduire des caractéristiques intrinsèques du matériau semi-conducteur. Les équations associées permettent de quantifier ces paramètres importants Chien (2013).

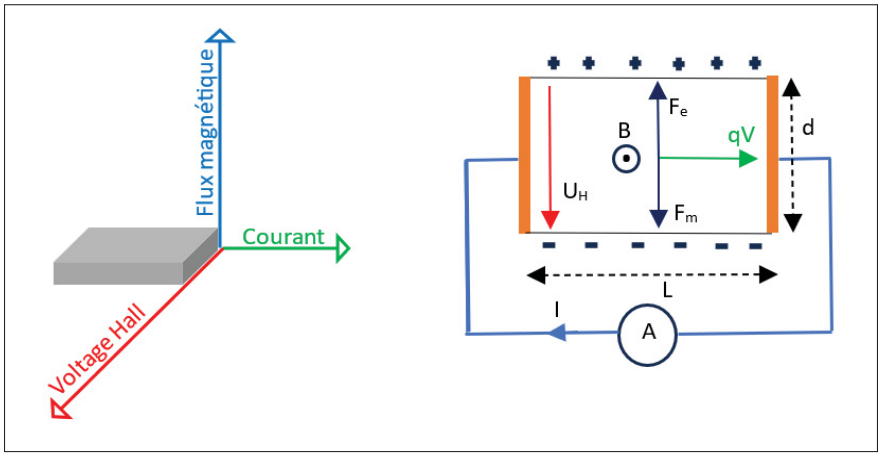


FIGURE 2.2 Illustration diffraction des rayons X

$$V_H = \frac{B \cdot I}{n \cdot q \cdot t} \tag{2.6}$$

$$R_H = \frac{1}{n \cdot q} \tag{2.7}$$

$$\mu = \frac{R_H \cdot I \cdot L \cdot V_r}{d \cdot L} \tag{2.8}$$

$$v = \mu \cdot E \tag{2.9}$$

$$\rho = \frac{R_H}{\mu} \tag{2.10}$$

Ou t est l'épaisseur du film, d largeur, D sa longueur, v vitesse d'entrainement des porteurs de charges, $V_H$ tension de Hall, E champs électrique, $R_H$ la constante de Hall, $\rho$ la résistivité et $\mu$ la mobilité des charges.

Les capteurs à effet Hall présentent de nombreux avantages. Tout d'abord, ils permettent une mesure sans contact, ce qui réduit l'usure et prolonge la durée de vie des dispositifs. Leur robustesse et fiabilité leur permettent de fonctionner efficacement dans des environnements difficiles, notamment en présence de fortes températures et de vibrations. Ces capteurs assurent également une mesure précise des champs magnétiques et des courants électriques, tout en réagissant rapidement aux changements dynamiques. De plus, ils sont insensibles à l'humidité, offrent une bonne linéarité, une large plage dynamique, et sont compatibles avec les technologies des semi-conducteur Crescentini, Syeda & Gibiino (2021). Ils permettent de détecter le type de porteurs de charge circulant dans le semi-conducteur. Toutefois, ils sont sensibles aux

interférences provenant de champs magnétiques externes indésirables, ce qui peut nuire à la précision des mesures Crescentini *et al.* (2021).

## 2.12 Photo-CELIV

L'extraction de charge photo-induite par augmentation linéaire de la tension (Photo-CELIV) est une technique temporelle utilisée pour étudier le transport et la recombinaison des charges dans les cellules solaires organiques et hybrides. Elle consiste à illuminer la cellule pour générer des porteurs de charge, puis à appliquer une tension croissante de manière linéaire afin d'extraire ces porteurs Sen & Islam (2022). La réponse en courant est mesurée, permettant d'analyser des paramètres essentiels comme la mobilité, la durée de vie et la densité des porteurs de charge. Cependant, il est important de noter que la méthode Photo-CELIV ne détecte que les porteurs rapides et ne permet pas de distinguer la mobilité des électrons de celle des trous. Malgré cette limitation, elle s'avère particulièrement utile pour les nouveaux matériaux photovoltaïques, tels que les semi-conducteurs organiques et les pérovskites. En offrant une évaluation directe du transport des charges, la Photo-CELIV contribue à l'optimisation de la conception des cellules solaires à couche mince, tout en restant une méthode non destructive pour les dispositifs étudiés. La mobilité de charges est décrite par l'expression suivante Aukštuolis, Girtan, Mousdis, Mallet, Socol, Rasheed & Stanculescu (2017) ; Stephen, Genevičius, Juška, Arlauskas & Hiorns (2017).

$$\mu = \frac{2d^2}{3A.t_{max}^2(1 + 0.36\frac{\Delta}{J_{max}})} \tag{2.11}$$

$A$ est la pente de la rampe de tension d'extraction, $t_{max}$ est le temps lié au pic de courant, et $\Delta$ est la différence entre le courant maximal et le plateau de courant de déplacement.

## 2.13 Conclusion

Dans ce chapitre, nous avons présenté diverses techniques de caractérisation utilisées tout au long de notre projet. La XRD et la GIXRD sont essentielles pour déterminer la structure cristalline,

la composition chimique et les phases des matériaux. La spectroscopie Raman et la FTIR fournissent des informations sur les vibrations moléculaires, les modifications structurelles, les liaisons chimiques et les interactions dans les matériaux. Le SEM et l'AFM permettent d'analyser la morphologie et la topographie à l'échelle nanométrique. Nous avons utilisé la spectroscopie d'absorption UV-Vis pour déterminer les propriétés optiques des matériaux. La spectroscopie d'impédance, l'effet Hall et la technique Photo-CELIV permettent quant à elles d'analyser les propriétés électroniques, telles que la résistance de transfert de charge, la diffusion, ainsi que la dynamique des porteurs de charge sous illumination. Ces aspects sont cruciaux pour les applications électrochimiques, notamment les batteries et les cellules solaires. L'utilisation de ces techniques permet d'obtenir une compréhension approfondie de la structure et des propriétés des matériaux, facilitant ainsi l'optimisation de la synthèse, du recuit et des processus de fabrication. Elles jouent un rôle clé dans le développement et l'amélioration des dispositifs semi-conducteurs, y compris les cellules solaires à base de pérovskites.

# CHAPITRE 3

## RECENT ADVANCES IN THE PHOTONIC CURING OF THE HOLE TRANSPORT LAYER, THE ELECTRON TRANSPORT LAYER, AND THE PEROVSKITE LAYERS TO IMPROVE THE PERFORMANCE OF PEROVSKITE SOLAR CELLS

Moulay Ahmed Slimani[1], Sylvain G. Cloutier[1], Ricardo Izquierdo[1]

[1] Département de Génie Électrique, École de Technologie Supérieure,
1100 Rue Notre-Dame Ouest, Montréal, Québec, H3C 1K3, Canada

Article publié dans la revue
« MDPI nanomaterials »
le 19 mai 2024.
https://doi.org/10.3390/nano14100886

**Résumé :** Les cellules solaires à pérovskite (PSC) suscitent un intérêt croissant dans la recherche, mais leurs performances dépendent à la fois du choix des matériaux et du processus utilisé. Les matériaux peuvent généralement être traités en solution, ce qui les rend bien adaptés aux méthodes de traitement de rouleau à rouleau, mais leur dépôt dans des conditions ambiantes nécessite de relever certains défis pour améliorer la stabilité et l'efficacité. Dans cette revue, nous mettons en lumière les dernières avancées en matière de recuit photonique (PC) pour les matériaux pérovskites, ainsi que pour les matériaux de la couche de transport de trous (HTL) et de la couche de transport d'électrons (ETL). Nous présentons comment les paramètres de recuit photonique peuvent être utilisés pour contrôler les propriétés optiques, électriques, morphologiques et structurelles des couches HTL, ETL et pérovskite. En soulignant l'importance de ces avancées pour les cellules solaires pérovskites, on pourrait mettre encore plus en évidence l'importance de cette recherche et souligner son rôle essentiel dans la création d'une technologie solaire plus efficace et durable.

**Abstract :** Perovskite solar cells (PSCs) have attracted increasing research interest, but their performance depends on both the choice of materials and the process used. The materials can typically be treated in solution, which makes them well suited for roll-to-roll processing methods, but their deposition under ambient conditions requires overcoming some challenges to improve stability and efficiency. In this review, we highlight the latest advancements in photonic curing (PC) for perovskite materials, as well as for hole transport layer (HTL) and electron transport layer (ETL) materials. We present how PC parameters can be used to control the optical, electrical, morphological, and structural properties of perovskite HTL and ETL layers. Emphasizing the significance of these advancements for perovskite solar cells could further highlight the importance of this research and underline its essential role in creating more efficient and sustainable solar technology.

**Keywords :** photonic curing ; ETL ; HTL ; perovskite solar cell

## 3.1 Introduction

Photonic curing (PC) is a method that is employed in several sectors, most notably printed electronics and coatings. It is a process of curing or drying inks, coatings, and other materials that employs powerful light pulses. Curing light is often in the ultraviolet (UV) and infrared (IR) spectra, as well as flash white light Hwang, Oh & Kim (2016). PC is a specialized process for producing nanoparticle-based thin films. The procedure involves using intense laser or light irradiation to rapidly cure and heat the material. It consists of three steps : (1) preparing the ink or paste, (2) drying the ink through a solvent elimination process, and (3) exposing the material to powerful light to generate a dense film.

Since 2006, NovaCentrix has led to advancements in printed electronics, including the introduction of the first commercial PC device. This technology has since evolved through innovations in flashlamp technology, digital control, and pulse tuning NovaCentrix (2024). The PC rapidly raises the temperature of the material and causes the solvent to evaporate, eventually producing a solid, cured coating. PC is widely used in the development of various types of printed electronics, including flexible displays, thin-film transistors Mudgal, Bhadrachalam, Bischoff, Cormier, Manley & Hirschman (2017), RFID tags Akbari, He, Juuti, Tentzeris, Virkki & Ukkonen (2017) ; Das, Cormier & Williams (2015b), sensors, and solar cells Chatterjee, Weidling & Swisher (2022) ; Schube, Fellmeth, Maier, Keding, Clement & Glunz (2018), but it is also increasingly used in the industrial sector, in the automotive, and solar industries Piper *et al.* (2021) ; Xu, Piper, Daunis, Schroder & Hsu (2020b) to enhance production and improve performance. PC is especially useful for printing on heat-sensitive substrates such as plastic or paper because it reduces heat exposure and potential substrate damage ; the material's temperature rises rapidly as an outcome of this exposure. The high-intensity light generates enough energy to start and finish the curing process in milliseconds, making it substantially faster than traditional thermal annealing (TA). PC is being researched and developed all the time, and it has the potential to change manufacturing processes in a variety of industries, making them more efficient and ecologically friendly. PC has evolved into a specialized technique for treating surfaces, presenting its importance in perovskite solar cell manufacturing through advancements like

optimizing curing parameters, adapting to delicate substrates, controlling layer morphology, and integration with manufacturing processes. Recently applied in perovskite solar cell fabrication, PC's potential for high efficiency and low processing cost is explored in this review, focusing on enhancing HTL, ETL, and perovskite material crystallization to improve the fabrication and processing of perovskite solar cells (PSCs).

### 3.2 Photonic Curing of the HTL Layer

Photonic annealing of HTL layers is an innovative and promising substitute for TA. It reduces the requirement for complex and time-consuming processes, making it a precise and efficient approach that has recently garnered significant interest. It is an annealing process using intense pulsed light (IPL). A brief pulse (25–100 ms) of broad-spectrum light (0.2–1.5 μm) turns energy into heat inside light-absorbing layers Xu *et al.* (2020a). The pulse intensity could be high; however, the cumulative energy is low due to the brief exposure Piper *et al.* (2021). To our knowledge, there has not been enough study of the photonic annealing of HTL, excluding sol-gel precursors, which were only used by the Hsu group as HTLs for flexible and rigid perovskite solar cells. Piper *et al.* (2021); Xu *et al.* (2020b). Similar to perovskite and other inks ($TiO_2$, $SnO_2$, $ZrO_2$), converting sol-gel precursors into a NiOx oxide film on a flexible substrate, presents many challenges. Nickel nitrate precursors are transparent, requiring higher energies, which could damage the flexible film; moreover, previous work has shown that NiOx is not a crystalline structure and remains transparent after photonic annealing, making it difficult to determine the degree of conversion of NiOx. To address this challenge, the ITO-coated flexible Corning Willow Glass (WG) substrate is used for the annealing process Hsu (2021). This option allows for roll-to-roll manufacturing compatibility and facilitates the comparison of both thermal and PC methods. In addition, low-cost solution methods (solution-based NiOx nanoparticles Sarda *et al.* (2023)) can also be employed to prepare efficient NiOx hole contacts. However, their application in flexible solar cells is restricted by the annealing process required at 300–500 °C Sajid, Elseman, Huang, Ji, Dou, Jiang, Liu, Wei, Cui & Li (2018); Subbiah, Halder, Ghosh, Mahuli, Hodes & Sarkar (2014). In addition, developing a one-step process to convert NiOx

from its sol-gel precursor is an interesting approach. Hsu's group has proven the possibility of creating a dense semiconducting metal oxide film from a sol-gel precursor through PC Piper *et al.* (2021). The choice of sol-gel nitrate precursors is justified by their lower decomposition temperature compared to other NiOx precursors, thus requiring less energy to convert the precursors into a dense film Liu, Chang, Lin, Zhou, Yang, Chen, Zhang, Liu & Hao (2018b) ; Sun, Chen, Wu, He, Zhang & Chen (2019). In their study, the authors compared the efficiency of various configurations of perovskite solar cells (PSCs) using thermal and photonic annealing for both NiOx HTL and perovskite active layer. All PC MAPI samples were treated with a single pulse at a lamp voltage of 300 V and a pulse duration of 20 ms, but the PC NiOx Champion was processed using a lamp voltage of 500 V for 10 ms with 10 pulses at a frequency of 0.2 Hz Piper *et al.* (2021). XRD analysis (Figure 3.1) showed that the crystal phase of perovskite was comparable for TA and PC, as were the microstructure, grain size, and topography (Figure 3.1B–D). TA and PC are applied to both NiOx and MAPI, enabling three different solar cell configurations : (1) TA NiOx and TA MAPI (TA/TA), (2) TA NiOx and PC MAPI (TA/PC), and (3) PC NiOx and PC MAPI (PC/PC). The maximum power conversion efficiencies (PCEs) are achieved by the TA/PC configuration (see Table 3.1). However, for the average PCE, we can see a slight improvement with the PC/PC and low dispersion compared to the other configurations. This is probably explained by the fact that PC, as opposed to TA, can provide excellent processing uniformity because the light source can be controlled very precisely, allowing the rapid and uniform heating of the material surface.

Tableau 3.1 Comparison of the 3 configurations

| **Annealing Process** | **NiOx** | **MAPI** | **PCEmax (%)** |
|---|---|---|---|
| TA/TA | TA | TA | 11.5 |
| TA/PC | TA | PC | 12.5 |
| PC/PC | PC | PC | 11.7 |

Table 3.1 presents a comparison of the maximum PCE of PSCs using NiOx. As shown in Table 3.1, PC treatment gives a similar maximum power conversion efficiency to conventional TA, which is consistent with previous studiesDas, Yang, Gu, Joshi, Ivanov, Rouleau, Aytug,

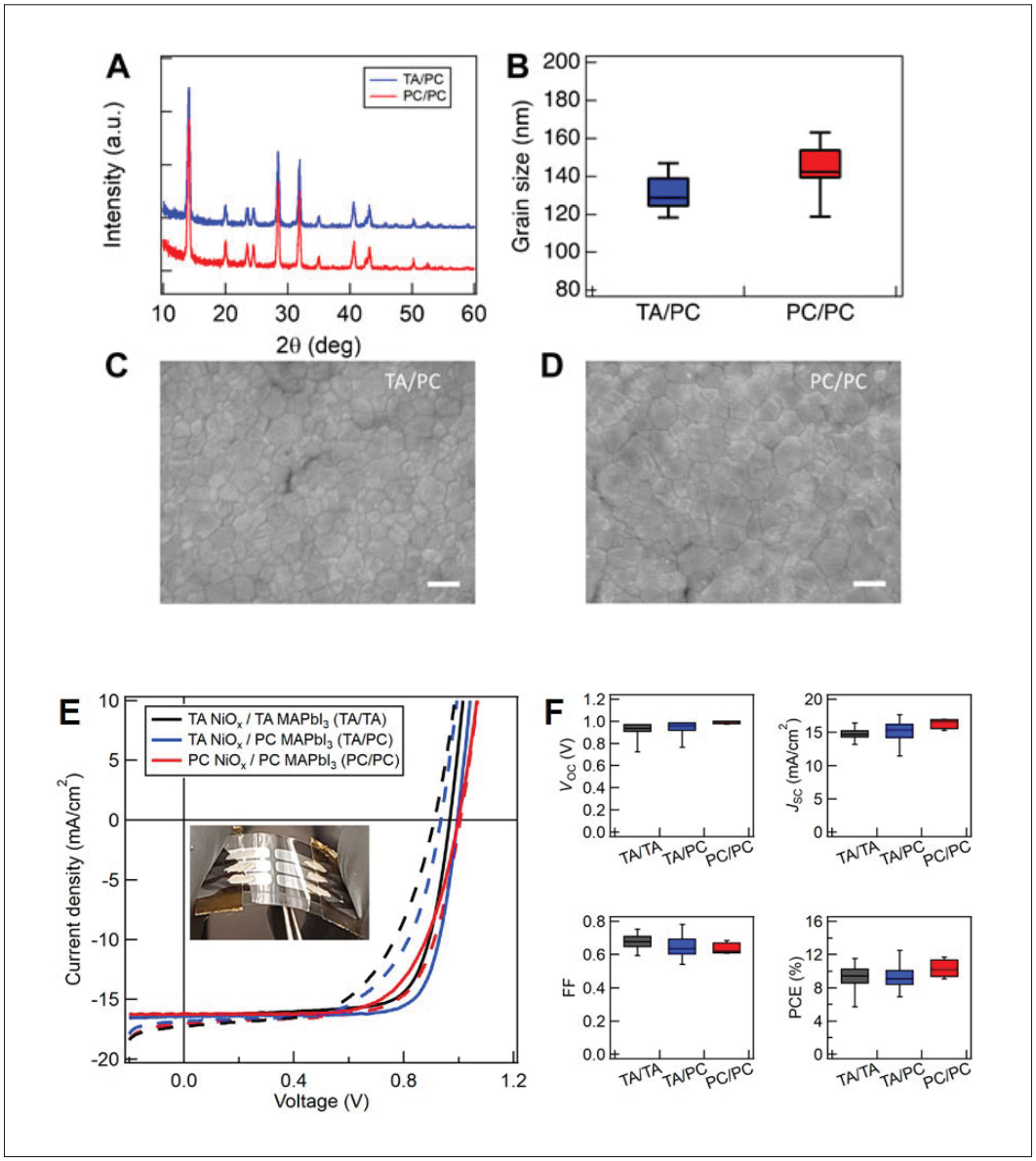


FIGURE 3.1 **A**) XRD of PC MAPI samples on TA and PC NiOx. (**B**) Grain size analysis of MAPI SEM images. SEM images of PC MAPI films on (C) TA NiOx and D) PC NiOx, respectively. (**E**) J-V measurements of flexible PSCs Reverse Champion (solid) and forward scan (dashed). (**F**) Box plots of $V_{oc}$, $J_{sc}$, FF and PCE variations for PSCs fabricated under ambient conditions (from Piper *et al.* (2021))

Geohegan & Xiao (2015a). Similarly, the PSC performance results were similar for TA and PC. (Figure 3.1 (E-F)). In addition, PC testing has shown that a single pulse can convert NiOx and MAPI films into dense, uniform films with excellent electrical properties and is sufficient to

achieve maximum performance for both NiOx and perovskite. TA is conducted in a glove box, while PC is performed under ambient conditions ; however, their performance is comparable.

The Hsu group's research focuses on the use of NiOx as an HTL layer for PSC on flexible and glass substrates Piper *et al.* (2021) ; Xu *et al.* (2020b). This work examines the impact of photonic curing on PSC efficiency, demonstrating how it can reduce production time and costs by rapidly heating and crystallizing the material. In addition, the group is examining the potential of photonic curing in perovskite solar cells, particularly in the context of high-throughput manufacturing.

### 3.3 Photonic Curing of ETL layer

Moreover, beyond HTL, photonic curing has been employed on various materials utilized in the production of PSCs, such as ETL. The preparation of the different HTL layers, the active layer, and the ETL layer requires sequence deposition and annealing, which sometimes limits the use of certain materials (ETL, HTL) and substrates due to high temperatures. $TiO_2$ is typically used in mesoporous Homola, Pospisil, Shekargoftar, Svoboda, Hvojnik, Gemeiner, Weiter & Dzik (2020) ; Kim, Choi, Choi, Song, Mo, An, Jo, Ahn, Ahn & Kim (2021a) or planar structures in PSCs Huang, Cui, Chen, Yan, Yue, Qu, Wang, Du, Liu & Zhang (2022) ; Otoufi, Ranjbar, Kermanpur, Taghavinia, Minbashi, Forouzandeh & Ebadi (2020). It is widely used in standard configurations as an ETL layer in PSCs. However, its crystallization into a compact layer requires a high temperature (400–500 °C)Ren, Wang, Wei, Cui, Li & Qin (2020) ; Seo, Shin, Kim, Jeong, Park & Shin (2021), which is not compatible with certain PSC configurations (p-i-n) or with flexible plastic-based substrates ( kapton, polyethylene terephthalate (PET), poly-ethylene naphthalate (PEN)). To overcome these issues, various approaches have been developed for fabricating compact $TiO_2$ coatings for PSCs, such as sputtering process, which showed power conversion efficiencies (PCEs) of 16.1 % and 23 % on glass substrates Lee, Bae, Cho, Kim, Hwang, Lee, Lee, Hyun, Lee & Choi (2019) ; Zhang, Zhang, Wang, Wang, Liu, Geng, Wang, Jiang & Ding (2022) ; electron beam evaporation, demonstrating 11.6 % Xue, Chen, Li, Chou, Wang, Tang, Zhang, Huang, Guo & Takaloo (2023) ; and solution treatment

methods, involving a lower temperature of 150 °C, which resulted in a PCE of 13.5 % Vaenas, Konios, Stergiopoulos & Kymakis (2015). In contrast to these techniques, the PC of $TiO_2$ is promising mainly because of its compatibility with R2R and sensitive substrates (PEN,PET) Feleki, Bex, Andriessen, Galagan & Di Giacomo (2017), Additionally, its reduced process time and low thermal budgets Das, Gu, Joshi, Yang, Aytug, Rouleau, Geohegan & Xiao (2016) make it appealing for large-scale industry. Several studies have confirmed that the use of PC is an effective technique to achieve the improved crystallization of $TiO_2$ films on glass and plastic substrates that are coated with ITO or FTO. The extremely short pulse duration emitted by the IPL system is sufficient to sinter the $TiO_2$ without damaging the substrate. It has been shown that surface pretreatment is necessary to replace high temperatures for $TiO_2$ crystallization by reducing surface tension, facilitating wetting, and decomposing the nitrate resulting from synthesis Zhang, Yao, Ali, Wei, Wang, Yeo, Friend & MacFarlane (2014). IPL, on the other hand, requires no additional treatment to eliminate the nitrate binder, which negatively affects the efficiency of PSCs Feleki *et al.* (2017). In the same study, Table 3.1 illustrates that both IPL and TA exhibit similar performance for all configurations within the energy density range of 10 to 20 $mA\,cm^{-2}$ and pulse duration range of 2 to 7 ms for glass substrates. However, the energy density needed for PEN substrates is less (2.35 $mA\,cm^{-2}$) than that of glass substrates due to their higher absorbance capacity. On flexible PEN substrates, the average yield reaches 10 %, which is an outstanding achievement for this type of configuration and appealing for R2R applications.

Figure 3.2 shows AFM analysis of the surfaces of unannealed, furnace-annealed (FA), and PC-annealed $TiO_2$ films. To explain the impact of PC on the optical, electrical, and structural characteristics of $TiO_2$ films, prior research indicated that roughness is more significant in furnace and PC-annealed films compared to as-cast $TiO_2$ films and the absence of anatase in untreated films Das *et al.* (2016). Figure 3.2 shows that the as-cast films exhibit a smooth surface, which is attributed to the presence of small grains. On the other hand, the treated films display higher roughness and larger grains, suggesting improved crystallinity and conductivity. This confirms the performance of both PC-annealed and furnace-annealed $TiO_2$ films (15.1–15 %),

as shown in Table 3.2. Another study examined the performance of PSCs on rigid and flexible substrates using a combination of the photonic annealing of $TiO_2$ and pulverization of perovskite $CH_3NH_3PbI_{3-x}Cl_x$. The results showed a performance of 11.5 % for PSCs on rigid substrates and 8.1 % for flexible PSCs (see Table 3.2). The latter demonstrated a retention of initial performance exceeding 60 % after 1000 bending cycles, displaying the compatibility of PSCs with lightweight and inexpensive flexible substrates. This suggests that PSCs are a feasible technique for roll-to-roll manufacturing Das *et al.* (2015a).

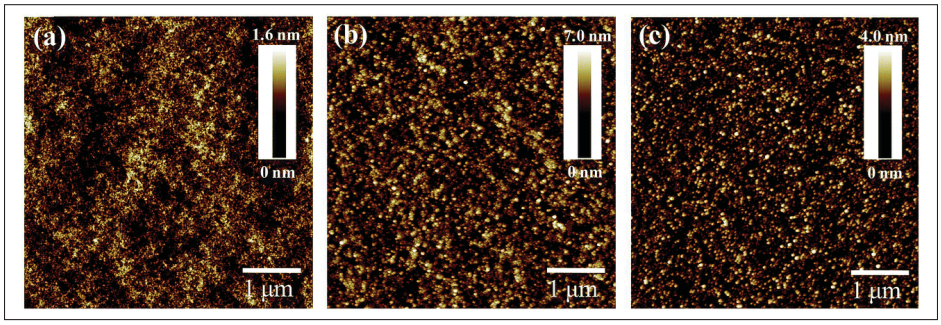


FIGURE 3.2 AFM images for $TiO_2$ films : (**a**) non-annealed, (**b**) PC-annealed, and (**c**) furnace-annealed ; Taken from Das *et al.* (2016)

TABLEAU 3.2 Performance parameters of PSCs with $TiO_2$, $SnO_2$ or Mix of both

| Annealing Process | Energy density Tension Energy | Pulse length (ms) | $V_{oc}$ (V) | $J_{sc}$ (mA cm$^{-2}$) | FF (%) | PCE (%) | Configuration | Ref |
|---|---|---|---|---|---|---|---|---|
| Glass-PC | 12.3 J.cm$^{-2}$ | 2 | 1.05 | 20.2 | 78.5 | 16.7 | ITO/compact$TiO_2$/MAPI Spiro-OMetad/ Au | Feleki *et al.* (2017) |
| Glass-TA | - | - | 1.05 | 20.2 | 76.5 | 16.3 | | |
| PEN-PC | 2.35 J.cm$^{-2}$ | 2 | 1.05 | 18.2 | 64.1 | 12.3 | | |
| Glass-PC | 200 | 7 | 1.04 | 19.9 | 60.9 | 15 | ITO/$TiO_2$/$CH_3NH_3PbI_{3-x}Cl_x$/ Spiro-OMetad/Au | Das *et al.* (2016) |
| Glass-FA | - | - | 1.04 | 19.4 | 65.7 | 15.1 | | |
| PET-PC | 200 | 7 | 1.09 | 16.9 | 61 | 11.2 | | |
| Glass-TA | - | 2 | 1 | 18 | 61.2 | 11.5 | ITO/$TiO_2$/$CH_3NH_3PbI_{3-x}Cl_x$/ Spiro-OMetad/Ag | Das *et al.* (2015a) |
| PET-PC | 17.3 J.cm$^{-2}$ | 2 | 1.03 | 15.3 | 51.4 | 8.1 | | |
| Glass-PC | 46 J.cm$^{-2}$ | 20 | 1.06 | 21.4 | 67 | 15.3 | FTO/$SnO_2$/MAPI/PTAA/Au | Zhu *et al.* (2017) |
| Glass-PC | 2100 J | 2 | 1.02 | 15.78 | 78.3 | 12.56 | FTO/$SnO_2$/MAPI/PTAA/Au | Ghahremani *et al.* (2020) |
| PET-PC | 2100 J | 2 | 0.99 | 11.33 | 64.75 | 7.6 | ITO/$SnO_2$/MAPI/PTAA/Au | |
| Glass-PC | 11.3 J.cm$^{-2}$ | 7 | 1.14 | 22.7 | 80.4 | 21.1 | FTO/$SnO_2$/$(FA_{0.83}MA_{0.17})_{0.95}$ $Cs_{0.05}PbI_{2.5}Br_{0.5}$/ Spiro-OMetad/Au | Sarda *et al.* (2023) |
| Glass-TA | - | - | 1.12 | 22.5 | 79.8 | 20.2 | | |

$SnO_2$ is a commonly used ETL in the fabrication of PSCs. It has received significant attention due to its remarkable stability under UV light, large bandgap, and greater electron mobility than ZnO and $TiO_2$Abulikemu, Neophytou, Barbé, Tietze, El Labban, Anjum, Amassian, McCulloch & Del Gobbo (2017) ; Zhu *et al.* (2017). Several approaches have proven the feasibility of fabricating planar PSCs based on solution treatment of $SnO_2$ nanoparticlesKe, Fang, Liu, Xiong, Qin, Tao, Wang, Lei, Li & Wan (2015) ; Xie, Yin, Chen, Liu, Yang, Que & Wang (2019), atomic layer deposition (ALD) Baena, Steier, Tress, Saliba, Neutzner, Matsui, Giordano, Jacobsson, Kandada & Zakeeruddin (2015) ; Ren, Zhu, Li, Mazumdar, Sun, Chen, Xu, Wang, Shi & Huang (2022), and $SnO_2$ sol-gel Yi, Wang, Mahmud, Haque, Upama, Xu, Duan & Uddin (2018). While these techniques have yielded high PCE, they necessitate extended annealing and growth periods, which could be a drawback for large-scale manufacturing. In this context, the IPL of $SnO_2$ appears to be a promising and compatible technique that avoids high-temperature annealing and significantly reduces the annealing time. Preliminary research on $SnO_2$'s PC has revealed a significant reduction in the roughness of $SnO_2$ films before and after photonic annealing, from 116.6 nm to 82.8 nm Zhu *et al.* (2017), with a performance of 15.3 % (Table 3.2). In a previous study, the IPL of the $SnO_2$ films on the FTO substrates indicates that the grain boundaries previously present in the FTO film (Figure 3.3a) have disappeared, validating that the optimized IPL parameters should make the $SnO_2$ film more compact and uniform (Figure 3.3b). Reducing the number of grain boundaries can increase shunt resistance and decrease recombination effects Ghahremani *et al.* (2020).

Table 3.3 displays PSCLs produced with identical techniques using different ETLs, $TiO_2$, $SnO_2$, or a combination of both (Mix). Based on the performance parameters of the PSCs reported in Figure 3.3c, we observe that $SnO_2$ exhibits significantly better performance than $TiO_2$, especially in terms of FF and Jsc. This is because $SnO_2$ has advantageous properties such as a wide bandgap, high transparency, high mobility, and excellent stability Xiong, Guo, Wen, Liu, Yang, Qin & Fang (2018); Yoo, Jung, Jung, Shen & Park (2021), which are ideal for use as an ETL for planar PSCs. However, a $TiO_2$ and $SnO_2$ bilayer, or a mixture of $SnO_2$ with $TiO_2$ dopants, offers even better performance than $SnO_2$. This is attributed to the excellent charge selectivity and low charge recombination in the interface perovskite/$SnO_2$ devices Baena *et al.* (2015).

TABLEAU 3.3 Performance parameters of PSCs with $TiO_2$, $SnO_2$ or Mix of both

| **ETL** | **Jsc** ($mA.cm^{-}2$) | $V_{oc}$**(V)** | **FF (%)** | **PCE (%)** | **Ref** |
|---|---|---|---|---|---|
| TiO_2/SnO_2 | 20.8/21.3 | 0.99/1.05 | 61.6/66.3 | 12.8/14.8 | Barbé *et al.* (2017) |
| ETL[1] | 19.92/21.63/22.06 | 1.09/1.11/1.02 | 65.54/70.24/72.6 | 14.18/16.92/18.46 | Li *et al.* (2020) |
| ETL[1] | 22/22.1/22.9 | 0.99/1.14/1.2 | 64.5/75.4/76.4 | 14/19/21.1 | Song *et al.* (2017) |
| ETL[1] | 22.85/23.45/23.91 | 1.13/1.14/1.69 | 75.2/75.8/76.5 | 19.33/20.34/21.4 | Tavakoli *et al.* (2018) |
| SnO_2/Mix | 23.4/24.2 | 1.03/1.1 | 75/77 | 18.09/20.5 | Hu *et al.* (2020a) |
| TiO_2/Mix | 22.06/22.58 | 1.01/1.04 | 72.4/75 | 16.16/17.64 | Sun, Li, Shen & Wang (2023b) |

[1] $TiO_2$/$SnO_2$/Mix

Figure 3.4a displays the transmittance spectra of the FTO, FTO/ $TiO_2$, and FTO/$SnO_2$ samples. It is evident that the $SnO_2$ film has higher transmittance compared to the $TiO_2$ film owing to its wider bandgap. This will enhance the Jsc current density and consequently the PCE. The optimization of photonic annealing time and $SnO_2$ concentration are critical factors in improving $SnO_2$ ETL crystallization. J-V curves for varying $SnO_2$ concentrations and photonic annealing times can be seen in Figure 3.4(b,c). To achieve optimal results, optimizing concentration and time sequencing is recommended. Figure 3.4d shows the XPS analysis of $SnO_2$ films synthesized from the original $SnCl_4$ solution. The figure shows a progressive decrease in the Cl 2p peak with increasing pulse duration, which finally disappears completely after a duration of 20 ms. This confirms that the chlorine is entirely photolyzed and $SnCl_4$ is fully converted to $SnO_2$ Shi, Li, Bu, Yang, Xiao, Peng, Li, Zhong, Ku & Cheng (2019); Zhu *et al.* (2017). Several comparative studies of the electron collection efficiency of compact $SnO_2$ and $TiO_2$ layers using photoluminescence (PL) have confirmed that the PL quenching resulting from

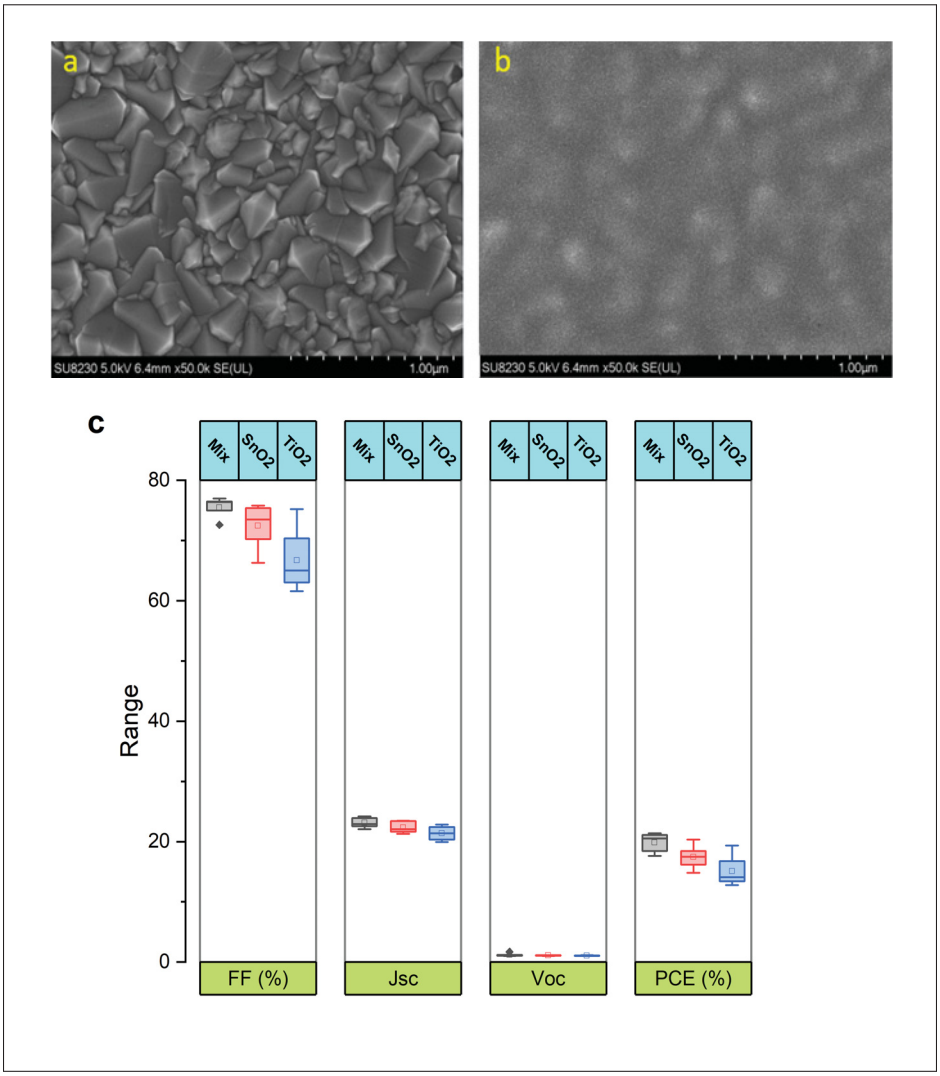


FIGURE 3.3 SEM image for (**a**) FTO and (**b**) SnO2 top surface after IPL treatment. (**c**) Box plot of the performance parameters of PSCs with different ETLs using the data from Table 3.3

charge carrier extraction across the ETL/perovskite interface is significant for the $SnO_2$ layer Regalado-Pérez, Díaz-Cruz, Landa-Bautista, Mathews & Mathew (2021). Figure 3.4e displays the photoluminescence analysis of $SnO_2$ films' TA and PC at various pulse durations. It can be observed that the PL quantum yield is significantly reduced for the 20 ms pulse duration compared to 5 ms. By optimizing energy density and pulse duration, quenching can be similar to or better than thermal annealing. The decrease in PL suggests more efficient separation of charge carriers within the perovskite layer and faster extraction and transfer facilitated by the

compact $SnO_2$ layers using PC annealing Xiong *et al.* (2018). The high electron mobility and lower conduction band of $SnO_2$ compact layers lead to efficient carrier dissociation in $SnO_2$ PSCs Chiang, Kan & Wu (2021); Wang, Xiao, Yu, Zhao, Awni, Grice, Ghimire, Constantinou, Liao & Cimaroli (2017a).

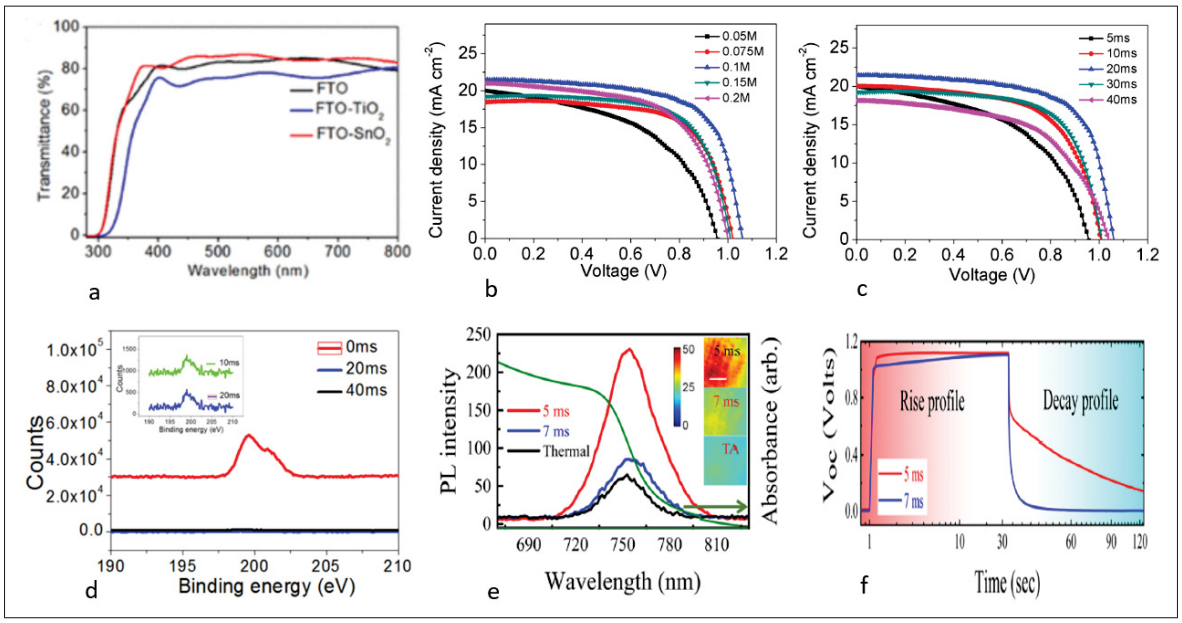


FIGURE 3.4 (**a**) Transmittance of FTO, $TiO_2$, and $SnO_2$ filmsKe *et al.* (2015). The J-V curves for PSCs with $SnO_2$ as ETL by (**b**) barying the concentration and (**c**) varying the PC duration. (**d**) XPS spectrum of the Cl 2p peak; the inset shows an enlarged view of the peak Cl 2p intensityZhu *et al.* (2017). (**e**) Evolution of PL intensity for devices utilizing the TA of $SnO_2$ ETL film and PC with varying pulse duration. (**f**) Open circuit voltage decay (OCVD) for $SnO_2$ PC-annealed devices at 5 ms and 7 ms Sarda *et al.* (2023)

Figure 3.4f shows the OCVD measurement for photonically annealed devices, which helps to understand the relevant changes in interface properties such as the recombination effect and trapping dynamics. We can see, in the light-off state, the high carrier concentration at the oxide–perovskite interface leads to rapid recombination Sarda *et al.* (2023), resulting in a faster drop in $V_{oc}$, which can be observed for 7 ms devices. Improving pulse time and selecting an appropriate ETL can enhance PSC performance. The $SnO_2$ plays an important role in charge separation (electron, hole) in the $SnO_2$/perovskite interface. The accumulation of negative charges within the perovskite leads to a dielectric polarization at the interface, which has been

able to maintain the $V_{oc}$ values and allows a slow decay of the $V_{oc}$ Pascoe, Duffy, Scully, Huang & Cheng (2015) when the light is turned off for devices fabricated with 5 ms pulses.

### 3.4 Photonic Curing of the Perovskite Layer

Photonic curing has the potential to benefit from the exceptional optical properties and substantial light absorption capacity of perovskite materials. This could lead to a more compatible approach with IPL processes, which present a multitude of alternatives to traditional thermal methods. The benefit of utilizing the PC method for perovskite is that it can quickly sinter vast areas at high temperatures in a short period without altering the substrate's composition, and it can be completely processed under ambient conditions. Studies indicate that the efficiency of PSC increases as the annealing temperature increases until 150 °C. Beyond this temperature, perovskite decomposes into $PbI_2$ Lavery, Kumari, Konermann, Draper, Spurgeon & Druffel (2016). The IPL can reach temperatures high enough to induce a phase transition, but no degradation occurred, because the rate of thermal response was too rapid Ghahremani *et al.* (2019). The improved quality of perovskite films depends on precise control of energy density and pulse duration to eliminate morphological defects, such as cracks or pinholes, in order to minimize series resistance and the possibility of charge recombination in PSC Ghahremani *et al.* (2019); Qiu, He, Yang, Deng & Peng (2016). This review will examine how energy density and pulse duration affect crystallization, microstructure, and topography and thereby influence PSC performance. The optimal approach for perovskite crystallization using pulsed light involves setting one parameter, either pulse duration or energy, and adjusting the other to determine the zones where the films are partially converted, fully converted, or degraded, based on SEM, XRD or absorbance characterization. This leads to two graphs, temperature vs. time or energy density vs. pulse duration, as displayed in Figure 3.5(a,b) Sanchez, Hua, Phung, Steiner & Abate (2018); Xu *et al.* (2020a). In both methods, increasing the energy density for PC or the pulse duration for FIRA leads to a rise in the annealing temperature. This phenomenon can produce partially converted perovskites due to the presence of the solvent, fully converted perovskites when the annealing temperature is optimized with the boiling point of the solvent, or overconverted

perovskites due to MAI evaporation at high temperatures, resulting in the thermal degradation of the perovskite. Figure 3.5(c,d) depict SEM images of perovskite films treated with both thermal and photonic annealing processes. The results show that for both PC and FIRA, an increase in energy density or pulse duration leads to an increase in grain size. In the case of FIRA 1.3s Figure 3.5c, individual domains are separated by regions that are likely non-crystalline. However, pulse durations of 1.7 and 3 seconds cause increases in grain size, leading to large crystalline domains with no pinhole in the perovskite films. This can be attributed to the much slower nucleation. Increasing either the energy density (20 ms HI sample, Figure 3.5c or the impulse time (FIRA 4s sample, Figure 3.5d results in film degradation, causing structural defects like cracks and voids. The energy induced in the film must be precisely controlled to enable the complete crystallization of the film without causing perovskite degradation Sanchez *et al.* (2018). At the optimum energy densities and pulse durations for PC and FIRA, respectively, the film quality is comparable to or better than that of TA control films. The growth temperature's control has a structural impact on the final crystal Nayak, Moore, Wenger, Nayak, Haghighirad, Fineberg, Noel, Reid, Rumbles & Kukura (2016). The pulse length and energy density are critical factors in controlling the nucleation density, which is imperative for enhancing the performance of PSCs.

Producing high-quality perovskite films in ambient conditions requires a precise precursor chemistry treatment. Binders and surfactants can improve film topography, but they can also leave organic residues that impair PSC performance. UV light, which is part of the IPL spectrum, can decompose these residues. In this section, we present the effect of PC on perovskite with an additive on the performance of PSCs. The performance of perovskite solar cells (PSCs) is significantly enhanced by its improved morphology. Various studies have suggested utilizing additives, including polymers, organic precursors, and alkyl halides, to enhance the morphology of perovskite films Ankireddy, Ghahremani, Martin, Gupta & Druffel (2018). Adding diiodomethane ($CH_2I_2$) or diidooctane to the perovskite formulation enhances device efficiency. $CH_2I_2$ decomposes into $I^-$ and $CH_2I^+$ when irradiated with ultraviolet (UV) light Ghahremani *et al.* (2019). Including iodine in the photonic annealing of perovskite should improve film quality by improving surface coverage, filling iodine vacancies in the crystal

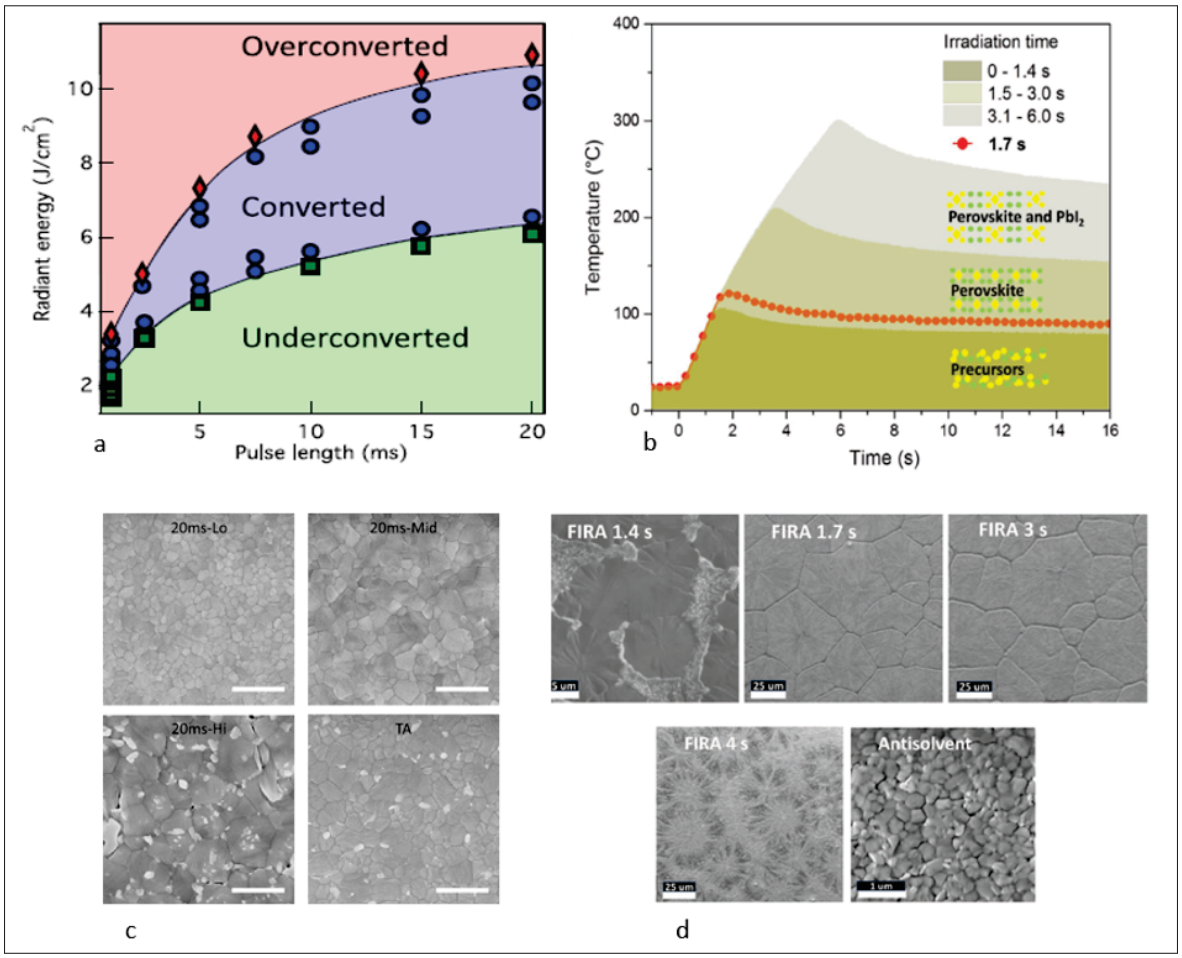


FIGURE 3.5 The three zones of perovskite crystallization can be defined through two methods : (**a**) PC, where the pulse duration is fixed and the energy density is varied from Xu *et al.* (2020a) ; (**b**) Flash Infrared Annealing (FIRA), where the energy density is fixed while the pulse duration is varied Sanchez *et al.* (2018). SEM images for thermal and photonic annealing, respectively, for (**c**) PC with increased energy density from Xu *et al.* (2020a) ; (**d**) FIRA with increased pulse duration from Sanchez *et al.* (2018)

lattice, reducing roughness, and promoting uniform crystallites with growth orientations aligned compared to the film without, $CH_2I_2$ Ghahremani *et al.* (2019) ; Liang, Liao, Chueh, Zuo, Williams, Xin, Lin & Jen (2014), thus improving device performance. SEM images (Figure 3.6A, B, F–H) reveal a surface that is filled without any holes and with larger grains for the $CH_2I_2$-treated films. The Nyquist diagram provides an overview of the film's electrical properties, including changes in impedance or conductivity due to PC and the presence of $CH_2I_2$. Figures 3.6(C,D) demonstrate that at high frequencies, the series resistance, which can be deduced from

the shift of the first semicircle, is smaller for the film with $CH_2I_2$ Matacena (2019). Moreover, in the low-frequency region, the second semicircle is wider, suggesting a higher recombination resistance Ankireddy *et al.* (2018). This indicates slower charge carrier recombination, better charge separation, and reduced losses Kay, Riley, Meredith, Armin & Sandberg (2024). This implies that the addition of diiodomethane has improved the quality and reduced the defect density of the perovskite film.

Tableau 3.4 Photovoltaic parameters for perovskite devices fabricated by PC

| **Year** | **Jsc** ($mA.cm^{-}2$) | $V_{oc}$**(V)** | **FF (%)** | **PCE (%)** | **Ref** |
|---|---|---|---|---|---|
| 2015 | 15.36 | 1.01 | 64.3 | 10 | Troughton *et al.* (2015) |
| 2016 | 16.55 | 1.02 | 69 | 11.5 | Lavery *et al.* (2016) |
| 2016 | 16 | 1.06 | 67 | 11.27 | Troughton *et al.* (2016) |
| 2018 | 22.7 | 1.11 | 74 | 19 | Sanchez *et al.* (2018) |
| 2018 | 20.7 | 0.97 | 62 | 12.6 | Hilt *et al.* (2018) |
| 2022 | 19.37 | 1.05 | 73.4 | 15.04 | Xu *et al.* (2022) |
| 2022 | 18.44 | 0.94 | 65.9 | 11.34 | Kim *et al.* (2022) |

The EDX technique (Figure 3.6I) confirms a deficiency of iodine ions in the PC of the perovskite films compared to those annealed by TA and PC+$CH_2I_2$. However, the PC promotes photolysis, decomposing $CH_2I_2$, which fills the holes and improves the crystallinity of the perovskite films. The addition of $CH_2I_2$ promoted vertical grain growth, reduced series resistance, and improved PCE from 11.86 % to 15.04 %, which is similar to the TA device of 15.81 % Xu *et al.* (2022). This study supports previous findings indicating that the use of alkyl-halide additives during the photonic curing process improves interactions between the perovskite precursor and solvent, leading to better surface coverage and higher PCE Ghahremani *et al.* (2020). Figure 3.6J illustrates the evolution of PC perovskite device performance compared to TA over almost a decade of development progress. The data reveal a substantial improvement in the performance of PC devices compared to those utilizing TA. The reduction in PCE gap between TA and PC can be attributed to the enhanced mastery of this technique and a better understanding of the crystallization dynamics induced by PC in recent years. Furthermore, PC technology offers significant opportunities and many advantages over TA. The most notable advantages are the shorter processing time and compatibility with low-heat-tolerant Piper *et al.* (2021), transparent

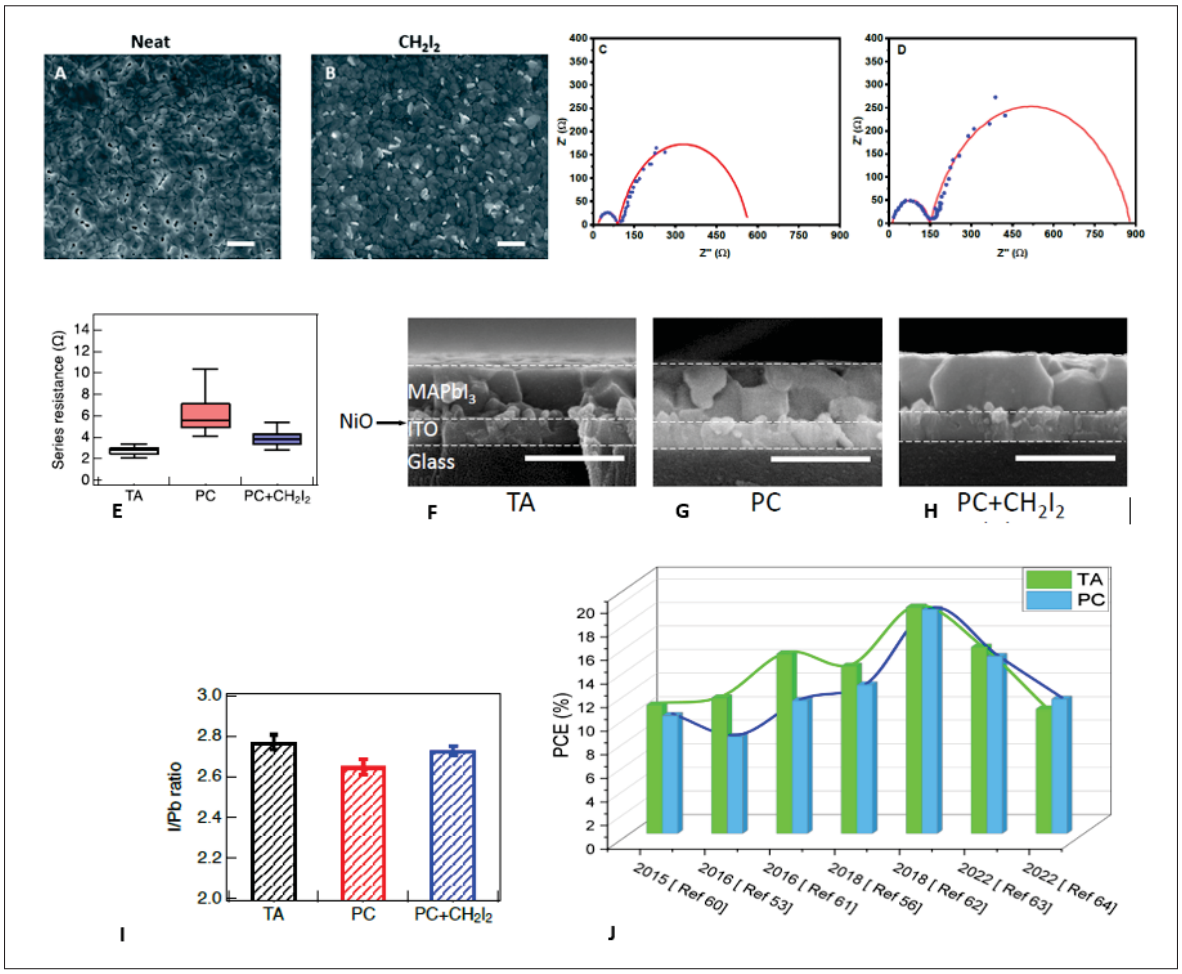


FIGURE 3.6 SEM images of photonic annealing of perovskite films : (**A**) neat, (**B**)+ additive $CH_2I_2$, (**C**,**D**) Nyquist plots for films without and with $CH_2I_2$Ankireddy *et al.* (2018). (**E**) Series resistance of devices annealed using a thermal annealing, PC, and PC with $CH_2I_2$ additive and (**F**–**H**) SEM cross-section images of devices annealed using TA, PC, or PC with $CH_2I_2$ additiveXu *et al.* (2022). (**I**) Comparison of I and Pb ratios in TA, PC, and PC+$CH_2I_2$ films utilizing the EDS technique fromXu *et al.* (2022). (**J**) PCE comparison for PC and TA since 2015 from (Hilt *et al.* (2018) ; Kim *et al.* (2022) ; Lavery *et al.* (2016) ; Sanchez *et al.* (2018) ; Troughton *et al.* (2015,1) ; Xu *et al.* (2022)) and data from Table 3.4

substrates, as shown in Table 3.5. This suggests that PC annealing will outperform traditional techniques in the near future.

PC significantly impacts the conversion of perovskite from the precursor to the crystalline phase. PC affects the optical, crystalline, and morphological properties of the films Xu *et al.*

Tableau 3.5 Advantages and disadvantages of PC and TA

| Aspect | PC | TA | Ref |
|---|---|---|---|
| **Advantages** | | | |
| Speed processing | Rapid (ms-s) | Longer (min-h) | de Boode *et al.* (2022) |
| Heat exposure reduction | Significantly reduces | High temperature requierd | Chatterjee *et al.* (2022) ; NovaCentrix (2024) |
| Heat sensitive substrat | Minimal risk | Potentiel risk | NovaCentrix (2024) |
| Temperature control | More presice | Must be carfully regulated to avoid damage | Wu (2017) |
| Selective processing | Yes | No | Garlapati *et al.* (2018) |
| Equilibrated heating | No | Yes | Xu *et al.* (2020a) |
| **Disadvantages** | | | |
| Initial cost | Higher due to specialized equipment | Lower | Schroder (2011) |
| Process complexity | May require additional technical expertise | Process may be simpler | |

(2020a). Notably, PC reduces surface bulk defects and enhances light absorption, resulting in denser films and influencing the performance of PSCs Gamal, Gamal, Okaz, Shehata & Kandas (2024) ; Xu *et al.* (2020a). Other studies also highlight PC's role in defect mitigation and absorption enhancement Serafini, Boix, Barea, Edvinson, Sánchez & Mora-Seró (2022). Bulk defect attenuation improves the crystallinity and stability, as well as the alignment of energy levels, enabling efficient charge extraction Iqbal, Zu, Musiienko, Gutierrez-Partida, Kobler, Gries, Sannino, Canil, Koch, Stolterfoht & others (2023). Furthermore, a recent study has shown that the incorporation of one- and two-dimensional halide perovskites as novel passivants enhances the performance of perovskite solar cells Zhao, Xiang, Ran, Zhou, Wang & Shao (2023). The integration of these perovskites into the serigraphy process Song (2022), combined with photonic annealing, has great potential for large-scale industrial applications.

The progress of perovskite-based solar cells has been significant, in part due to advancements in photonic processing Wang, Cui, Hou, Zhu, Yan & Su (2016). In addition to work on transport layers and electronic contacts, techniques such as encapsulation Xu, Xia, Gao, Wang, Zhu, Xiong, Yuan & Ding (2023c), efficient surface nanostructuring Li & Ning (2024), and optimized light management have improved both the efficiency and stability of perovskite-based cells Jiang, Wang, Li, Yu, Wang & Tan (2024). These advances pave the way for more efficient, durable, and economically viable perovskite devices.

## 3.5 Conclusion

This paper presents a literature review on the rapid annealing of HTL (NiOx), ETL ($SnO_2$ and $TiO_2$), and photoactive perovskite layers under ambient conditions. The photonic annealing of perovskite and ETL/FTL layers, which require high temperatures, enabled rapid sintering in the order of milliseconds with photovoltaic performance comparable to standard techniques. The addition of $CH_2I_2$ has been shown to enhance the formation of perovskite morphology with larger grains by releasing iodine during the PC processes. This approach provides significant advantages for quick, cost-effective, R2R production. The integration of photonic curing techniques into PSCs has led to a notable enhancement in efficiency and performance, as evidenced by the refinement of morphology, crystallinity, and interface quality. However, challenges remain, including the complexity of experimentation for optimal curing and the limitations of material compatibility. The precise control of parameters such as energy density and duration is crucial to prevent the damage of layers. Further investigations are necessary to comprehend and explore the science and dynamics of thin film crystallization, as well as to extend the PC process to diverse materials for various perovskite solar cell (PSC) configurations and other applications. In summary, the evolution of PC has considerably enhanced the understanding of curing parameters, expanded its applicability to different substrates, improved control of layer morphology, and integrated it into manufacturing processes more effectively. These advances position PC as a fascinating tool in the process of perovskite solar cell manufacturing, offering substantial benefits for device efficiency and stability.

## Funding

The authors would like to acknowledge the financial support received from NSERC with the following Discovery grants (RGPIN-2023-05211, RGPIN 2022-03083) as well as the Canada Research Chairs (CRC-2021-00490).

## Author Contributions

Writing—original draft, M.A.S. Review and editing, S.G.C. and R.I. All authors have read and agreed to the published version of the manuscript.

## Conflicts of interest

The authors declare no conflicts of interest.

## Abbreviations

The following abbreviations are used in this manuscript :

| | |
|---|---|
| PSCs | Perovskite solar cells |
| PC | Photonic curing |
| TA | Thermal annealing |
| FA | Furnace annealing |
| ETL | Electron transport layer |
| HTL | Hole transport layer |

# CHAPITRE 4

## IMPACT OF RESIDUAL STRAINS ON THE CARRIER MOBILITY AND STABILITY IN PEROVSKITE FILMS

Moulay Ahmed Slimani[1], Luis Felipe Gerlein[1], Ricardo Izquierdo[1], Sylvain G. Cloutier[1]

[1] Département de Génie Électrique, École de Technologie Supérieure,
1100 Rue Notre-Dame Ouest, Montréal, Québec, H3C 1K3, Canada

Article publié dans la revue
« MDPI nanomaterials »
le 03 Aout 2024.
https://doi.org/10.3390/nano14151310

**Résumé :** Les pérovskites d'halogénures inorganiques et organiques en solution présentent un grand intérêt pour les chercheurs en raison de leurs propriétés optoélectroniques uniques et de leur facilité de traitement. Cependant, les films de pérovskite polycristallins présentent souvent une inhomogénéité due à la déformation résiduelle induite pendant la phase de post-traitement du film. Ces déformations peuvent avoir un impact sur leur stabilité et leurs performances. Une étude exhaustive des déformations résiduelles peut permettre de mieux comprendre et contrôler la manière dont elles affectent les performances et la stabilité des films de pérovskite. Dans ce travail, nous explorons cette relation complexe entre les déformations résiduelles et les propriétés électriques des films de méthylammonium $CH_3NH_3PbI_{3-x}Cl_x$ en utilisant la diffraction des rayons X à incidence rasante (GIXRD). Nous corrélons leur résistivité et la mobilité des porteurs en utilisant l'effet Hall. La technique $\sin^2(\psi)$ est utilisée pour optimiser les paramètres de recuit des films de pérovskite. Nous établissons également que la relaxation induite par la température peut entraîner une amélioration significative du transport des porteurs de charge dans les films de pérovskite. Enfin, nous utilisons la microspectroscopie Raman pour évaluer la dégradation des films de pérovskite en fonction de leurs contraintes résiduelles.

**Abstract :** Solution-based inorganic–organic halide perovskites are of great interest to researchers because of their unique optoelectronic properties and easy processing. However, polycrystalline perovskite films often show inhomogeneity due to residual strain induced during the film's post-processing phase. In turn, these strains can impact both their stability and performance. An exhaustive study of residual strains can provide a better understanding and control of how they affect the performance and stability of perovskite films. In this work, we explore this complex interrelationship between residual strains and electrical properties for methylammonium $CH_3NH_3PbI_{3-x}Cl_x$ films using grazing incidence X-ray diffraction (GIXRD). We correlate their resistivity and carrier mobility using the Hall effect. The $\sin^2(\psi)$ technique is used to optimize the annealing parameters for the perovskite films. We also establish that temperature-induced relaxation can yield a significant enhancement of the charge carrier transports in perovskite films. Finally, we also use Raman micro-spectroscopy to assess the degradation of perovskite films as a function of their residual strains.

**Keywords :** Williamson Hall ; GIXRD ; $CH_3NH_3PbI_{3-x}Cl_x$ ; Hall effect ; Raman

## 4.1 Introduction

Perovskite is a promising material with unique optical and electrical properties Rong, Hu, Mei, Tan, Saidaminov, Seok, McGehee, Sargent & Han (2018). However, it can be very sensitive to environmental factors, including humidity, oxygen, and heat Kim, Seo & Park (2016) ; Liu, Yang, Li, Xue & Hu (2020). These can make the perovskites unstable and limit their integration into commercial devices. Recently, reports have suggested that stability enhancement could be achieved by the release of residual strains Wang, Zhu, Liu, Ma, Liu, Wu, Shi, Du, Hao & Xiang (2019). Although residual strains are well known, the first studies on strains in perovskites were reported less than a decade ago Wu, Liu, Li, Wang, Xue, Lin & Hu (2021). The problems associated with residual strains and their impact on material and device stability remain an active research field Grote & Berger (2015). In time, this deeper understanding could translate into a significant improvement in perovskite devices. In this work, we use thermally-induced strain release to explore the origin of residual strains in perovskite films and their impact on their electrical and optical properties, as well as their stability.

### 4.1.1 Stress Origin in Perovskite Films

Generally, stresses in perovskite films mainly have three origins : intrinsic, mechanical, and thermal Hutchinson (1996). Because of the polycrystalline and heterogeneous nature of perovskite films, residual strains can stem from macroscopic, mesoscopic, or microscopic deformations Peng (2006) ; Tennyson, Doherty & Stranks (2019). Residual strains in thin films are usually the consequence of thermal stresses or other external conditions occurring during grain coalescence or growth Abadias, Chason, Keckes, Sebastiani, Thompson, Barthel, Doll, Murray, Stoessel & Martinu (2018) ; Wang *et al.* (2019). Indeed, it is largely due to the coefficient of thermal expansion (CTE) and lattice offset between the film and substrate Namvar, Dehghany, Sohrabpour & Naghdabadi (2016) ; Wu *et al.* (2021). These stresses can modify the structure of the crystal lattice and consequently impact the mobility of charge carriers, the band gap, and the stability of the film Lee, Deng, Bristowe, Bristowe & Cheetham (2018) ; Rolston, Bush, Printz, Gold-Parker, Ding, Toney, McGehee & Dauskardt (2018). Kay *et al.* (2024)

### 4.1.2 Impact on Electrical, Optical Properties and Stability

Recently, perovskite-based solar cells (PSCs) have achieved a certified efficiency of 26.1% Zhang, Li, Zhang, Li, Zuo, Odunmbaku, Chen, Chen, Zhang, Li & others (2023). However, instability remains the main factor limiting their large-scale commercialization Mohammad & Mahjabeen (2023). Efforts were made to reduce the moisture sensitivity of perovskite materials and improve the chemical stability of the electron and hole transport layers Hu, Chen, Yang, Li, Zhou, Larson, Johnson, Lu, Zhong & Xu (2020b); Rong, Hou, Hu, Mei, Liu, Wang & Han (2017). Strains can cause distortion of the crystal structure of perovskite materials Lei, Liu, Li, Da, Zheng, Wu & Ran (2024); Wang *et al.* (2019). Band structure calculations suggest that the band gap increases as the strain changes from compressive to tensile Zhu, Niu, Fu, Li, Hu, Chen, He, Na, Liu, Zai, Ge, Lu, Ke, Bai, Yang, Chen, Li, Sui, Zhang, Zhou & Chen (2019). Small lattice strains in perovskite thin films can have major consequences for carrier recombination, electronic band structure, crystallinity, and crystal phase stability Jones, Osherov, Alsari, Sponseller, Duck, Jung, Settens, Niroui, Brenes & Stan (2019b); Qiao, Fang, Long & Prezhdo (2021); Wang, Hu, Wang, Cui, Chen, Niu & Hao (2022a). The bandgap variations due to strains can result in a change in the absorption spectrum of the perovskite film Wu *et al.* (2021). The presence of surface defects and grain boundaries in perovskite films also creates trap states, impacting their stability Zheng, Chen, Dai, Fang, Bai, Lin, Wei, Zeng & Huang (2017). It is also well known that strains can weaken the bonds and increase the defect density and degradation in perovskite films Ghosh, Aziz, Dawson, Walker & Islam (2019); Rolston *et al.* (2018); Steele, Jin, Dovgaliuk, Berger, Braeckevelt, Yuan, Martin, Solano, Lejaeghere & Rogge (2019).

### 4.1.3 Regulation of Strain in Perovskite Films

Residual strains in perovskite films can affect their physical, optical, and electrical properties and impact their stability Jin, Cao, Yuan, Cai, Wu & Zheng (2023). In turn, releasing residual strains in perovskite films could potentially be used to controllably improve their properties or stability. Several techniques can be used to release strains, including (1) regulation of local strains through synthesis, (2) stress release by thermal expansion, or (3) adjusting the lattice offset between film

and substrate Wu *et al.* (2021). It has been established that the intrinsic instability of perovskite films can result from annealing-induced residual strain accelerating their degradation Rolston *et al.* (2018); Zhao, Deng, Wei, Zheng, Yu, Shao, Shield & Huang (2017). This work will focus exclusively on the temperature-induced strain relaxation of methylammonium lead halide perovskite films in order to improve their optical and electrical properties and increase their stability. A comprehensive study of how residual strain impacts the electrical properties of perovskite films can be conducted using the Williamson-Hall plot, Grazing Incidence X-ray Diffraction (GIXRD), Hall effect measurements, and Raman spectroscopy. The Williamson-Hall plot quantifies strain by analyzing the broadening of X-ray diffraction peaks. GIXRD provides detailed structural information about surface layers, phase analysis, degree of crystallinity, texture, and depth profiling, revealing the strain distribution Pandey, Dalal, Dutta & Dixit (2021). Hall effect measurements determine carrier concentration and mobility, showing how strain affects electrical conductivity. Raman spectroscopy detects changes in lattice vibrations due to strain, offering insights into the correlation between lattice dynamics and electronic structure. Together, these techniques elucidate the influence of residual strain on both the structural and electrical properties of perovskite films, guiding their optimization for enhanced performance. Our findings indicate that achieving temperature-induced relaxation requires annealing within the temperature range of 75 to 85 °C to achieve a high carrier mobility, low activation energy, high mean free path, and improved stability. We also find that this optimized annealing process reduces defect density.

## 4.2 Experimental Section

Glass substrates (25 mm × 25 mm) were cleaned sequentially with acetone, isopropanol, and DI solution for 15 min each. Perovskite layers were prepared with commercial $CH_3NH_3PbI_{3-x}Cl_x$ ink from Ossila, Sheffield, UK (used as received). The films were deposited on the substrates by spin-coating at 2000 rpm for 30 s (the ink quantity used per film is 70 µL). The resulting films are annealed on a hot plate for 2 h at different temperatures, ranging from 50 °C to 110 °C. The residual strains are characterized using XRD. Hall-effect measurements are used for carrier

mobility. Finally, UV-Vis absorption and Raman micro-spectroscopy are used to assess perovskite film degradation. Raman characterization was done using a WITec Alpha 300 confocal Raman microscope (Ulm, Germany) equipped with a continuous-wave 60 mW laser emitting at 532 nm whose power output was attenuated mechanically. XRD was done using a Bruker D8 Advance (Billerica, MA, USA), equipped with a Cu source. SEM imaging was done using a SU8230 from Itachi (Tokyo, Japan). Optical absorbance was done using a UV-VIS-NIR spectrophotometer by Perkin Elmer (Waltham, MA, USA), model Lambda 750, with an integrating sphere. The Hall effect measurement was done using a Room-Temperature Hall Effect system fabricated by TeachSpin (Buffalo, NY, USA), which uses a permanent magnet that generates fields of about 0.7 T to create the Hall effect. The system is designed to accommodate TeachSpin sample holders, which are printed circuit boards. The perovskite film was deposited on the sample board, which was then mounted on the device chassis and connected to a DC power source, allowing current to flow along the perovskite sample under the effect of the permanent magnetic field, enabling Hall voltage measurement.

## 4.3 Results and Discussion

In Figure 4.1, characterization of the films by X-ray diffraction (XRD) confirms the crystallization of a sample in a perovskite structure, with the presence of the standard peaks associated with the (110), (220), and (330) reflection planes, respectively. The peak intensity at 14° suggests that the main orientation of the perovskite film is (110) Głowienka, Miruszewski & Szmytkowski (2018). XRD is also useful to characterize the residual strains through the lattice parameters. Indeed, the tensile or compressive strains can be respectively associated with the shift of the peaks to lower or higher diffraction angles. Residual strains are often non-uniform and complex to analyze from the peak position alone. Another indicator of strain is the broadening of the XRD peaks compared to the fully relaxed state Zak, Majid, Abrishami & Yousefi (2011); Zhu *et al.* (2019).

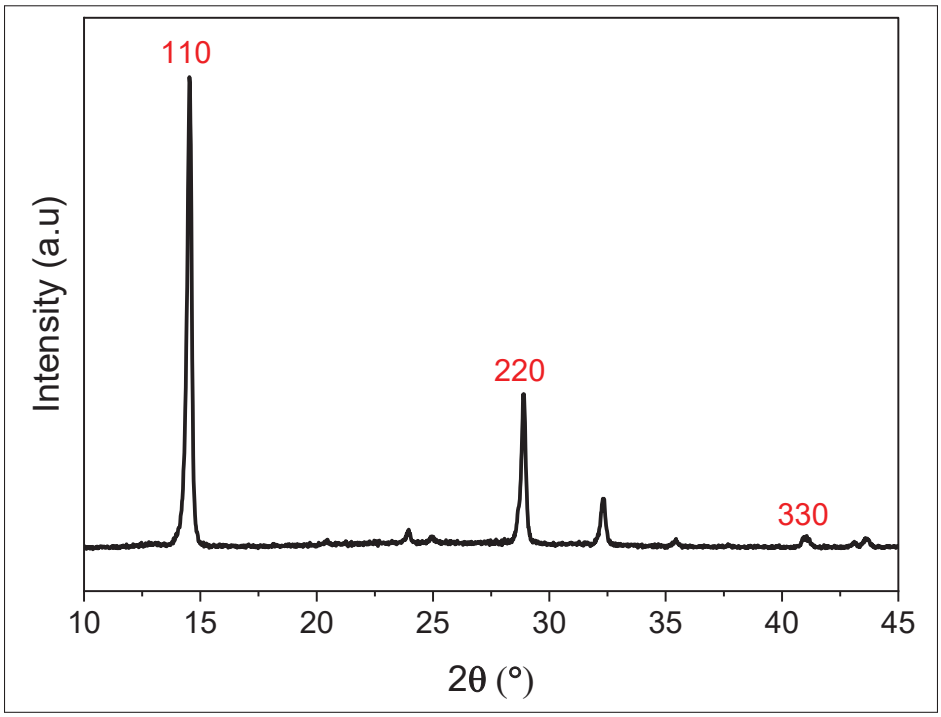


FIGURE 4.1 XRD spectra of perovskite film annealed at 80 °C

### 4.3.1 Williamson Hall Characterization

The Williamson Hall (W-H) analysis, described by Equation (4.1) can be used to quantify the strain-induced broadening of the XRD peaks resulting from crystal imperfections Hall (1949); Mote *et al.* (2012); Nishimura, Hirotani, Kamarudin, Shen, Toyoda, Iikubo, Minemoto, Yoshino & Hayase (2019), and the structural imperfections such as dislocations, vacancies and stacking defects Pramanick, Wang, Hoffmann, Diallo, Jørgensen & Wang (2015); Robinson & Harder (2009) :

$$\beta_{hkl} \cdot cos\Theta_{hkl} = k\frac{\lambda}{D} + 4\varepsilon \cdot sin\Theta_{hkl} \tag{4.1}$$

where $\beta_{hkl}$ is full width at half maximum (FWHM) of the XRD peak, k is the Scherrer constant equal to 0.94, $\lambda$ is the X-ray source wavelength, D is the crystallite size, $\theta_{hkl}$ is the peak position (°) and $\epsilon$ is the strain. The fundamental difference between W-H's method and Scherrer's method is that W-H considers both the crystallite size and microstrains which are often interrelated.

The Williamson-Hall plot in Figure 4.2(a) show the $\cos\theta_{hkl}$ vs $4\sin\theta_{hkl}$ evolution measured from $CH_3NH_3PbI_{3-x}Cl_x$ films annealed at 25, 50, 70, 80, 90 and 110 °C. The residual strain can be calculated directly from the slope for each curve fitting. In Figure 4.2(b), the strain values calculated reveal an interesting trend. It starts with a relatively high compressive strain at low annealing temperatures, below 40 °C. The residual strains decrease as the annealing temperature increases to 70 °C. Over 90 °C, the residual strains become increasingly tensile. We can conclude from this first test that the annealing temperature can generate three types of strain : compressive, tensile, and a relaxed strain at a temperature around 80 °C. Based on our observations, we can expect improved performance from the perovskite film.

It is important to note that a full profile analysis, which involves a comprehensive examination of all aspects of the diffraction data -including peak shapes, positions, and asymmetry factors- a more robust approach than the Williamson-Hall method presented in this manuscript. The Williamson-Hall method often simplifies certain aspects of the analysis by focusing on the broadening of diffraction peaks to estimate deformations and crystallite sizes. For this reason, we will be combining GIXRD analysis with Williamson-Hall analysis to confirm residual strain trends in perovskite films, validate the results obtained, and overcome the limitations and potential inconsistencies of the Williamson-Hall method.

### 4.3.2 Gixrd Characterization

Grazing incidence XRD is a very useful technique to characterize the structure of thin films. It can also directly probe the strain distribution in perovskite films Wu *et al.* (2021). As such, we can use GIXRD to analyze the variations in the in-plane residual strains for the perovskite films annealed at different temperatures. The measurements shown in Figure 4.3a are performed in the $\omega$-mode Song (2010) ; Wu *et al.* (2021), by fixing the angle $\theta_{hkl}$ and varying the instrument's tilt angle $\psi$.

In Figure 4.3(b,c), we analyze the strains in perovskite films annealed at 50, 70, 80, 90, and 110 °C using GIXRD. Figure 4.3b illustrates the plot of $2\theta$ vs. $\sin^2(\phi)$, where the slope of the

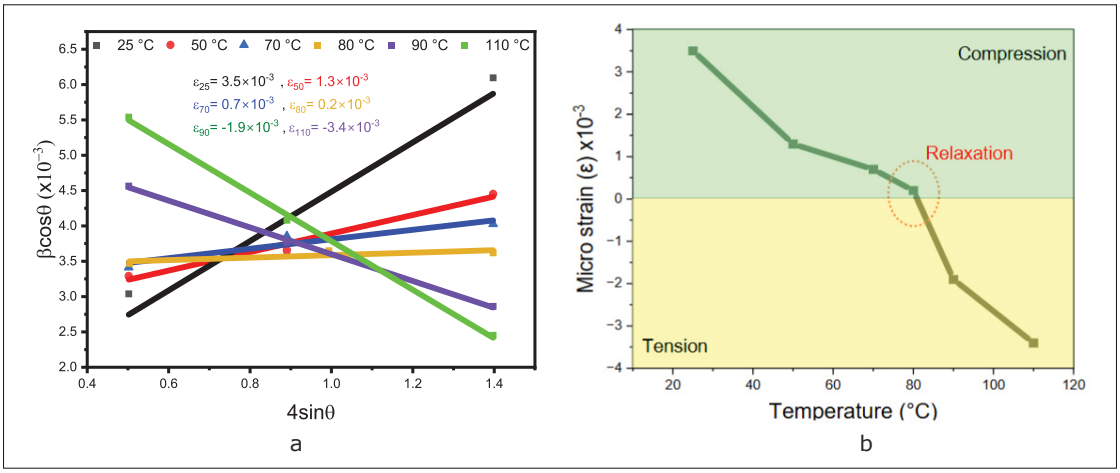


FIGURE 4.2 (a) Williamson-Hall plotfrom which the value of micro-strain was estimated for perovskite films annealed at 50, 70, 80, 90, and 110 °C, (b) Residual strain extracted from the slope of the plots in (a) using Equation (4.1)

fitted curves yields the strain coefficients. A negative slope suggests tensile strains, while a positive slope suggests compressive strains. Figure 4.3(d–h) clearly illustrates the distribution of compressive and tensile strain gradients for annealing temperatures from 50 to 110 °C, respectively. While thermal energy can cause significant strain levels in the crystal lattice, it should be noted that the perovskite crystal structure still remains thermally stable between 50 °C and 110 °C Murali, Yengel, Peng, Chen, Alias, Alarousu, Ooi, Burlakov, Goriely & Eddaoudi (2017). These GIXRD strain measurements are consistent and strongly support the W-H results presented in Figure 4.2. In Figure 4.3, residual strains appear compressive at temperatures below 70 °C and tensile at temperatures above 90 °C. We can infer that strain relaxation can be achieved between 75 and 85 °C. Based on the W-H XRD and GIXRD analysis, we concur that $CH_3NH_3PbI_{3-x}Cl_x$ has a relaxed cubic structure when annelaed at 80 ± 5 °C (At 80 °C and up, the mixed crystals of perovskite transform from tetragonal to cubic phase), and this relaxed symmetrical structure is favorable to improved electrical properties Francisco-López, Charles, Alonso, Garriga, Campoy-Quiles, Weller & Goñi (2020); Murali *et al.* (2017).

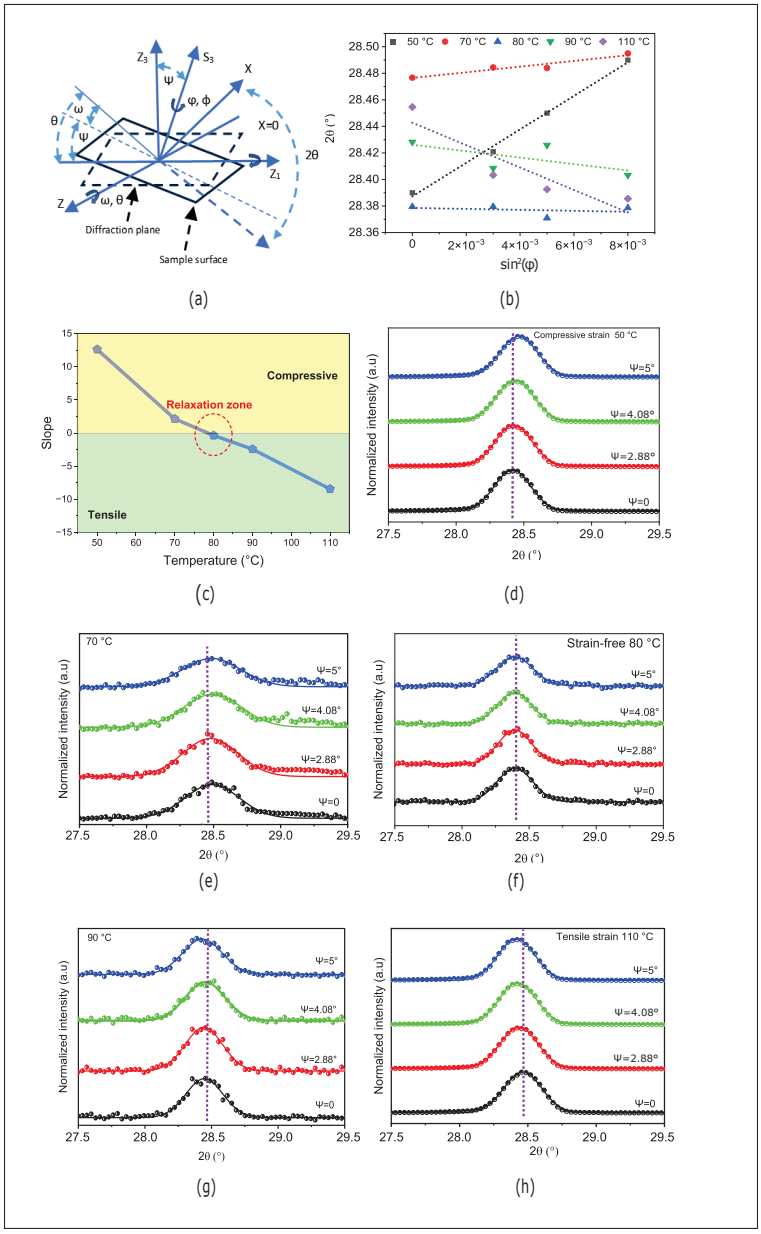


FIGURE 4.3 (a) Schematic of the strain measurement using GIXRD in the $\omega$-mode, where $Z_3$ is normal to the diffraction plane, $S_3$ is normal to the sample surface and $\psi$ is the instrument's tilt angle. (b) $2\theta$ vs $\sin^2(\phi)$ from which the value of micro-strain was estimated of the perovskite films annealed at 50, 70, 80, 90 and 110 °C. (c) Strain coefficients extracted from the GIXRD slope. (d,e) Compressively-strained films annealed below 80 °C. (f) strain-free film (g, h) Tensile-strained films annealed above 80 °C

### 4.3.3 SEM Characterization

SEM analysis can be used to examine the change in granularity and microstructure caused by the residual strains. Distortions and internal strains can arise from the growth of superstructures and nanostructures, as well as from substitutions with elements of different sizes Grote & Berger (2015). Figures 4.4(a–e) show SEM micrographs of the perovskite films after annealing at 50, 70, 80, 90, and 110 °C, respectively. The grain size evolution indicates that grains appear at 50 °C (Figure 4.4a). The presence of solvents in the precursor leads to high pinhole densities due to minimal evaporation. Increasing the annealing temperature reduces pinhole density and increases the average grain size Ren, Yang, Yang, Zhang, Cui, Liu, Wei, Fan & Liu (2016). The maximum average size of 795 nm is achieved with 80 °C annealing (Figure 4.2h). At 90 °C and above, microstructural changes (grain size and surface filing) start to appear (Figures 4.4(d,i)). These strain-induced alterations in the perovskite film's granularity and microstructure could potentially compromise its stability and accelerate its degradation.

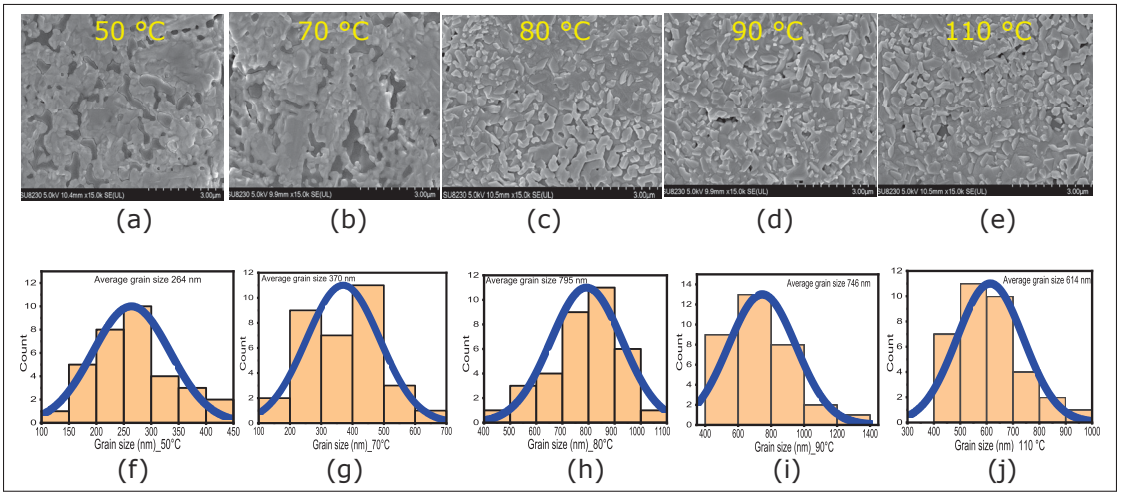


FIGURE 4.4 SEM micrographs for the perovskite films annealed (a) 50 °C, (b) 70 °C, (c) 80 °C, (d) 90 °C and (e) 110 °C. The scale bars correspond to 3 µm. (f-j) Grain size distributions extracted from the SEM images using ImageJ. The blue lines show the Gaussian distribution that describes the data

### 4.3.4 Hall effect characterization

Carrier mobility can be directly measured using the Hall-effect technique represented in Figure 4.5(a). Here, a transverse magnetic field of 0.7 T is applied to all samples. The applied magnetic field will induce a Lorentz force opposing the movement of charge carriers, separating holes from electrons and creating a potential difference, the Hall voltage ($V_H$). From this measurement, we can deduce the carrier density (n), Hall constant ($R_H$), charge carrier mobility ($\mu$), and resistivity ($\rho$), and charge carrier mobility ($\mu$) using the following expressions Bouras (2019) ; Choi, Paterson, Fusella, Panidi, Solomeshch, Tessler, Heeney, Cho, Anthopoulos, Rand & others (2020) :

$$V_H = \frac{B \cdot I}{q \cdot n \cdot d} \tag{4.2}$$

$$R_H = \frac{1}{q \cdot n} \tag{4.3}$$

$$\mu = \frac{V_H \cdot L}{W \cdot B \cdot V_r} \tag{4.4}$$

$$\rho = \frac{1}{n \cdot e \cdot \mu} \tag{4.5}$$

With B : magnetic induction, I : injected current, n : carrier concentration, q : carrier charge, W : perovskite sample width, L : its length, and d : its thickness.

In Figure 4.5(b), all samples display a p-type behavior indicated by the positive Hall voltage. This expected result can be explained by the large amounts of Pb, $CH_3NH_3I$, Cl vacancies and I present in the film Xie, Feng, Xiong, Chen, Liang, Abid & Xu (2021) ; Xiong, Hou, Zou, Lu, Yang,

Hao, Zhou, Xu, Zeng & Xiao (2021). Due to their lower formation energies, Pb and $CH_3NH_3$ vacancies are known to play a significant role in the p-type behavior of $CH_3NH_3PbI_{3-x}Cl_x$ thin films Frolova, Dremova & Troshin (2015); Karim, Khan & Hossain (2021); Wang, Shao, Xie, Lyu, Liu, Gao & Huang (2014); Yin, Shi & Yan (2014). Figure 4.5(c) shows the Hall effect results illustrating the corresponding change in carrier mobility and resistivity with increasing annealing temperatures. The carrier mobility reaches its highest value of 10 $cm^2\ V^{-1}\ s^{-1}$ at 80 °C, which is consistent with previous reports Luo, Yu, Wang, Zou, Luo, Liu & Lu (2015); Wehrenfennig, Eperon, Johnston, Snaith & Herz (2014). We already established that $CH_3NH_3PbI_{3-x}Cl_x$ films annealed at this temperature are strain-relaxed. Above 75 °C (relaxation zone), the structure adopts cubic symmetry and can achieve high stability since the entropy reduction in the inorganic cage compensates for the high dynamic disorder of the organic cations in methylammonium Francisco-López *et al.* (2020); Saffari, Mohebpour, Soleimani & Tagani (2017). This cubic phase is also known to offer better electronic properties than the orthorhombic and tetragonal phases for symmetry reasons Berdiyorov, Kachmar, El-Mellouhi, Carignano & El-Amine Madjet (2016a); Berdiyorov, Madjet, El-Mellouhi & Peeters (2016b); Leguy, Azarhoosh, Alonso, Campoy-Quiles, Weber, Yao, Bryant, Weller, Nelson & Walsh (2016).

The thermal behavior for the Hall mobility can be described by the expression Shan, Tong, Cao, Tang, Xu, Yu & Chen (2019) :

$$\mu_T(T) = \mu_0(T) \cdot exp\left(\frac{E_a}{k_B \cdot T}\right) \tag{4.6}$$

where, $\mu_0$ is the exponential prefactor, $k_B$ is the Boltzmann constant and $E_a$ is the activation energy. Figure 4.6(a) shows $ln(\mu_H)$ as a function of 1000/T measured between 25 and 110 °C. The activation energy $E_a$ corresponds to the potential energy barrier height Shan *et al.* (2019), and it can be directly extracted from the slope of the linear fit. From Figure 4.6(a), the activation energy for perovskite films with compressive strains is found to be 400 meV, while tensile strain reduces the activation energy to 50 meV. These results are also consistent with previous reports Brenner, Egger, Kronik, Hodes & Cahen (2016). This change in activation energy originates

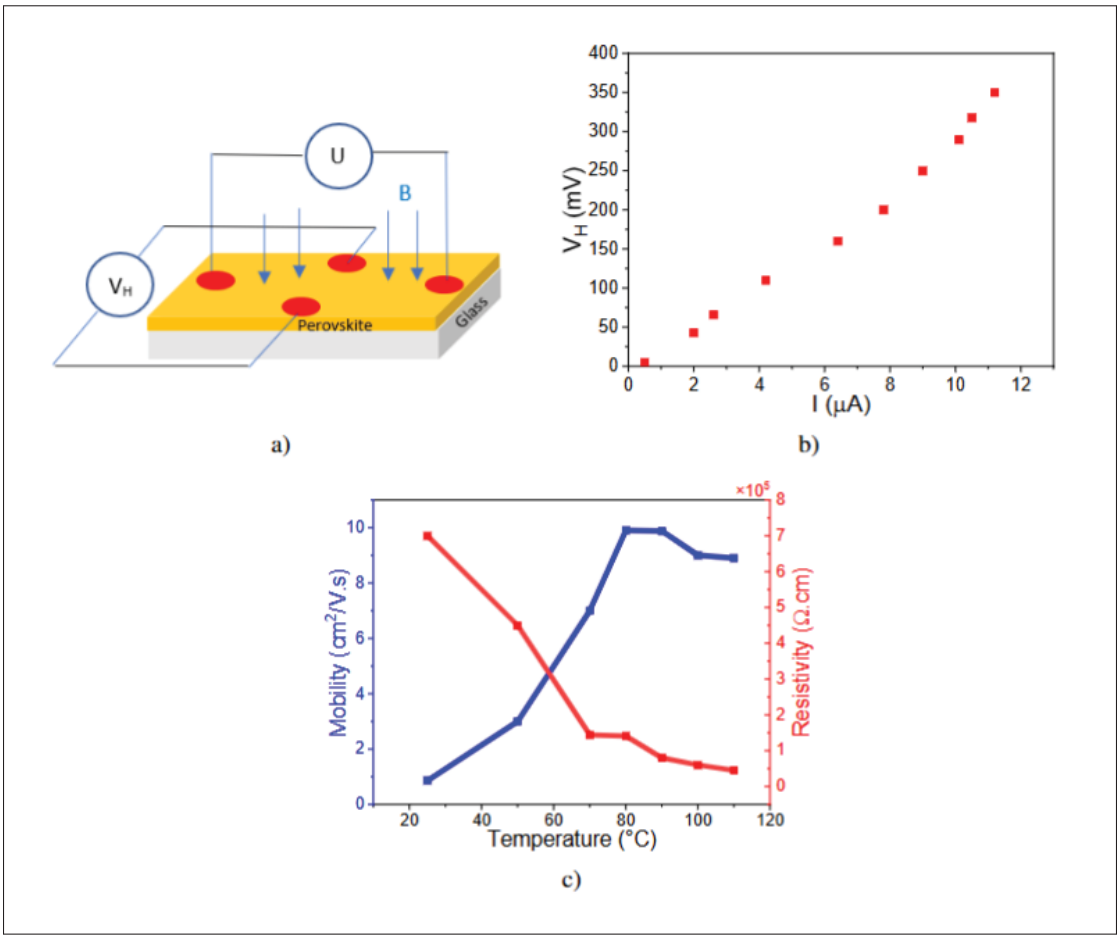


FIGURE 4.5 (a) Schematic of the Hall effect measurement setup. (b) Hall-voltage measured as a function of the current flowing through the device. (c) Resistivity and mobility values extracted from the Hall measurements for different annealing temperatures

from the slope at approximately 80°C, suggesting significantly-reduced activation energy due to film relaxation. It has been previously reported that $CH_3NH_3$ and $I^-$ vacancies can easily migrate to a neighboring site due to their low activation energy Eames, Frost, Barnes, O'regan, Walsh & Islam (2015). This variation of the activation energy with temperature can be directly associated with the film's residual strains Bhargava, Sharma, Kumar, Pandey & Kumar (2010).

Using the Hall mobility measurements from Figure 4.6(a), it becomes possible to access the mean carrier path length $L_m$ and the mean free time $\tau_m$, both represented in Figure 4.6(b), in the

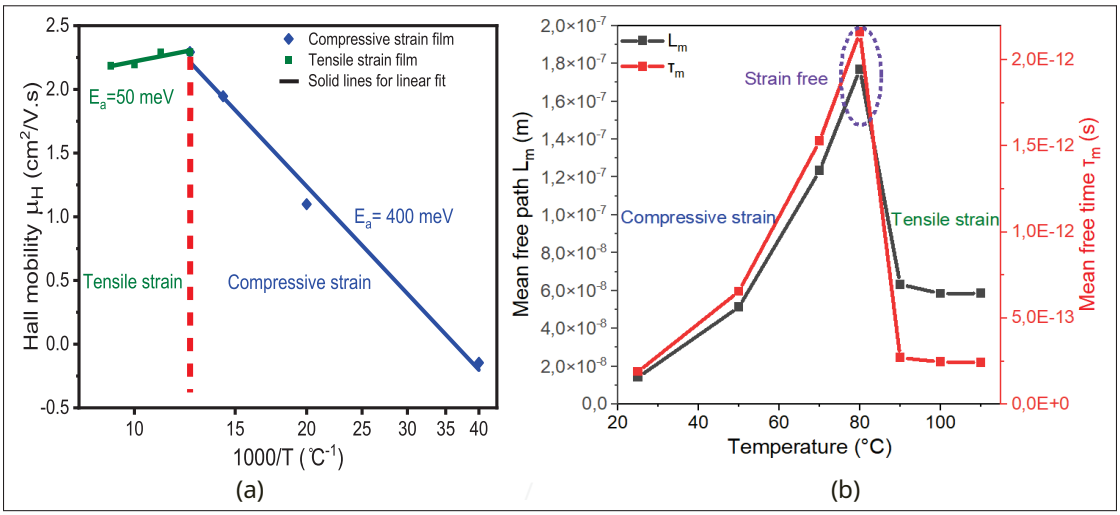


FIGURE 4.6 (a) Activation energy ($E_a$) and (b) Mean free path (Lm) and mean free time ($\tau_m$) for the $CH_3NH_3PbI_{3-x}Cl_x$ films as a function of their annealing temperature

$CH_3NH_3PbI_{3-x}Cl_x$ thin films using the conventional Drude-Sommerfeld model Karim *et al.* (2021) :

$$\mu_T(T) = \mu_0(T) \cdot exp\left(\frac{E_a}{k_B \cdot T}\right) \tag{4.7}$$

$$L_m = \mu_H \left(\frac{(3m_h^* \cdot k_B \cdot T)^2}{e}\right) \tag{4.8}$$

Where $m_h{}^*$ is the effective mass of the hole given by the expression :

$$E_a = \frac{e^4 \cdot m_h^*}{2(2\varepsilon_0 \cdot \varepsilon_r \cdot h)^2} \tag{4.9}$$

Where $\epsilon_0$ is the permittivity of free space, and $\epsilon_r$ is the relative dielectric constant used between 5.6 (high frequency) and 25.7 (low frequency) Karim *et al.* (2021). For the calculation of $m_h{}^*$ we assumed $\epsilon_r$= 9 based on the hydrogen model Miyata, Mitioglu, Plochocka, Portugall, Wang, Stranks, Snaith & Nicholas (2015). The values of $m_h{}^*$ are estimated at 0.3 meV and 2.4 meV

for the tensile and compressive films respectively Davies, Filip, Patel, Crothers, Verdi, Wright, Milot, Giustino, Johnston & Herz (2018); Karim *et al.* (2021); Yang, Meissner, Yamaguchi, Zhang, Ueba, Cheng, Ideta, Tanaka, Zeng & Ueno (2018), where $m_e$ represents the rest mass of the electron.

Results from Figure 4.6(b) suggest that films subjected to compressive and tensile strains respectively have lower $L_m$ and $\tau_m$, respectively. Both parameters peak at 80 °C, which corresponds to the relaxation region (strain-free) regime. At this temperature, mixed halide perovskites make the transition from the tetragonal to the cubic phase due to the tilt of the inorganic $PbI_6$ octahedron and the rotational shift of the organic $CH_3NH_3$, resulting in increased average mobility Berdiyorov *et al.* (2016b). Consequently, these results confirm reports that phase shift can change the physical properties of mixed halide perovskites films and positively influence their electrical properties Karim *et al.* (2021).

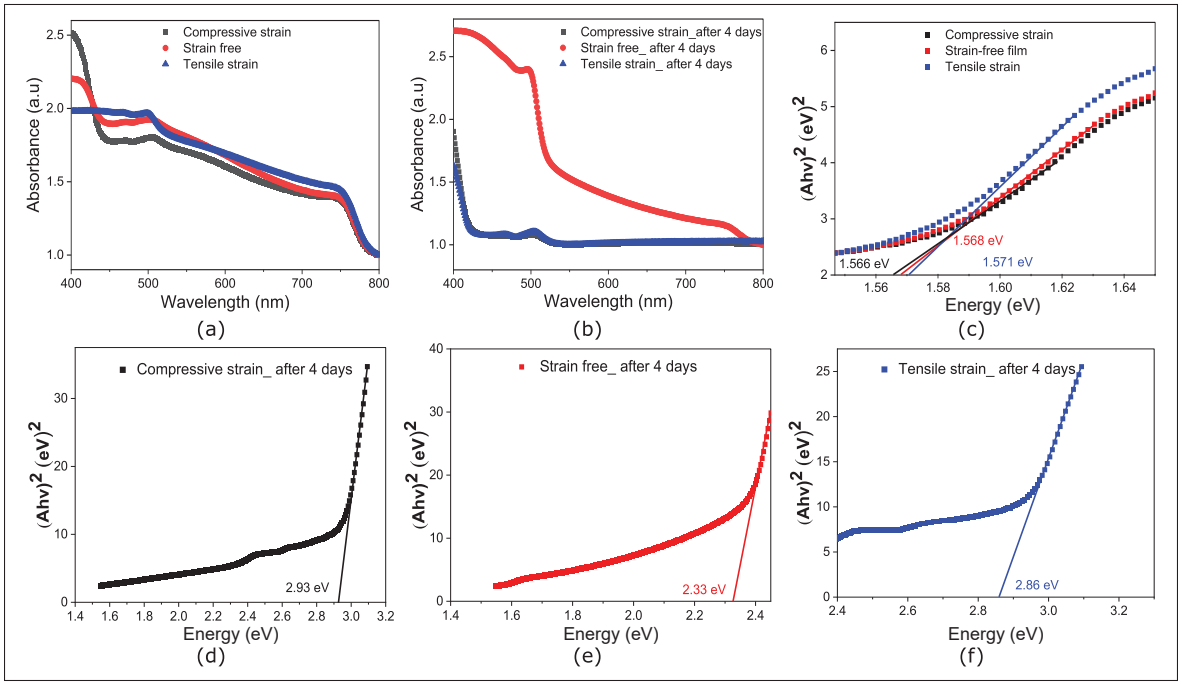


FIGURE 4.7 Absorption spectra for perovskite films annealed at 60, 80 and 110 °C. (a) Pristine films following fabrication (b) After 4 days of degradation in ambient conditions. (c) Tauc plot showing the bandgap evolution under temperature induced strain variation.(d,e,f) Tauc plots measured after 4 days in ambient environment

Figure 4.7(a,b) displays the absorption spectrum for samples annealed at 60°C, 80°C, and 110°C exhibiting compressive, relaxed, and tensile residual strains, respectively. The spectra in Figure 4.7(a) show stronger UV absorption for the tensile-strained and relaxed samples. When the residual strains transition from compressive to tensile, the bandgap of the film in Figure 4.7(c) show a slight increase from 1.56 eV to 1.57 eV. After four days of storage in an ambient environment, the absorption spectra in Figure 4.7(b) is significantly reduced for both tensile- and compressive-strained samples, compared to the sample annealed at 80 °C. Moreover, as the strained samples become transparent, this degradation also translates in a significant bandgap increase from 1.59 eV to 2.34 eV seen in Figure 4.7(d-f). The low absorption of these samples can be attributed to incomplete crystallization during annealing at 60 °C. Poor-quality perovskite films often result from incomplete DMF solvent evaporation. Conversely, high-temperature annealing at 100 °C promotes rapid solvent evaporation, preventing uniform surface filling and poor film quality as shown in Figure 4.4(d).

### 4.3.5 Raman characterization

Raman micro-spectroscopy measurements from Figures 4.8(a,b) are performed with a very low laser power of 0.5 mW at 532 nm wavelength, using a 10x objective, to avoid any laser-induced damage. All measurements are done under ambient conditions. To perform the Raman measurements, we slowly increase the laser power until the main perovskite peaks are visible. Then the laser is shifted to a new position to record the Raman spectrum for a pristine perovskite. To avoid the laser intensity from impacting the perovskite film's crystallization, we utilized equation 4.10 to estimate the sample's temperature based on the intensity ratio between Stokes/Anti-Stokes peaks Barbillat, Bougeard, Buntinx, Delhaye, Dhamelincourt & Fillaux (1999); Kauffmann, Kokanyan & Fontana (2019) as shown in Figure 4.8(b) :

$$\frac{I_s}{I_{as}} = \left(\frac{\vartheta_0 + \vartheta_v}{\vartheta_0 - \vartheta_v}\right)^4 e^{\left(\frac{E_p}{k_B \cdot T}\right)} \tag{4.10}$$

Where $k_B$ is the Boltzmann constant, $\nu_0$ is the frequency of the excitation source, and T is the sample's temperature.

The inorganic-organic sublattices of the perovskite have different vibrational frequencies covering the range from 50 to 150 $cm^{-1}$ with phonon energies of 6-11 meV (50-90 $cm^{-1}$) and 11-20 meV (90-150 $cm^{-1}$) Chang, Cho, Chen, Chen, Kinaci, Diroll, Wagner, Chan, Lin & Schaller (2016). Figures 4.8(c-e) display the statistical temperature graphics calculated using Eq (4.10), for samples with residual tensile strains, no strains, and compressive strains for a phonon energy of 12 meV at a peak Raman shift of 100 $cm^{-1}$ Chang *et al.* (2016). The maximum temperature reached by the samples due to laser-induced heating is 324 °K (50.85 °C). This value remains lower than the lowest annealing temperatures, ensuring that the 532 nm laser-induced heating does not impact the crystalline structure of the different perovskite samples.

Finally, we can also evaluate the impact of different strain levels on the film degradation using Raman micro-spectroscopy. To do so, measurements are performed every 30 minutes for 4 days at a sufficiently low excitation power to prevent laser-induced heating. The Raman spectrum in Figure 4.8(a) clearly indicates the presence of vibrational peaks at 53, 65, 92, and 100 $cm^{-1}$ with a broader Raman band at 170 $cm^{-1}$, which can be attributed to the Pb-I and Pb-Cl perovskite layers Singh, Jain, Singh & Kumar (2017). The sharp peaks between 53 $cm^{-1}$ and 92 $cm^{-1}$ are attributed to the bending and stretching of Pb-I bonds, which are modes of inorganic cages Ardimas, Pakornchote, Sukmas, Chatraphorn, Clark & Bovornratanaraks (2023). Meanwhile, the bands at 100 $cm^{-1}$ can be attributed to the vibrations of the organic $CH_3NH_3$ cations Liang, Zhang, Xu, Wang, Wang, Wang, Bi, Xu, Yuan & Ding (2015). After 24 hours, the peak intensity decreases, and no new vibrational bands are observed, implying the structure remained unaltered. It is known that incorporation of $H_2O$ into the crystal lattice is measured by solvating of $MA$ and the dissolving of the cations Leguy, Hu, Campoy-Quiles, Alonso, Weber, Azarhoosh, Van Schilfgaarde, Weller, Bein & Nelson (2015); Segovia, Qu, Peng, Sun, Shi & Gao (2018). The absence of $MA$ can increase defect density and cause a slight displacement of atoms in the crystalline structure, leading to fluctuations in vibrational bands Byranvand & Saliba (2021); Segovia *et al.* (2018). Figure 4.8(a) shows a redshift for all bands, suggesting an increased length

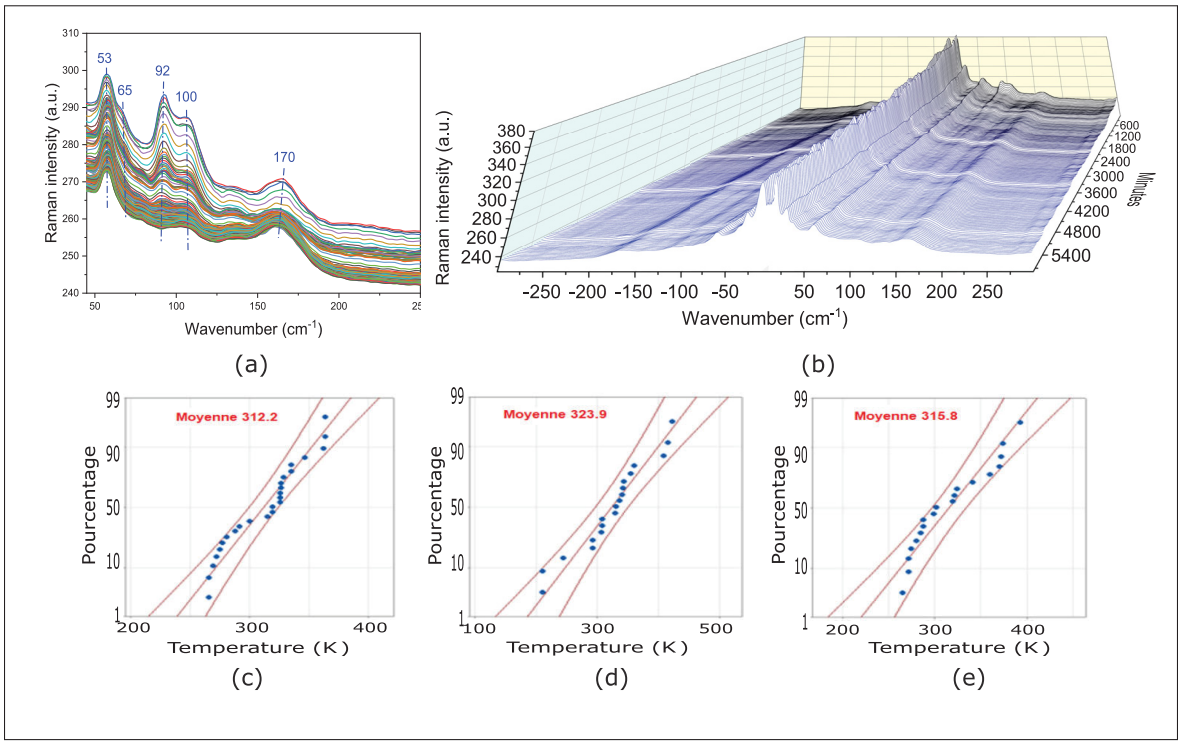


FIGURE 4.8 (a) Raman peaks shifting of the thermally-relaxed sample during 4 days of analysis. Each line corresponds to a spectrum taken after 30 minutes, b) Stokes/ani-Stokes for samples without strain. Evaluation of the samples based on Stokes/anti-Stokes intensity ratios. Calculated temperature of the (c) compressively-strained sample annealed at 60 °C, (d) thermally-relaxed sample annealed at 80 °C and (e) tensile-strained sample annealed at 110 °C

of the chemical bond. Previous research confirms that the redshift in these bands results from stress exerted by the $H_2O$ molecule on the atomic bond related to this vibrational mode and the shift induced by the $MA$ vacancies Segovia *et al.* (2018). However, the observed shift is not consistent, as the penetration of moisture in the film is not uniform due to the heterogeneity of the microstructural morphology, defects, and internal stresses.

In Figure 4.9(a-c) we compare the degradation of the strained films. As expected, results from 4.9(d-f) clearly suggest that thermally-relaxed films show lower degradation compared with tensile- or compressively-strained films. Indeed, the average peak intensity decrease for the thermally-relaxed film never exceeds 10 %. In contrast, films with residual tensile and compressive strains respectively show a decrease in peak intensity of more than 20 % and 45

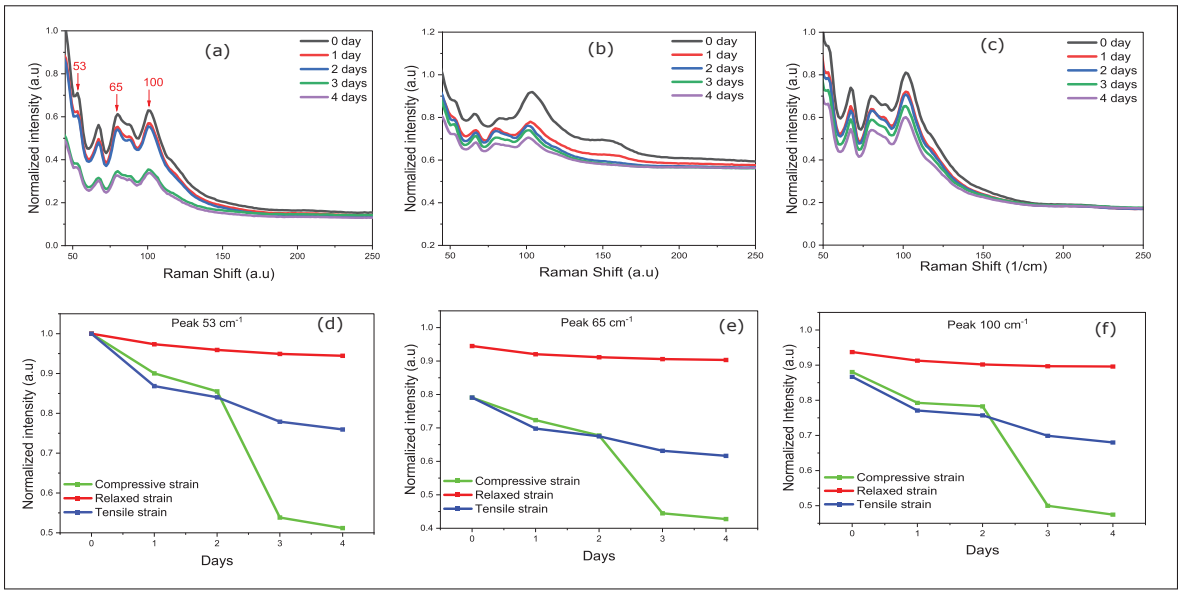


FIGURE 4.9 Raman spectra of film degradation of a different time from 0 day to 4 days. (a) With residual compressive strains, (b) Thermally-relaxed, (c) tensile-strained film. (d,e,f) Degradation measured from Raman peaks evolutions at 53, 65 and 100 $cm^{-1}$

%. This is consistent with previous observations that strained films degrade more rapidly due to their crystal structure enabling easier incorporation of $H_2O$ molecules. Surface defects and strain-induced distortions in the crystal lattice weaken the structure, rendering it less resilient to external factors and thus accelerating its degradation Aydin, De Bastiani & De Wolf (2019); Chen, Rudd, Yang, Yuan & Huang (2019).

## 4.4 Conclusion

This study shows a clear relationship between temperature-induced strains, charge carrier mobility, and the long-term stability in solution-based perovskite films. Our findings show that these factors are interrelated and must be carefully considered to optimize the performance of perovskite materials. Our findings indicate that achieving temperature-induced relaxation requires annealing within the temperature range of 75 to 85 °C for this specific precursor formulation. As a result, the $CH_3NH_3PbI_{3-x}Cl_x$ films annealed at 80 °C demonstrate optimal performance shown by higher carrier mobility, lower activation energy, high mean free path,

and improved stability. We find that these annealing temperatures reduce defect density and promote strain relaxation. These results could potentially minimize the impact of residual strain on optoelectronic properties and offer an alternative approach to optimize the performance of perovskite solar cells and other perovskite-based optoelectronic devices.

## Author Contributions

Writing - original draft, Methodology, Resources, Conceptualization, Characterization, Formal analysis, Data curation M.A.S ; Raman test Review and editing L.F.G ; Supervision, visualization, validation, Review and editing, RI and S.G.C. All authors have read and agreed to the publication of the manuscript.

## Funding

The authors would like to acknowledge the financial support received from NSERC with the following Discovery grants (RGPIN-2023-05211, RGPIN 2022-03083) as well as the Canada Research Chairs (CRC-2021-00490),

## Data availability

The data that support the findings of this study are available from the corresponding author upon reasonable request.

## Conflicts of interest

The authors declare no conflicts of interest.

## Abbreviations

The following abbreviations are used in this manuscript :

| | |
|---|---|
| GIXRD | grazing incident X-ray diffraction |
| CTE | coefficient of thermal expansion |
| PSC | perovskite solar cell |
| XRD | X-ray diffraction |
| FWHM | full-width half-maximum |

## CHAPITRE 5

# ENHANCING PERFORMANCE OF NANOCRYSTALLINE SNO2 FOR SOLAR CELLS THROUGH PHOTONIC CURING USING IMPEDANCE SPECTROSCOPY ANALYSIS

Moulay Ahmed Slimani[1], Jaime A. Benavides-Guerrero[1], Ricardo Izquierdo[1], Sylvain G. Cloutier[1]

[1] Département de Génie Électrique, École de Technologie Supérieure,
1100 Rue Notre-Dame Ouest, Montréal, Québec, H3C 1K3, Canada

Article publié dans la revue
« MDPI Nanomaterials »
le 17 Septembere 2024.
https://doi.org/10.3390/nano14181508

**Résumé :** Les couches minces d'oxyde d'étain à large bande interdite ($SnO_2$) sont fréquemment utilisées comme couches de transport d'électrons dans les cellules solaires à pérovskite en raison de leur stabilité thermique et environnementale supérieure. Cependant, sa cristallisation par des méthodes thermiques conventionnelles nécessite généralement des températures élevées et de longues périodes de temps. Ces conditions de post-traitement limitent considérablement le choix des substrats et réduisent les capacités de fabrication à grande échelle. Ce travail décrit la cristallisation induite par la lumière pulsée de couches minces de $SnO_2$ en utilisant seulement 500 $\mu s$ de temps d'exposition. Les propriétés des couches minces sont étudiées à l'aide de la spectroscopie d'impédance et des mesures caractéristiques de photoconductivité. Une analyse du diagramme de Nyquist établit que les paramètres du processus ont un impact significatif sur les comportements électroniques et ioniques des films $SnO_2$. Plus important encore, nous démontrons que la cristallisation induite par la lumière produit une topographie améliorée et d'excellentes propriétés électriques grâce à un meilleur transfert de charge, une meilleure morphologie interfaciale et un meilleur contact ohmique par rapport aux films $SnO_2$ recuits thermiquement (TA).

**Abstract :** Wide-bandgap tin oxide ($SnO_2$) thin-films are frequently used as an electron-transporting layers in perovskite solar cells due to their superior thermal and environmental

stabilities. However, its crystallization by conventional thermal methods typically requires high temperatures and long periods of time. These post-processing conditions severely limit the choice of substrates and reduce the large-scale manufacturing capabilities. This work describes the intense-pulsed-light-induced crystallization of $SnO_2$ thin-films using only 500 µs of exposure time. The thin-films' properties are investigated using both impedance spectroscopy and photoconductivity characteristic measurements. A Nyquist plot analysis establishes that the process parameters have a significant impact on the electronic and ionic behaviors of the $SnO_2$ films. Most importantly, we demonstrate that light-induced crystallization yields improved topography and excellent electrical properties through enhanced charge transfer, improved interfacial morphology, and better ohmic contact compared to thermally annealed (TA) $SnO_2$ films.

**Impedance spectroscopy ; Photonic curing ;** $SnO_2$ **; Dark injection current transient, Photo-Celiv.**

## 5.1 Introduction

Electron-transporting layers (ETLs) are critical components in most optoelectronic device architectures, including perovskite solar cells (PSCs). These PSC devices rely on organic-inorganic perovskite materials to efficiently absorb light and generate charge carriers Jing, Zhu, Peng, Li, Xiong, Wang, Liu & Wang (2020); Wei, Zhao, Jiang, Yan, Feng & Ma (2020); Yang, Lai, Zhu, Tan, Luo & Ye (2022). ETL layers are essential to promote efficient electron transport, block holes, align energy levels, and ultimately enhance the efficiency and stability of the perovskite solar cells. Choosing appropriate ETL materials is essential for the performances of PSCs. Typical ETL materials require processing between 150 and 500 °C, resulting in higher processing times and energy costs. Most importantly, this prevents their integration on most low-cost substrates requiring processing temperatures below 150 °C Jiang, Chu, Wang, Yang, Liu, Wang, Yin, Wu, Zhang & You (2017); Liu, Hu, Zhou, Wu, Zhang, Kong, Li, Zhao, Dai & Xu (2018a). In this context, intense pulsed light annealing also sometimes referred-to as photonic curing (PC) Schroder (2011) is an emerging technique ideally suited for large-scale manufacturing as is relies on short, high-intensity light pulses to anneal materials selectively and rapidly Akhavan, Schroder & Farnsworth (2022); Secor, Ahn, Gao, Lewis & Hersam (2015). In this process, the optical energy absorbed by the active material can sustain carefully-controlled light-induced annealing with minimal substrate damage. As a result, even metals with relatively high melting-points can be successfully sintered on low-cost plastic- or paper-based substrates Altay, Turkani, Pekarovicova, Fleming, Atashbar, Bolduc & Cloutier (2021); Piper *et al.* (2021); Zhu *et al.* (2017). As such, this technique is also especially well-suited for roll-to-roll (R2R) manufacturing Maskey, Koirala, Kim, Park, Yadav, Park, Sun & Cho (2019). $SnO_2$ metal-oxide thin films were first utilized as ETL for perovskite-based solar cells nearly a decade ago Dong, Shi, Wang, Li, Wang, Zhang, Xing, Du, Bai & Ma (2015); Matacena, Guerriero, Lancellotti, Alfano, De Maria, La Ferrara, Mercaldo, Miglietta, Polichetti & Rametta (2023). It has since emerged as the preferred material for PSC over $TiO_2$ and ZnO due to its large band gap, higher charge mobility, and better stability under ambient conditions Hu *et al.* (2020a); Irfan, Ünlü, Lê, Fischer, Ullah & Mathur (2022); Martínez-Denegri, Colodrero, Kramarenko & Martorell

(2018). A few years later $SnO_2$ films were photonically annealed in just 20 ms, enabling the fabrication of PSCs with reduced hysteresis and a 15 % power conversion efficiency Zhu *et al.* (2017). However, these previous studies did not address the effect of photonic curing on the electronic properties of SnO2 films. To investigate this, we used impedance spectroscopy (IS), a rapid technique for evaluating these properties. IS is a powerful tool to shed light on the kinetic processes taking place within electrochemical systems Magar *et al.* (2021) ; Pascoe *et al.* (2015). During measurement, a small alternative current (AC) signal is coupled with a direct (DC) voltage applied to the device. The phase difference between the DC voltage and AC current is measured over a wide frequency range to identify the various physical effects in the device. As a result, IS measurements can access the physical and chemical processes of various types of devices, including optoelectronic devices, fuel cells, and solid state batteries Sinclair (1995). It is a non-destructive Matacena *et al.* (2023) ; Middlemiss, Rennie, Sayers & West (2020) ; Shohan, Harm, Hasan, Starly & Shirwaiker (2021) tool that can effectively be used to optimize the stability and performance of these devices by characterizing their charge transport properties Cherian, Zheng, Reddy, Chowdari & Sow (2013) ; Magar *et al.* (2021). Typically, the IS measurements exhibit two arcs corresponding to low frequency (LF) and high frequency (HF) responses Dıaz-Flores, Ramırez-Bon, Mendoza-Galvan, Prokhorov & Gonzalez-Hernandez (2003) ; Suo *et al.* (2023). The series resistance (Rs), charge-transfer resistance ($R_{CT}$) and parallel capacitance can be determined from the HF and LF responses.

This work explores the impact of the photonic curing parameters on the thin-film $SnO_2$ properties using IS and photocurrent characteristic analysis to unveil and control the ionic and electronic kinetics within the treated $SnO_2$ layer. As we demonstrate, this improved understanding and control leads to enhanced electronic properties with great potential for improved perovskite solar cell manufacturability.

## 5.2 Experimental section

The commercial patterned FTO substrates (SHENZHEN HUAYU UNION TECHNOLOGY, resistance 7 Ohm/sq) doped with fluorine are cleaned using a sequential process of DI water,

acetone, and IPA in an ultrasonic bath for 10 minutes each. After drying with a nitrogen spray gun, residual organic contaminants are removed by performing a 15 min $O_2$ plasma treatment (Plasma Etch, PE-100LF). To prepare the $SnO_2$ solution, a colloidal precursor of $SnO_2$ obtained from Alfa Aesar (15 % in $H_2O$ colloidal dispersion CN : 044592.A3), were diluted with DI water to a concentration of 3 % by volume. The $SnO_2$ solution is spin-coated onto the clean FTO substrate in one step in air (3000 rpm for 30 s. The edges of the FTO electrodes are then cleaned with a dry cotton swab to enable electrical and IS measurements (figure 5.1). For TA, $SnO_2$ films were annealed using a hot plate at 150 °C for 30 minutes under ambient air. For photonic curing, each sample is treated using Novacentrix PulseForge system (500 V/3 A) power supply with 3 capacitors provides a radiant energy greater than 20 J.cm$^{-2}$ using lamp system (7.6 cm x 60.8 cm) with an illumination area of 300 mm x 75 mm. The light source ensures uniform curing over a large area and delivers short (20 µs to 100 ms) but intense light pulses from a broadband xenon flash lamp (200-1500 nm). The Paois (Fluxim AG, SN :20121) tool was used for all electrical and IS measurements. SEM (SU8230 Hitachi) and AFM (Bruker, MultiMode8) were used for topography inspection. For impedance spectroscopy, the FTO edges used as electrodes are connected to the Paois to measure impedance over a range of frequencies (10 Hz to 10 MHz) in the dark at 0.07 V perturbation at room temperature. Impedance data can be analyzed using Nyquist and Bode plots to interpret electrochemical properties, such as charge transfer resistance, capacitance, and dielectric properties. Temperature was simulated using NovaCentrix SimPulse software. The configuration is modeled as follows (from bottom to top) : Aluminum Chuck 6 mm, Glass 2.2 mm, FTO 600 nm and 50 nm of $SnO_2$. Glass and FTO layer thicknesses are supplied by the manufacturer. X-ray diffraction (XRD) was done using a Bruker D8 Advance (Billerica, MA, USA) and Optical absorbance was done using a UV−Vis-NIR spectrophotometer by Perkin Elmer (Waltham, MA, USA).

## 5.3 Results and discussion

After deposition of colloidal $SnO_2$ films using the protocol, samples are post-processed using varying pulse durations and energy densities using the methodology described in the Expe-

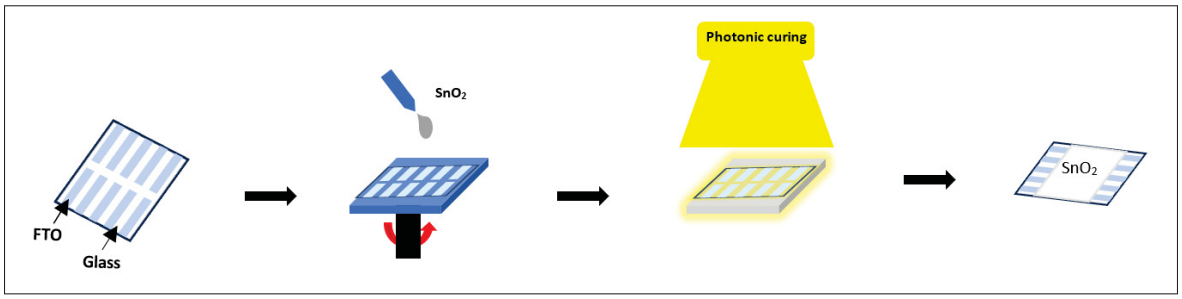


FIGURE 5.1 Illustration of the $SnO_2$ sample fabrication process

rimental section. To investigate the impact of PC on the electrical properties of $SnO_2$ films, we conduct flash annealing for pulse durations of 500, 1500, 2500, and 3500 µs, followed by photocurrent measurements. This allowed us to optimize our photonic annealing parameters and define the high photoconductivity range for $SnO_2$ films. Photocurrent analysis is used to map the different zones photoconductivity. Pulses ranging from 500 to 3500 µs are utilized to complete the photo-responsivity characterization. Figure 5.2a shows the I-V responses in the dark and under illumination for two samples photonically treated using pulse duration of 2500 µs and respectively 2 J.cm$^{-2}$ and 4 J.cm$^{-2}$. A low photo-responsivity indicates that the illumination and dark curves approach the overlap limit, while a high photo-responsivity indicates a clear offset (more than 0.5 order of magnitude) between the I-V characteristics in the dark and under illumination. Based on such measurements, Figure 5.2b displays photo-responsivity map for samples photonically-treated using different pulse duration vs energy density. To shed light on these results, IS and SEM characterization are conducted. $SnO_2$ is highly transparent, which makes it difficult to using photonic curing Piper, Xu & Hsu (2022). To mitigate this problem, we used substrates with FTO patterns that act as a structural support and a stable base for the growth of $SnO_2$ nanoparticles. This helps promote the transmission of heat generated when light is absorbed by the nanoparticles Albrecht, Rivadeneyra, Abdellah, Lugli & Salmerón (2016), which can increase the local temperature around the nanoparticles and promote the recrystallization process. FTO substrates exhibit rougher surfaces than glass Pan, Fan, Li, Wang, Huang, Jiao & Yao (2017), promoting superior adhesion and growth of $SnO_2$ nanoparticles Hamdi, Saleh & Poulis (2020). Their conductivity enhances the electrical properties of resulting

$SnO_2$ films. The FTO substrate's roughness directly influences both the diameter and alignment of $SnO_2$ nanoparticles Bandara, Aththanayake, Kumara, Samarasekara, DeSilva & Tennakone (2021). Areas with FTO patterns acting as a blanket allow for changes in nanoparticle recrystallization depending on the energy density used.

Figure 5.2c displays SEM images of the bare FTO substrate and $SnO_2$ films deposited on FTO and photonically-treated using energy densities of 0.15, 2.06 and 2.46 J.cm$^{-2}$ (Figure 5.2(d-f)). As the energy density is increased from 0.15 to 2.06 and 2.46 J.cm$^{-2}$ using 1500 µs pulse durations, the $SnO_2$-covered films appear granular, and the distinct grain boundaries that were clearly observed in the FTO/glass film are less apparent. The recrystallization of the $SnO_2$ film better follows the substrate topography, revealing the underlying FTO grain profile. This process indicates that higher energy densities lead to improved film-substrate adhesion and more pronounced exposure of the underlying grain structure. The photonic curing of $SnO_2$ wet films enables water evaporation and subsequent crystallization of $SnO_2$ nanoparticles Ghahremani *et al.* (2020). The degree of crystallization will greatly affect the photoconductivity of $SnO_2$ films and their ability to carry charge carriers Mukhamedshina & Beisenkhanov (2012) ; Zhu, Bai, Liu, Chueh, Yang & Jen (2016). Its properties will largely depend on two independent parameters : the energy density and pulse duration of the pulsed light.

To obtain quantitative information and better understand surface morphology and roughness, we also conduct AFM analysis on samples subjected to different types of annealing treatments. Figure 5.2g shows the surface roughness of the films samples with a scan area of 5x5 µm$^2$. It highlights the improvement in surface topography after optimal photonic treatment of $SnO_2$, with a root-mean-square roughness of 14.01 nm, compared to 45.57 nm for the thermally-annealed sample. Roughness is defined as the microscopic and macroscopic variations on a material's Creager, Hockett & Rowe (1992). It measures the irregularities present in the surface. These variations can have a significant impact on the physical and chemical properties of materials, such as recombination rates in ETL films for solar cells. Low-roughness films can reduce recombination rates and thus improve performance Keshtmand, Zamani-Meymian,

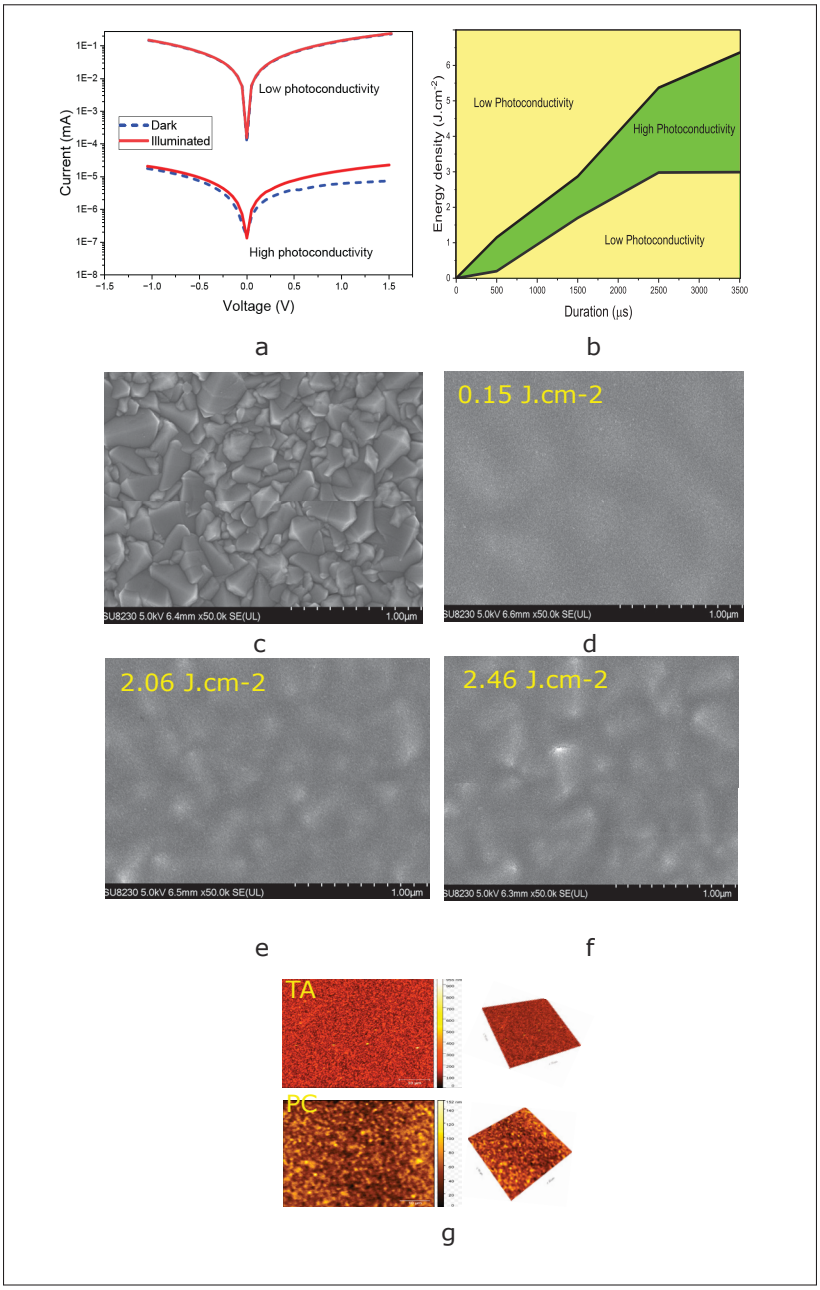


FIGURE 5.2 a) I-V responses in the dark and under illumination for two samples photonically treated using pulse duration of 2500 µs and respectively 2 and 4 J.cm$^{-2}$, b) Photo-response map for samples photonically treated using different pulse duration vs. energy density based on the criterion of Figure 5.2a, c) SEM images of FTO/glass, d-f) SEM images of PC of $SnO_2$ samples on FTO/glass. g) Atomic Force Microscopy (AFM) images 2D and 3D of thermally and photonically-annealed samples

Mohamadkhani & Taghavinia (2021). The morphological effect of PC processing could be beneficial in terms of device performance. This significant improvement underscores another important advantage of photonic treatment in enhancing the quality of $SnO_2$ as an electron transport layer (ETL) in perovskite solar cells.

This section focuses on the variation of IS results for $SnO_2$ films treated with different energy densities and pulse durations of 500, 1500, 2500, and 3500 µs. For these measurements, the $SnO_2$ film is deposited onto FTO glass, and its electrochemical behavior can be represented by an equivalent circuit that produces a semicircle on the Nyquist diagram. Figure 5.3(a–d) displays IS results for $SnO_2$ samples treated using these different pulse durations and energy densities. When the pulse duration is fixed and the energy density is increased, the semicircle decreases until it reaches its minimum, and then the arc widens. The frequency response exhibits two distinct behaviors. At high frequencies (*HF*), it is dominated by the resistance attributed to electronic transport ($R_{CT}$). At low frequencies ($L_F$), it is dominated by the recombination resistance ($R_{rec}$) related to ionic diffusion and charge accumulation at the contacts Li *et al.* (2020); Salado, Contreras-Bernal, Caliò, Todinova, López-Santos, Ahmad, Borras, Idígoras & Anta (2017). In Figure 5.3, it corresponds to the second semicircle inclined at 45° to the real axis in the Nyquist graph Shibuya, Inoue & Ihara (2009). The semi-circle in the high-frequency region is generally related to the counter-electrode and its interface Abdulrahim, Ahmad, Bahadra & Al-Thani (2020). A smaller half-circle suggests a lower $R_{CT}$ and better photoconductivity of the device. These Nyquist plots suggest that our devices' equivalent circuits can be accurately modeled by a resistor–capacitor (RC) pair in the dark AC regime Bredar, Chown, Burton & Farnum (2020). As such, the interface contribution can be derived from the equivalent circuit's parameters Chang & Park (2006). The series resistance (Rs) can be obtained by measuring the shift of the semi-circle from the origin along the horizontal axis Matacena (2019). However, the time constant related to the physical phenomena dominating at both the low and high frequencies is described by $\tau_{HF}.\omega_{HF} = 1$ and $\tau_{LF}.\omega_{LF} = 1$, with $\omega_{HF,LF} = 2\pi \cdot f_{max,HF,LF}$ Bredar *et al.* (2020). The time constants can be deduced from the IS results by identifying the peak of the semicircle, which corresponds to the maximum frequency, or by calculating $\tau = Req.Ceq$, as shown in Table 5.1.

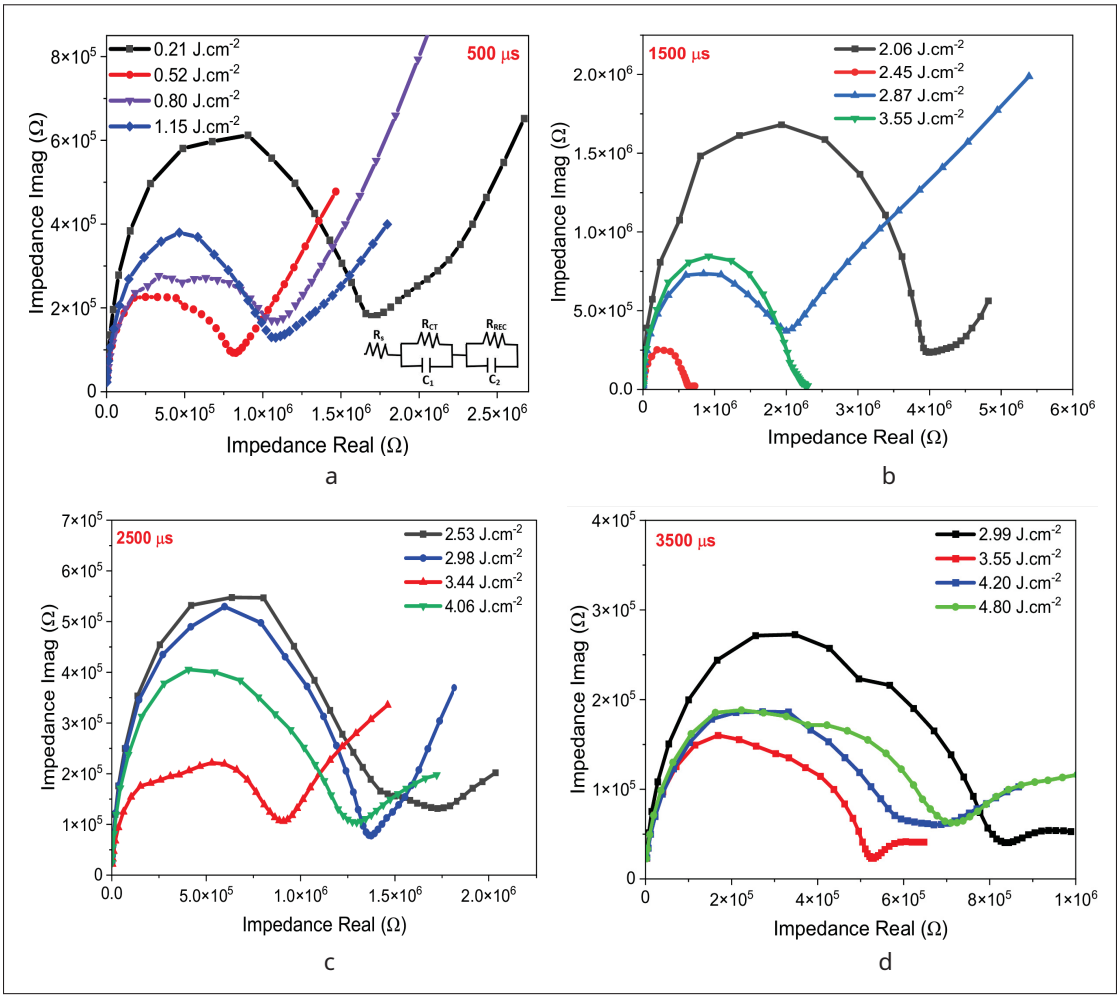


FIGURE 5.3 Imaginary versus real components of impedance for photonically annealed films with pulse durations of 500, 1500, 2500, and 3500 µs, respectively

TABLEAU 5.1 IS parameters extracted from the Nyquist plots for thermally annealed and photonically treated samples at 0 V in dark conditions with 0.07 V perturbations. Photonic treatment is performed using a 3500 µs pulse duration at 3.55 J.cm$^{-2}$ energy density

| **Device** | **Rs** (kΩ) | $R_{CT}$ (MΩ) | **Ceq** (pF) | $\tau_{HF}$ (µs) |
|---|---|---|---|---|
| Thermally annealed | 1.96 | 0.99 | 0.88 | 0.87 |
| Photonically treated | 3.06 | 0.49 | 0.78 | 0.38 |

Figure 5.4 compares the Cole–Cole plots for films that are photonically treated using 500, 1500, 2500, and 3500 µs pulses with respective energy densities of 0.52, 2.45, 3.44, and 3.55 J.cm$^{-2}$

with a typical film sample crystallized using standard thermal annealing.Clearly, the physical and chemical properties of the resulting $SnO_2$ films appear greatly affected by the pulse duration and energy density. When the pulse duration is 3500 µs and the energy density is 3.55 J.cm$^{-2}$, the high-frequency arc is smallest, suggesting that the film is less resistive and facilitating charge transfer. In comparison, the thermally annealed sample exhibits a larger semicircle than all of the photonically treated samples. This suggests increased imaginary impedance associated with a decrease in charge transfer. Figure 5.4(b–d) compare the imaginary impedance, capacitance, and conductance versus the frequency for the best thermally annealed and the best photonically treated films for the conditions 3.55 J.cm$^{-2}$ and 3500 µs. In Figure 5.4b, the high-frequency ( *HF*) peaks appear between $10^5$–$10^6$ Hz for both samples. The response time can be obtained by taking the inverse of the peak frequency from the imaginary impedance graph. Table 5.1 presents the IS parameters extracted from the spectra. There, the $R_{CT}$ value for the thermally annealed sample is roughly twice the value achieved using optimal photonic curing conditions. This suggests that the $SnO_2$/FTO interface provides a low $R_{CT}$ under the effect of photonic annealing, which facilitates charge carrier transport. The resulting time constant is 0.8 µs for the thermally annealed film, compared to 0.38 µs for the optimal photonic curing conditions. This suggest that photonically induced crystallization promotes a faster response time, resulting in low recombination and more dominant ionic diffusion behavior Alvarez, Arcas, Aranda, Bethencourt, Mas-Marzá, Saliba & Fabregat-Santiago (2020); Prochowicz, Trivedi, Parikh, Saliba, Kalam, Mahdi Tavakoli & Yadav (2021). At low frequencies, the thermally annealed device does not exhibit any measurable peak, which is consistent with the presence of the single semicircle in Figure 5.4a. In contrast, the impedance plot of the photonically treated device is curved at low frequencies, explaining the start of the second semicircle in this region. Frequency, time constant, and conductivity values are good indicators of process kinetics Hernández, Reynoso, González, Morán, Hernández, Ruiz, Hernández & Cruz (2020); Laschuk, Easton & Zenkina (2021). Indeed, the dark IS can be directly related to the carrier density, mobility, and conductivity Shibuya *et al.* (2009). Figure 5.4c,d show capacitance and conductivity evolutions as a function of the operation frequency. Figure 5.4c illustrates two distinct capacitance behaviors, each corresponding to a specific polarization process.

This distinction makes it possible to identify specific capacitive processes directly from the plot Almora, Zarazua, Mas-Marza, Mora-Sero, Bisquert & Garcia-Belmonte (2015); Guerrero, Garcia-Belmonte, Mora-Sero, Bisquert, Kang, Jacobsson, Correa-Baena & Hagfeldt (2016). The high-frequency capacitance $C_{HF}$ (above 100 kHz) exhibits a plateau in the order of 1 pF for both thermally and photonically treated devices and is rather similar for both annealing processes. This region represents the geometric capacitance and is due to the intrinsic dielectric polarization of the $SnO_2$ layer Guerrero *et al.* (2016). However, photonic treatment achieves higher capacitance values at low frequencies (below 1 KHz) compared to the thermally annealed device. This is primarily due to the accumulation of charges or ions Mahapatra *et al.* (2020); Todinova, Contreras-Bernal, Salado, Ahmad, Morillo, Idígoras & Anta (2017) resulting from the polarization of the interfaces between the $SnO_2$ layer and the electrodes. At low frequencies, the increase in capacitance is dominated by ionic movement in the dark and electronic movement in the light Zarazua, Bisquert & Garcia-Belmonte (2016a); Zarazua, Han, Boix, Mhaisalkar, Fabregat-Santiago, Mora-Seró, Bisquert & Garcia-Belmonte (2016b). In circuits that exhibit capacitive behavior, the capacitor offers less resistance to the flow of alternating current as the frequency increases. Accordingly, Figure 5.4d shows increases in conductance for both devices in the high-frequency region. This behavior is consistent with that of semiconductors, where capacitance and conductance vary inversely Heeger, MacDiarmid & Shirakawa (2000); Li & Ferrari (2018); Namsheer & Rout (2021).

The temperature simulation results using the photonic annealing parameters shown in Figure 5.4e reveal a relationship between the energy density, pulse duration, and resulting temperature of the $SnO_2$ film. As the energy density increases from 0.52 to 3.55 J.cm$^{-2}$, the temperature increases from 122 to 364°C then decreases to 329°C for the film treated with an energy density of 3.55 J.cm$^{-2}$ and a pulse duration of 3500 µs. These parameters are crucial to determine the energy transferred to the $SnO_2$ film, but they show a non-linear trend with temperature. Figure 5.4f shows X-ray diffraction (XRD) measurements of the thermally and photonically annealed $SnO_2$ films. The prominent peaks are determined to correspond to (110), (101), (200), (211), (220), and (002), confirming the tetragonal crystal structure of $SnO_2$ for both the TA and PC films Deva Arun Kumar, Valanarasu, Capelle, Nar, Karim, Stolz, Aspe & Semmar (2024); Patil, Kajale,

Gaikwad & Jain (2012); Peiris, Benitez, Sutherland, Sharma, Michalska, Scully, Vak, Gao, Weerasinghe & Jasieniak (2022).

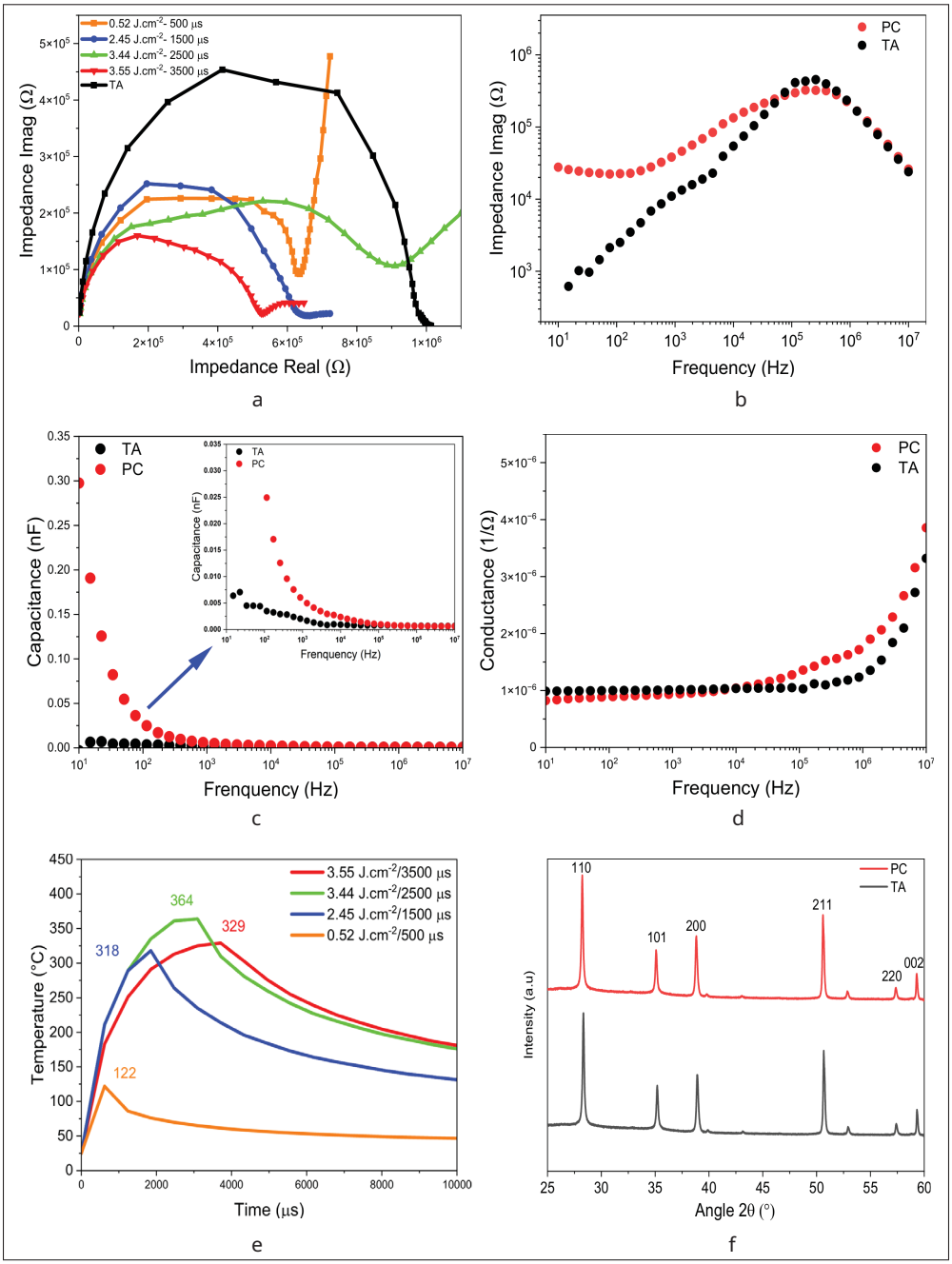


FIGURE 5.4 (**a**) Cole–Cole plot for films thermally and photonically treated using 500, 1500, 2500, and 3500 µs with energy densities of 0.52, 2.45, 3.44, and 3.55 J.cm$^{-2}$, respectively. (**b–d**) Comparison of imaginary impedance, capacitance, and conductance vs. frequency for typical thermally annealed and photonically treated samples. (**e**) SimPulse simulations of temperature profiles of photonically annealed SnO2 film Cole–Cole plots for films photonically treated using 500, 1500, 2500, and 3500 µs with energy densities of 0.52, 2.45, 3.44, and 3.55 J.cm$^{-2}$, respectively. (**f**) XRD spectra of thermally and photonically annealed $SnO_2$ films at 3.55 J.cm$^{-2}$ and 3500 µs

The optical properties of the prepared samples are characterized by UV–Vis absorption spectra. As shown in Figure 5.5a, the transmittance of PC-treated films is higher than that of TA-treated films, which is desirable for solar cell applications. $SnO_2$ is a direct bandgap (BG) semiconductor; its BG can be calculated using a Tauc plot Wang, Su, Liu, Lin, Wang, Guo, Zhang, Qin, Liu, Zhang & others (2022b), as shown in Figure 5.5b. The calculated BGs are 3.45 eV and 3.43 eV for the TA- and PC-treated films, respectively, which explains why the TA film is slightly more transparent than the PC film. Measurements in Figure 5.5(c,d) compare the dark injection transients for the photocurrent rise and decay for the thermally and photonically treated (3.55 J.cm$^{-2}$, 3500 µs) samples. This time-of-flight technique is useful for determining majority carrier mobility and trapping, especially in thin-films Esward, Knox, Jones, Brewer, Murphy, Wright & Williams (2011). Figure 5.5c illustrates that the current for the photonically treated film rises to 2.7 mA, compared to 2.3 mA for the thermally annealed film. The current also increases more rapidly in the photonically treated sample, reflecting the interrelationship between charge carrier generation and recombination. Therefore, the rapid increase in current for the PC sample can be attributed to the fast accumulation of photogenerated carriers Sarda *et al.* (2023). Figure 5.5d compares the decay of the transient current. After reaching its maximum, the current decay depends on the charge capture coefficient Knapp & Ruhstaller (2012). The decay graph illustrates the speed of charge recombination after being excited by a 1.2 V pulse voltage. A shorter carrier lifetime suggests faster recombination and a high carrier capture rate, which implies more rapid current decay for the thermally annealed sample. In contrast, photonic curing yields a lower recombination rate, resulting in slower decay and longer current holding times. The photogeneration and recombination processes have a significant impact on the density and mobility of charge carriers. Figure 5.5e compares the charge mobility using the photo-CELIV technique using the following expression Aukštuolis *et al.* (2017); Sen & Islam (2022); Stephen *et al.* (2017) :

$$\mu = \frac{2d^2}{3A.t_{max}^2(1 + 0.36\frac{\Delta}{J_{max}})} \tag{5.1}$$

where $d$ is the $SnO_2$ film thickness, $A$ is the slope of the extraction voltage ramp, $t_{max}$ is the time related to the current peak, and $\Delta$ is the difference between the maximum current and the displacement current plateau. Photo-CELIV is a technique used to extract the charge mobility by illuminating the device. The measurement displays the current overshoot and the time at which the current reaches its maximum, which is an essential parameter for quantifying mobility. However, it should be noted that Photo-CELIV only measures fast carriers and cannot distinguish between the mobility of electrons and holes. The Photo-CELIV measurements for the film after optimized photonic treatment yield $4.56 \times 10^{-2}$V cm$^2$ s$^{-1}$, compared with $3.66 \times 10^{-2}$V cm$^2$ s$^{-1}$ for the thermally annealed film. This measurement does not precisely reflect the mobility of the $SnO_2$ material. However, it serves as a characterization for comparing the fastest or maximum carrier mobility values. This higher maximum mobility compared to thermal annealing is consistent with previous results.

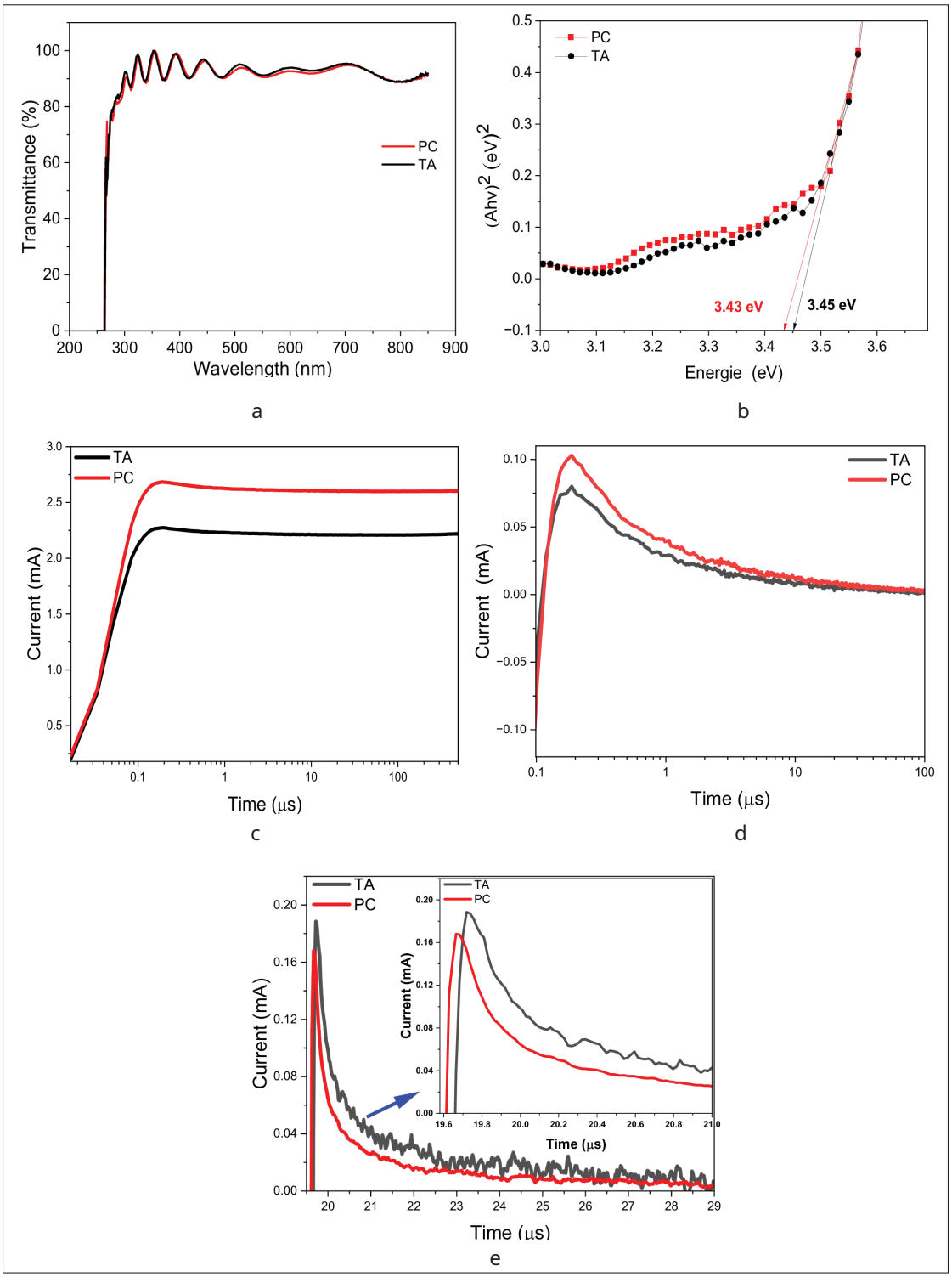


FIGURE 5.5 (**a**,**b**) Transmittance spectra and Tauc plots of thermally and photonically annealed $SnO_2$ samples. (**c**,**d**) Dark injection transients for the photocurrent rise and decay for the thermally and photonically treated samples. (**e**) Charge mobility using the photo-CELIV technique for the thermally and photonically treated samples

## 5.4 Conclusion

In summary, we propose an optimized photonic annealing approach to improve electrical properties of $SnO_2$ thin-films compared to standard annealing. $SnO_2$ thin-films play an essential role in emerging device architectures, especially as the electron-transporting layer (ETL) for perovskite-based solar cells. We use impedance spectroscopy to analyze the electrical behavior of $SnO_2$ films in the dark. The results indicate that the impedance spectroscopy response depends significantly on both energy density and pulse duration, shedding light on the resulting ionic and electronic transfer. Additionally, we demonstrate that the photonic treatment yields $SnO_2$ layers with enhanced electrical performance and a significantly-reduced manufacturing time compared to standard thermal annealing. This would be a great advantage for large-scale manufacturing of better and cheaper perovskite-based solar cells.

### Author Contributions

Writing - original draft, Methodology, Resources, Conceptualization, Formal analysis, M.A.S ; Simulation and manuscript review, J.B.G ; Supervision, visualization, Review and editing, S.G.C and R.I. All authors have read and agreed to the published version of the manuscript.

### Funding

The authors would like to acknowledge the financial support received from NSERC with the following Discovery grants (RGPIN-2023-05211, RGPIN 2022-03083) as well as the Canada Research Chairs (CRC-2021-00490).

### Data availability

The data that support the findings of this study are available from the corresponding author upon reasonable request.

## Conflicts of interest

The authors declare no conflicts of interest.

## Abbreviations

The following abbreviations are used in this manuscript :

| | |
|---|---|
| ETL | Electron-transporting layer |
| PSC | perovskite solar cell |
| TA | Thermal annealing |
| PC | Potonic curing |

# CHAPITRE 6

## CONTROLLING THE OPTICAL AND ELECTRICAL PROPERTIES OF PEROVSKITE FILMS AND THE PERFORMANCE OF SOLAR CELLS USING PHOTONIC CURING PROCESS

Moulay Ahmed Slimani[1], Wadhwa Arjun[1], Luis Felipe Gerlein[1], Jaime A. Benavides-Guerrero[1], Mohamad Hassan Tehrian[2], Ricardo Izquierdo[1], Sylvain G. Cloutier[1]

[1] Département de Génie Électrique, École de Technologie Supérieure,
1100 Rue Notre-Dame Ouest, Montréal, Québec, H3C 1K3, Canada
[2] Département de Génie Mécanique, Université du Québec à Trois-Rivières,
3351 Bd des Forges, Trois-Rivières, QC G8Z 4M3, Canada

Article publié dans la revue
« MDPI Nanomaterials »
le 09 Décembre 2024.
https://doi.org/10.3390/nano14231975

**Résumé :** La méthode la plus courante de traitement des films minces d'oxydes métalliques et de pérovskites en laboratoire est le recuit thermique (RT), ce qui représente une contrainte pour la commercialisation des cellules solaires à pérovskite à grande échelle. Ici, nous présentons un processus de photonic curing (PC) pour produire des cellules à pérovskite entièrement recuites par photonique - un processus rapide avec des impulsions lumineuses courtes et bien contrôlées - pour développer des dispositifs photovoltaïques à pérovskite avec une haute efficacité. Nous avons également démontré comment utiliser les paramètres du système de recuit photonique pour contrôler les propriétés optiques, électriques, morphologiques et structurelles des couches de pérovskite pour les applications dans les dispositifs photovoltaïques. L'effet du traitement par PC sur la microstructure, la granularité et les propriétés électroniques a été étudié par microscopie électronique à balayage (MEB), photoluminescence (PL) et photocourant transitoire (TPC). Le degré de conversion du précurseur de pérovskite et son influence sur la structure électronique ont été identifiés. Les films de $SnO_2$ et de pérovskite ont été traités avec une impulsion unique et ont produit un rendement de conversion de puissance (PCE) comparable aux échantillons de contrôle traités par RT.

**Abstract :** The most common method of processing metal oxide and perovskite thin films in the laboratory is thermal annealing (TA), which is a constraint for the commercialization of large-scale perovskite solar cells. Here, we present a photonic curing (PC) process to produce fully photonically annealed perovskite cells—a fast process with well-controlled, short light pulses—to develop perovskite photovoltaic devices with high efficiency. We also demonstrate how to use the parameters of the photonic annealing system to control the optical, electrical, morphological, and structural properties of perovskite layers for photovoltaic device applications. The effect of PC treatment on the microstructure, granularity, and electronic properties was studied by scanning electron microscopy (SEM), photoluminescence (PL), and transient photocurrent (TPC). The degree of conversion of the perovskite precursor and its influence on the electronic structure have been identified. $SnO_2$ and perovskite films were treated with a single pulse and produced PCE comparable to control samples treated by TA.

**Perovskite solar cell ; Photonic curing ; Transient photocurrent , photoluminescence.**

## 6.1 Introduction

Perovskite solar cells (PSCs) have shown remarkable results in terms of power conversion efficiency (PCE), which has exceeded 26.7% in the last decade Zhu, Zhang, Hu, Wan, Huang, Chu, Hao, Cheng, Simonov & Lu (2024). This success is mainly due to the perovskite material, which is considered a promising candidate for thin-film solar cells due to its low-cost processing capability Dunlap-Shohl, Zhou, Padture & Mitzi (2018) ; Jena, Kulkarni & Miyasaka (2019) and excellent optoelectronic properties. These properties include superior light absorption over a wide range of wavelengths in the solar spectrum, due to their tunable bandgap and long charge carrier (electrons, holes) diffusion length Aljuaid (2023) ; Calvo (2017) ; Semerci, Buyruk, Emin, Hooijer, Kovacheva, Mayer, Reus, Blätte, Günther & Hartmann (2023). These characteristics allow perovskite cells to achieve energy conversion efficiencies comparable to, or even surpassing, those of other established solar cells, such as silicon and cadmium telluride (CdTe) Jena *et al.* (2019) ; Saraf (2020). Currently, these energy conversion records are obtained in laboratories primarily by using TA to convert precursors into a crystalline perovskite structure. However, this technique is incompatible with roll-to-roll (R2R) fabrication and presents a major drawback for large-scale production of perovskite solar cells, limiting their contribution to the transition to renewable energy Ghahremani *et al.* (2020) ; Liao, Li, Xie, Yuan, Wang, Cao, Ding & Hao (2020). Additionally, TA, which is based on equilibrium heating, can cause failures in flexible plastic devices (which are sensitive to high temperatures) due to the mismatch of the thermal coefficient of expansion (TCE) between the layers and the substrate. It is therefore essential to replace TA with PC in the PSC manufacturing process, as PC is compatible with R2R manufacturing. Due to their quick processing times and low energy requirements, photo-irradiation techniques such as near-infrared radiation Troughton *et al.* (2015,1), flash infrared annealing Sánchez, Vallés-Pelarda, Alberola-Borràs, Vidal, Jerónimo-Rendón, Saliba, Boix & Mora-Seró (2019) ; Sánchez, Jerónimo-Rendon, Saliba & Hagfeldt (2020), laser annealing Jeon, Jin, Lee, Lee, Park, Kim, Lee, Shin & Kim (2016) ; You, Li, Tang, Cao & Yan (2020), and ultraviolet light have recently been researched as alternatives to TA in PSC manufacturing. PC has significantly reduced annealing time, from 10 min for TA to a few milliseconds for PC, which could lower

associated costs. Recent studies have used PC or intense pulsed light to crystallize perovskite precursors into a crystalline phase in just a few milliseconds Lavery *et al.* (2016); Troughton *et al.* (2016); Xu *et al.* (2020a). This technique has not been limited to the perovskite active layer but has also been extended to other PSC layers, such as transparent metal oxides (TMOs) like $TiO_2$ Das *et al.* (2016); Hu, Zhang, Chen & Luo (2020c), $SnO_2$ Ghahremani *et al.* (2020); Sarda *et al.* (2023), and NiO Piper *et al.* (2021); Xu *et al.* (2020b), enabling the fabrication of a complete PSC using PC. The PC delivers short, intense pulses of light from a broadband xenon flash lamp (200–1500 nm). The difference in absorption between the perovskite precursors and the substrate allows for selective heating, with the energy being absorbed primarily by the perovskite film without damaging the substrate.

Previous studies have investigated the potential for printed carbon-based perovskite solar cells to be enhanced in terms of performance through the use of humidity-assisted heat treatment Perrin, Lemercier, Planès, Berson & Flandin (2021). By precisely controlling relative humidity and temperature conditions during the annealing process, the quality of perovskite films is improved, leading to more efficient and stable devices. The results demonstrate a reduction in defects in the crystalline structure and a notable enhancement in photovoltaic performance, while maintaining a cost-effective, metal-free manufacturing process. Furthermore, it is established that the identification of optimal materials and the precise timing of antisolvent ejection significantly improve the quality of the perovskite film, leading to enhanced PCE and long-term device reliability Ghufran Hashmi, Martineau, Ibrahim Dar, T. Myllymäki, Sarikka, Ulla, Mohammed Zakeeruddin & Grätzel (2017).

In this work, the combined effect of antisolvent treatment and photonic annealing on perovskite conversion is investigated. We used different antisolvents to create an intermediate phase that facilitates crystallization by increasing the heating capacity of the perovskite precursors. The antisolvents used are chlorobenzene (CB), ethyl ether (EE), and a mixture of chlorobenzene and ethyl ether (CB :EE) with a molar ratio of (3 :1). The objective of this study is to evaluate the performance of fully photonically annealed perovskite solar cells (PSCs) compared to thermally annealed PSCs. This will provide insight into the impact of PC parameters on the

optical, electrical, morphological, and structural properties of perovskite films. By examining these effects, we aim to elucidate and control the properties of perovskite layers. The findings clearly show that optimizing these parameters will lead to the development of more efficient and cost-effective solar cells with significant potential for large-scale commercialization.

## 6.2 Experimental Section

$PbI_2$ was purchased from Alfa, and methylammonium iodide from GreatCell Solar. $SnO_2$ was obtained from Alfa Aesar (15% in $H_2O$ colloidal dispersion, CN : 044592.A3); the particles were diluted with DI water to a concentration of 3% by volume. Patterned fluorine-doped tin Oxide (FTO) substrates were purchased from sf-international (SHENZHENHUAYU UNION TECHNOLOGY, Shenzhen, China), and all other materials were sourced from Sigma-Aldrich (ON, Canada). All purchased products were used as received. FTO-coated glass substrates (15 ohm/sq) were cleaned sequentially in soapy water, acetone, IPA, and DI water for 10 min and dried with $N_2$. They were then treated with $O_2$ plasma (Plasma Etch, Carson City, NV, USA, PE-100LF) for 15 min. For perovskite ink, a 0.85 M solution was prepared by mixing equimolar amounts of MAI and $PbI_2$ in anhydrous DMSO. The hole transport material 2,2,7,7-tetrakis(N,N-dimethoxyphenylamine) 9,9-spirobifluorene (Spiro-OMeTAD) was dissolved in anhydrous chlorobenzene (CB) at a concentration of 80 mg $L^{-1}$ and doped with 25 mL lithium bis(trifluoromethanesulfonyl)imide (LiTFSI) ( 170 mg $L^{-1}$ in acetonitrile) and 28.8 µL of 4-tert-butylpyridine (tBP) solution. $SnO_2$ was spin-coated onto the glass substrate at 3000 rpm for 30 s in an ambient environment. For TA, the films were annealed at 150 °C for 30 min. For PC, the films were cured using the parameters (3.55 J.$cm^{-2}$, 3500 ms) presented in our previous work Slimani, Benavides-Guerrero, Cloutier & Izquierdo (2024a). For both TA and PC, the perovskite precursor solution (70 mL ) was spin-coated on the $SnO_2$ (treated with $O_2$ plasma) at 4000 rpm for 30 s inside an $N_2$-purged glovebox. The antisolvent (150 µL) was applied to the film 15 s before the end of spin-coating (SC). For PC, the films were prepared inside the same glovebox and processed using PulseForge (500 V, 3 A) power supply, three-capacitor bank with a maximum radiant energy delivery of 20 J·$cm^{-2}$, xenon flash lamp with 150 mm × 75 mm illumination

area, and a wide bandwidth (200–1500 nm). For TA samples, $MAPbI_3$ films were annealed at 100 °C for 10 min in the glovebox. Afterwards, a spiro-OMeTAD-based HTL was spin-coated at 2000 rpm for 30 s. Finally, a 100 nm Ag electrode was thermally evaporated at a pressure of $10^{-6}$ torr to complete the device. The PSC configuration and materials are identical for TA and PC except for the annealing process used for $SnO_2$ and perovskite. For PC, the perovskite films were all processed in air at ambient temperature (22–24 °C) and relative humidity (25–40%). UV-Vis absorption, SEM, FTIR, and PL were used for characterization. For PL, the spectra were normalized by reducing the duration to 1 s and laser power to 1 mW. The full width at half maximum (FWHM) and the position of the maximum were obtained by fitting the spectra with a Gaussian function. XRD was conducted using a Bruker D8 Advance (Billerica, MA, USA), equipped with a Cu source. The temperature is simulated using NovaCentrix SimPulse software (simulation package is standard on the PulseForge Version 3, TX, USA). The configuration was modeled from bottom to top, with the following layers : aluminum chuck 6 mm, glass 2.2 mm, FTO 600 nm, and 300 nm of perovskite. The glass and FTO layer thicknesses were supplied by the manufacturer. Current density–voltage (J-V) measurements were carried out under an AM 1.5 G 100 mW $\cdot cm^{-2}$ solar simulator (Oriel, MA, USA). All other electrical measurements were taken using PAIOS (Fluxim AG, SN :20121Winterthur, Switzerland).

### 6.3 Results and Discussion

FTIR, SEM, and absorbance characterizations presented in Figure 6.1 enabled us to choose the appropriate solvent for our photonic process. FTIR analysis of the solvents studied shows the appearance of the first broad peak at 3180 $cm^{-1}$, corresponding to the stretching of the N-H bond, while the narrow peak is associated with the C-O bond at 1468 $cm^{-1}$ (Figure 6.1a) Abdelmageed, Mackeen, Hellier, Jewell, Seymour, Tingwald, Bridges, Zhang & Carter (2018) ; Wang, Mahmoudi, Rho, Yang, Seo, Bhat, Ahmad & Hahn (2017b), confirming the MAPI signature for all the solvents studied. The intensity of the FTIR peaks and the absorption spectrum (Figure 6.1a,b) are both significantly greater for the CB solvent. Figure 6.1c illustrates that the film treated with this solvent is more compact, uniform, and exhibits larger grains. However,

films treated with EE and CB display small grains and surface defects (holes), respectively. To understand how PC affects the electrical and optical properties of perovskite films, the crystallinity and morphology of the films were studied. MAPI films are generally light yellow, which makes the photonic annealing process on glass difficult due to its transparency. First, we studied the effect of solvents on the crystallinity and morphology of the films, finding that the CB solvent creates an intermediate phase, and the color becomes darker, facilitating light absorption and consequently perovskite crystallization, as shown in Figure 6.1d. The effect of the solvent is not limited to an instant color change (intermediate phase), but also affects granularity and microstructure Gedamu, Asuo, Benetti, Basti, Ka, Cloutier, Rosei & Nechache (2018). The improved quality of the active layer highlights the importance of interface quality in optimizing device performance Mehdi, Matheron, Mhamdi, Cros & Bouazizi (2021); Pan, Shao, Zhang, Shen & Wang (2021).

The optical absorbance of perovskite films is a critical element for evaluating the conversion of precursors into a crystalline structure. We measured the absorbance of perovskite films produced by PC immediately after SC. It is known that the crystallization process is spontaneous in air, as film crystallinity and surface morphology are sensitive to environmental conditions Cheng, So & Tsang (2019); Li, Zhang, Wu, Wang, Hong, Rao, Pan & Zhong (2023). To understand and elucidate how PC parameters affect the crystallinity of MAPI films, we performed photonic annealing of perovskite films at different energy densities and pulse durations, followed by absorbance measurements. This approach enabled us to optimize the PC parameters and map the distinct MAPI conversion zones. We employed an absorbance criterion at a wavelength of 774 nm to compare the absorbance of PC films with that of the reference thermally annealed film Xu *et al.* (2020a).

Figure 6.2 shows the change in absorbance of photonically annealed films. The energy density delivered to the film has a significant impact on the film's conversion status. When the energy density is low, $\Delta A_{774}$ of the PC is below 90% of the TA reference (Figure 6.2a, blue curve), indicating that the film is partially converted. Conversely, when the energy density is increased, $\Delta A_{774}$ exceeds 90% (Figure 6.2(a), green curve), signifying that the film has fully converted.

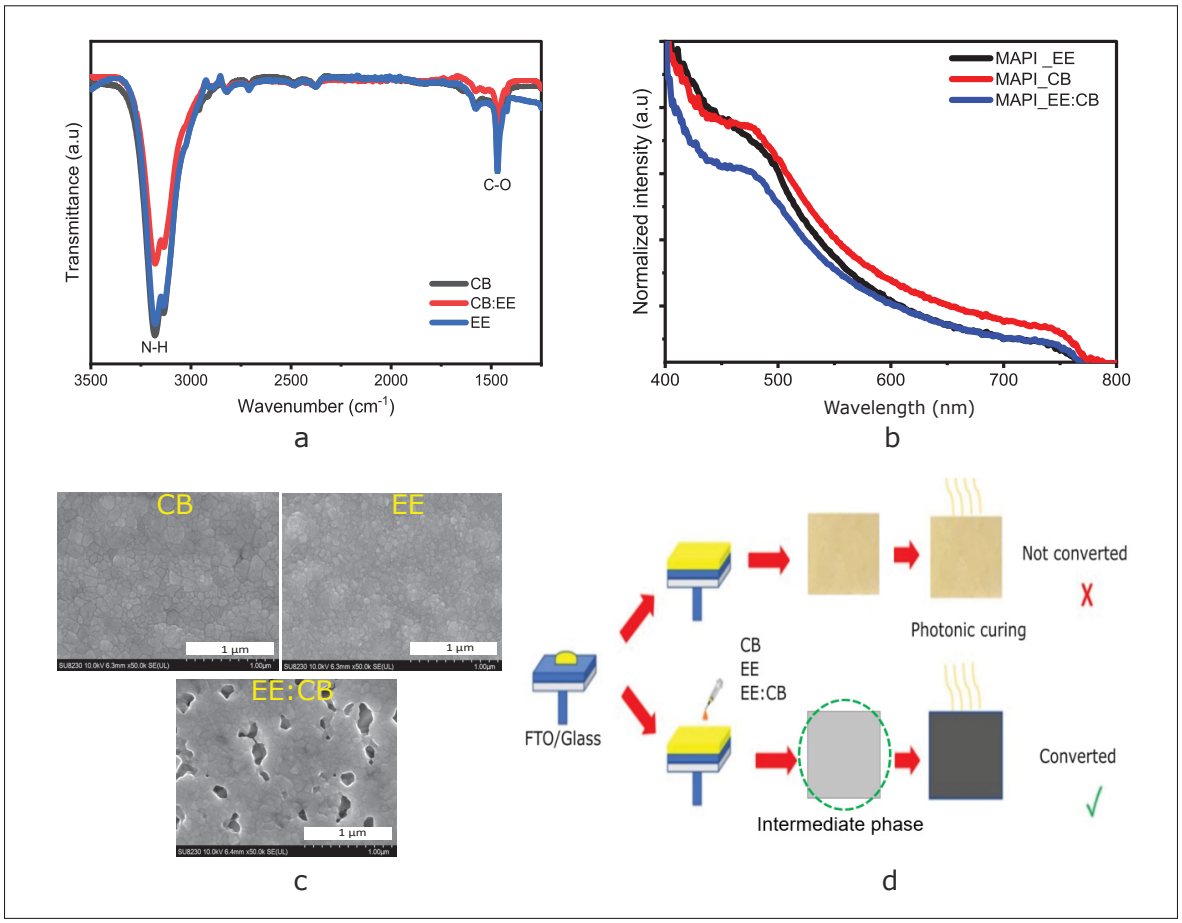


FIGURE 6.1 (**a**) FTIR spectra of perovskite films with different solvents, CB (black line), EE (blue line), and CB :EE (red line); (**b**) UV-Vis absorption spectra of MAPI films obtained from different antisolvents CB (red line), EE (black line), and EE :CB (blue line); (**c**) SEM images of surface of MAPI films prepared by CB antisolvent, diethyl-ether antisolvent, and a mix of CB and EE at a ratio 1 :1. (**d**) Illustration of PC process

However, at a certain energy density threshold, the perovskite film begins to degrade, exhibiting low absorbance (Figure 6.2a, red curve). The use of UV-Vis absorbance has enabled the mapping of three different conversion zones of perovskite precursors, which were achieved using PC's two independent variables : pulse duration and energy density. The results of the temperature simulation, as illustrated in Figure 6.2c–g, demonstrate a complex relationship between energy density, pulse duration, and the resulting temperature on the perovskite film when photonic annealing parameters are employed. The applied energy density ranges from 2.5 to 7.5 J·cm$^{-2}$, and the pulse duration varies from 2500 to 25,000 µs. These parameters are of great consequence

in determining the energy transferred to the perovskite film. In general, an increase in energy density and pulse duration results in an elevation of temperature, although the effect is not entirely linear. The recorded temperatures on the perovskite film ranged from 117 to 148 degrees Celsius (Figure 6.2h). In the initial stages, an increase in energy density and pulse duration results in a corresponding rise in temperature. For example, at an energy density of 2.5 J.cm$^{-2}$ and a pulse duration of 2500 µs, the temperature is 117 °C. An increase in energy density to 3.52 J·cm$^{-2}$ and pulse duration to 7500 µs results in a temperature rise to 139 °C. However, a non-linear behavior is observed when the energy density reaches 6 J·cm$^{-2}$ with a pulse duration of 15,000 µs, where the temperature slightly decreases to 129 °C. This phenomenon is probably attributed to a saturation effect or a redistribution of energy within the material, which impacts the heat transfer process. At the highest energy density (7.5 J·cm$^{-2}$) and the longest pulse duration (25,000 µs), the temperature rises significantly to 148 °C. This substantial increase suggests that the combination of high energy density and extended pulse duration maximizes heat transfer to the perovskite film, resulting in a more pronounced temperature increase and, consequently, an impact on perovskite crystallization.

To confirm the formation of the perovskite structure, we analyzed the compositional and structural characteristics of the films using X-ray diffraction (XRD). Measurements were performed for perovskite films corresponding to the three conversion zones with the following annealing parameters : 1.01 J.cm$^{-2}$/5000 µs, 3.52 J·cm$^{-2}$/5000 µs, and 7.02 J·cm$^{-2}$/500 µs. As shown in Figure 6.2i, the primary diffraction peaks were observed at 14.03°, 28.38°, and 31.75°, corresponding to the (110), (220), and (310) planes, respectively, confirming the formation of the MAPI structure Belayachi, Boujmiraz, Zouhair, Yaşaroğlu, Schmerber, Rehspringer, Fix, Slaoui, Abd-Lefdil & Dinia (2021). Additionally, the presence of the (211) and (112) peaks in all films indicates a tetragonal crystal structure Montaño, Diaz, Koudriavtsev, Cosme, Korneev & Mansurova (2023). At lower energy densities (partially converted zone), the diffraction peak at 12.8° assigned to the (001) plane corresponds to residual $PbI_2$, suggesting the presence of small grains or incomplete crystallization. For the film treated with the optimum photonic annealing energy, maximum crystallization was achieved, as evidenced by more intense and

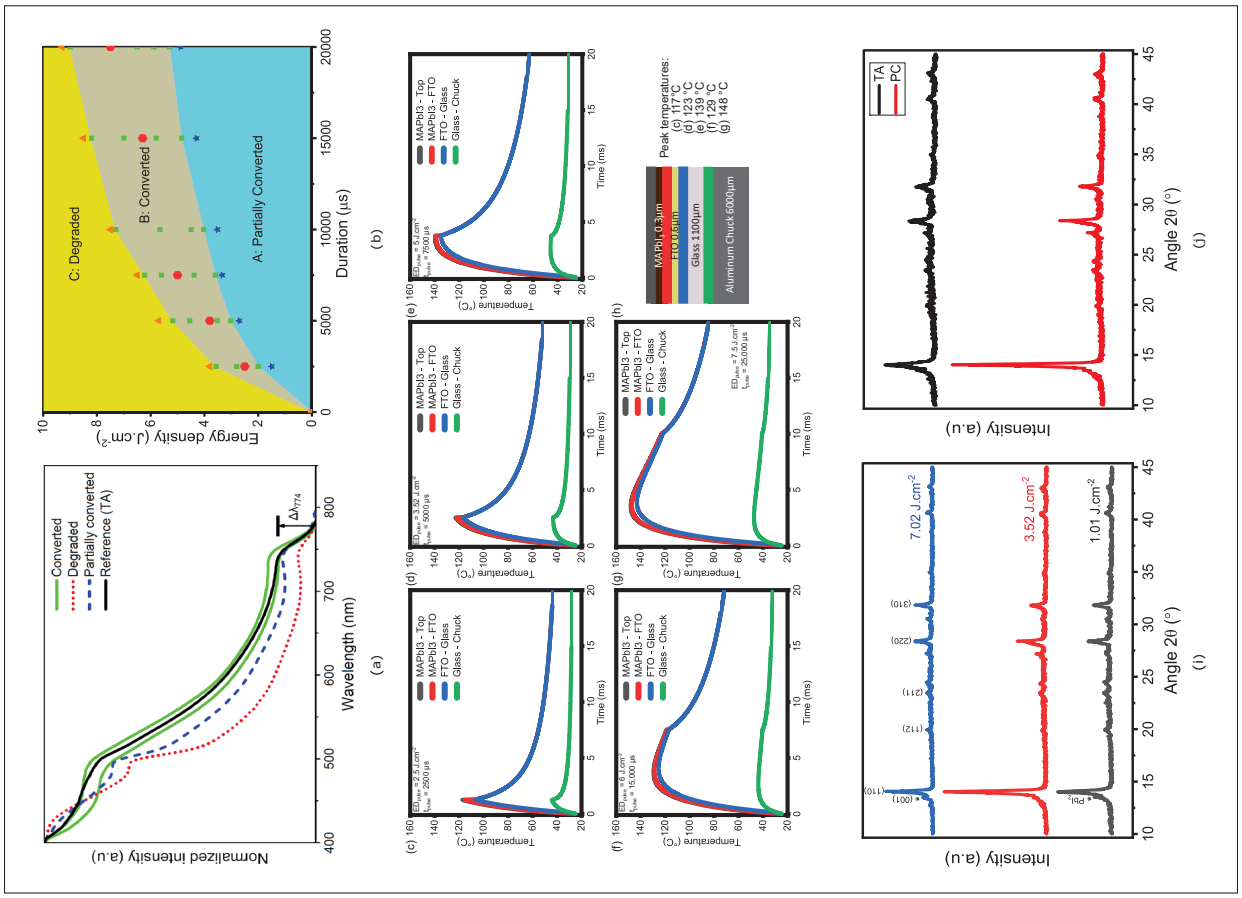


FIGURE 6.2 (**a**) Absorbance spectra of TA MAPI films (black line) partially converted PC (dashed blue line) when $\Delta\ A_{774}$ of the PC is below 90% of the TA reference (low energy density), converted PC (green line) when $\Delta\ A_{774}$ of the PC is superior to 90% (medium energy density), and degraded PC (dashed red line) when $\Delta\ A_{774}$ is inferior to 90% (high energy density). (**b**) Mapping of photonically annealed perovskite films based on criterion 2a, partially converted (turquoise zone), fully converted (gray zone), and degraded (yellow zone). SimPulse simulations of MAPI film temperature profiles at pulse lengths and density energies corresponding to the center of the conversion zone (red hexagon); (**c**) 2.5 J.cm$^{-2}$/2500 µs; (**d**) 3.52 J·cm$^{-2}$/5000 µs; (**e**) 5 J·cm$^{-2}$/7500 µs; (**f**) 6 J·cm$^{-2}$/15,000 µs; (**g**) 7.5 J·cm$^{-2}$/20,000 µs. (**h**) The configuration used for the temperature simulation, and the maximum temperature for each photonic annealing. (**i**) XRD patterns of MAPI films deposited on a glass substrate and photonically annealed at 5000 µs pulse duration and energy densities of 1.01 J·cm$^{-2}$ (black line), 3.52 J.cm$^{-2}$ (red line), and 7.02 J.cm$^{-2}$ (blue line), * corresponds to the diffraction of the $PbI_2$ peak associated with the (001) plane. (**j**) XRD patterns for the MAPI films, the thermally annealed reference film (black line), and the photonically annealed film at 5000 µs and 3.52 J·cm$^{-2}$ (red line)

sharper XRD peaks, reflecting larger crystallite size and improved crystalline orientation. However, beyond the optimum energy, the perovskite films degraded due to excessive energy input. This degradation is characterized by a decrease in peak intensity and the reappearance of the $PbI_2$ peak. Furthermore, Figure 6.2j compares the XRD spectra of TA and PC films. The results reveal that the intensity of the peaks is significantly higher for the films annealed using photonic curing at 3.52 J·cm$^{-2}$/5000 µs compared to the reference film. This indicates that the photonic annealing process promotes enhanced crystallization. To gain a deeper insight into this crystallization phenomenon, we will analyze the influence of the photonic annealing parameters (energy density and pulse duration) on the granularity and microstructure of perovskite films in the following section.

PC of perovskite films involves using intense pulsed light to rapidly anneal the material. This process can enhance the crystallinity and reduce defects, leading to significant changes in PL spectra. Figure 6.3 depicts the results of PL and SEM measurements for CB-treated MAPI samples that were subjected to annealing at energy densities of 2.5, 3.52, 5, 6, and 7.5 J·cm$^{-2}$, which correspond to the respective states 1, 2, 3, 4, and 5. As illustrated in Figure 6.3b, the PL peaks are found to be sensitive to both ED and pulse duration. The sample annealed at 3.5 J·cm$^{-2}$ for 5000 µs exhibited the highest intensity peak with a relatively narrow FWHM. The higher PL intensity indicated a higher-quality material with a reduction in trap states and suppression of non-radiative recombination Chen, Jia, Qiu, Zhuang, Hua & Zhang (2022); Luo, Liu, Zhang, Wang, Wen, Zhang, Chen & Zheng (2023). Additionally, a decrease in FWHM indicated a more uniform crystal size distribution and passivation of surface defects, reflecting increased crystallinity Kim, An, Kim, Myoung, Heo & Cho (2021b); Zhou, Fernando, Wan, Liu, Shrestha, Tisdale, Sheehan, Jones, Tretiak & Tsai (2021). Another noteworthy observation is the shift in peak wavelength observed with the increase in ED. First, a redshift is observed at low energy density for annealed films from 2.5 J·cm$^{-2}$ to 5 J·cm$^{-2}$ (766 nm–774 nm). Beyond this ED, a transition to a blueshift occurs (774 nm–761 nm), which can be explained by the grain size distribution and phase transition in MAPI Min, Hossain, Adhikari & Kaul (2020); Yamada, Yamada & Kanemitsu (2020). Figure 6.3c–g show SEM images of photonically annealed films

at 2.5, 3.52, 5, 6, and 7.5 J·cm$^{-2}$, respectively. These images illustrate the formation of uniform topographies with a large grain size distribution. As energy density increases, grain size reaches an average of 851 nm (Figure 6.3h), with a compact, uniform structure. Subsequently, grain size begins to decrease, and at higher energy densities, holes and cracks emerge (Figure 6.3g). Based on the simulation of temperature peaks at the surface of the perovskite film for each photonic treatment, the (7.5 J·cm$^{-2}$/20,000 µs) treatment corresponds to a peak temperature of 148 °C. This high temperature causes film degradation, which can be explained by the easy release of methylammonium iodide (MAI) at this temperature Ali Akhavan Kazemi, Jamali & Sauvage (2021); Meng, Chen, Xiao, Sun, Zhang, Han, Gao, Zhang & Yan (2021). This high temperature corresponds to the weak power peak of 282 W.cm$^{-2}$, and the degradation is likely due to the long pulse duration of 20,000 µs (Figure 6.3i), which extends the annealing time and thus impacts the material stability or quality.

This observation aligns with the PL test presented above. This phenomenon can be attributed to the solvent evaporating too rapidly, leading to surface defects. Controlling the solvent evaporation rate is crucial for determining both the nucleation and growth rates of perovskite films Chao, Niu, Gao, Ran, Song, Chen & Huang (2021); Ding, Li, Huang, Chu, Li, Li & Yang (2017); Zhang, Zuo & Ding (2021). When the solvent evaporation rate is high, the concentration of precursors increases rapidly. This leads to grain growth being restricted by the limited time and space available, resulting in a perovskite film that is fully coated but composed of uniformly small grains Chao *et al.* (2021). To achieve a perovskite film with high coverage, large grain size, and uniformity, it is essential to precisely control the solvent evaporation rate Kwang, Chang, Hsieh, Wei & Lu (2018).

The shift in the PL peak as a function of its width (FWHM) provides an indication of the evolution of crystallinity when the energy is increased from the initial state (state 1) to the final state (state 5). Initially, an increase in energy density leads to a rapid red shift in the PL peak, accompanied by a simultaneous decrease in the FWHM. This behavior is attributed to the reduction in defects and the achievement of a significant degree of crystallization. During this phase, the evolutionary trend is perfectly linear, which can be explained by a decrease in the

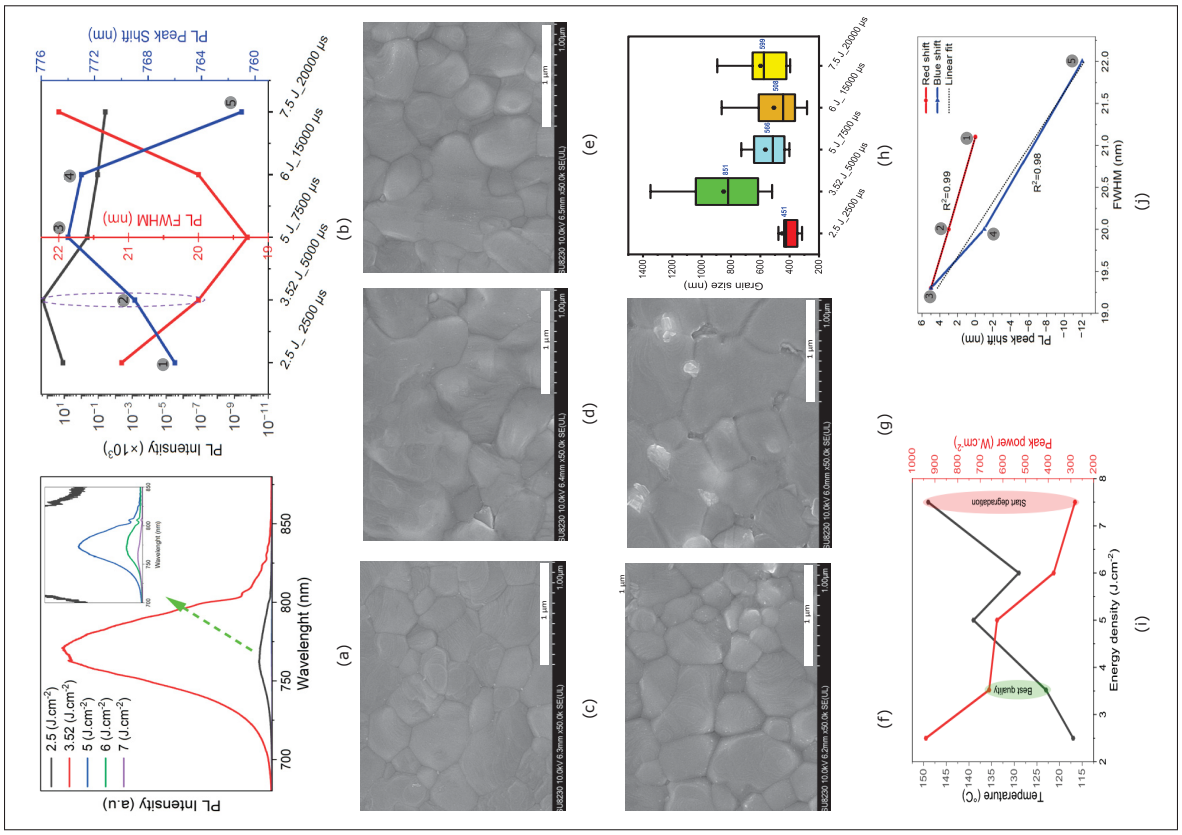


FIGURE 6.3 (**a**) PL spectra of photonically annealed perovskite films. (**b**) PL intensity, pic shift, and FHWM as a function of ED and pulse duration of photonically perovskite films. (**c**–**g**) SEM images of photonically annealed perovskite films at energy density and duration 2.5 J.cm$^{-2}$/2500 µs, 3.52 J·cm$^{-2}$/5000 µs, 5 J·cm$^{-2}$/7500 µs, 6 J·cm$^{-2}$/15,000 µs, and 7.5 J·cm$^{-2}$/20,000 µs. (**h**) Grain size distribution vs. ED and pulse duration. (**i**) Peak power and simulated temperature as a function of annealing density energy for photonically annealed samples ; PL peak shift as a function of peak width (FWHM) for photonically annealed sample. (**j**) The shift of the PL peak as a function of the FWHM of photonically annealed perovskite films at energy density and duration 2.5 J.cm$^{-2}$/2500 µs, 3.52 J·cm$^{-2}$/5000 µs, 5 J·cm$^{-2}$/7500 µs, 6 J·cm$^{-2}$/15,000 µs, and 7.5 J·cm$^{-2}$/20,000 µs correspond to states 1, 2, 3, 4 and 5 respectively, states 1, 2 and 3 correspond to redshift (red line) and states 3, 4 and 5 correspond to blueshift (blue line), The dotted black line represents the fitted line

effect of phonon localization within the structure Cloutier, Guico & Xu (2005). However, at higher energy densities, starting from stage 3, a blue shift in the PL peak is observed. Beyond this point, the appearance of new defects disrupts the crystalline structure, leading to a non-linear relationship between the PL peak shift and the FWHM width, indicating the onset of structural degradation (Figure 6.3j).

In other words, the photonic annealing coupled with CB antisolvent treatment created considerably larger and more uniform grain sizes. The UV-Vis absorption results, SEM topography, and PL measurements clearly demonstrate that the photonic annealing with the antisolvent used in this work can generate a PSC device with a power conversion efficiency (PCE) comparable to the standard TA method. As shown, films treated by photonic annealing have shown significant improvements in terms of crystallinity and defect density. In the following section, we will conduct a performance comparison study between a typical TA device and an optimized PC device (3.52 J·cm$^{-2}$, 5000 µs) to evaluate the contribution of PC to the improvement of perovskite cell fabrication.

Figure 6.4a,b shows contact angle measurements before and after $O_2$ plasma treatment of $SnO_2$ ETL layers. The decrease in contact angle signifies that this treatment has increased the surface energy and wettability of $SnO_2$, ensuring fewer surface defects, better adhesion, and greater uniformity of the perovskite layer Park & Zhu (2022). This enhancement in surface properties leads to a more uniform and defect-free perovskite film, which is crucial for improving the overall efficiency and stability of the solar cell Gong, Cui, Li & Liu (2023). The plasma treatment, therefore, plays a significant role in optimizing the interface between the $SnO_2$ ETL, and the perovskite layer, contributing to enhanced device performance. Figure 6.4c,d present a performance comparison for typical TA and optimized PC devices (3.52 J·cm$^{-2}$, 5000 µs). The data in Figure 6.4d show that open-circuit voltage (Voc) is similar and relatively high, indicating that the perovskite films are of better quality with reduced electron-hole recombination Carnie, Charbonneau, Davies, O'Regan, Worsley & Watson (2014); Wolff, Zu, Paulke, Toro, Koch & Neher (2017). FF is slightly low for TA, probably due to its higher series resistance and the sensitivity of perovskite to moisture, light, and heat Sun, Guo, Liang, Heger, Liu, Yin, Reus, Spanier, Deschler & Bernstorff (2023a); Wozny, Yang, Nardes, Mercado, Ferrere, Reese, Zhou & Zhu (2015). However, the variation in efficiency between the PC and TA samples is primarily attributed to the Jsc. We propose that this is due to interface effects arising from differences in topography, which could impact the transport of charge carriers Banerjee, Askari & Das (2023); Xu, Hart, Moss, Caprioglio, Macdonald, Furlan, Panidi,

Oliver, Pacalaj & Heeney (2023a). Furthermore, all PC samples are processed in an ambient environment, which explains the relatively lower PCE of the PC samples compared to the TA samples due to their sensitivity to humidity. Figure 6.4e illustrates the transient photocurrent (TPC) comparison between the champion solar cells TA and PC. This comparison involves analyzing the time-dependent response of the photocurrent when the solar cells are exposed to light. The TA solar cell typically exhibits a fast rise time due to high-charge-carrier mobility and lower recombination rates. However, in the context of Figure 6.4f, which illustrates the effect of light intensity on the open-circuit voltage (Voc) for two types of solar cells (PC and TA), the greater sensitivity of Voc to light intensity in the PC solar cell compared to the TA solar cell suggests important differences in their photovoltaic behavior. This observation may be linked to the presence and impact of stronger trap states in TA than in PC Jia, Qin, Zhao, Tang, Song, Guo, Li, Li, Cui & Hu (2021). Figure 6.4g,h show SEM images of thermally and photonically annealed perovskite films. Figure 6.4i illustrates that the average grain size in the PC samples is approximately six times larger than that in the TA samples. To our knowledge, no other grain size ratio has been reported to reach this magnitude of difference. This significant performance is mainly attributed to the photonic annealing process. Overall, the average PCE remains comparable to the TA process, even with the disadvantage of the environmental conditions. Figure 6.4j illustrates the significantly faster processing time of the photonic curing process, which uses 5000 $\mu$s, compared to the 10 min required for thermal annealing. This results in a 12,000-fold reduction in processing time, making perovskite cells produced by photonic curing compatible with R2R and high-throughput manufacturing.

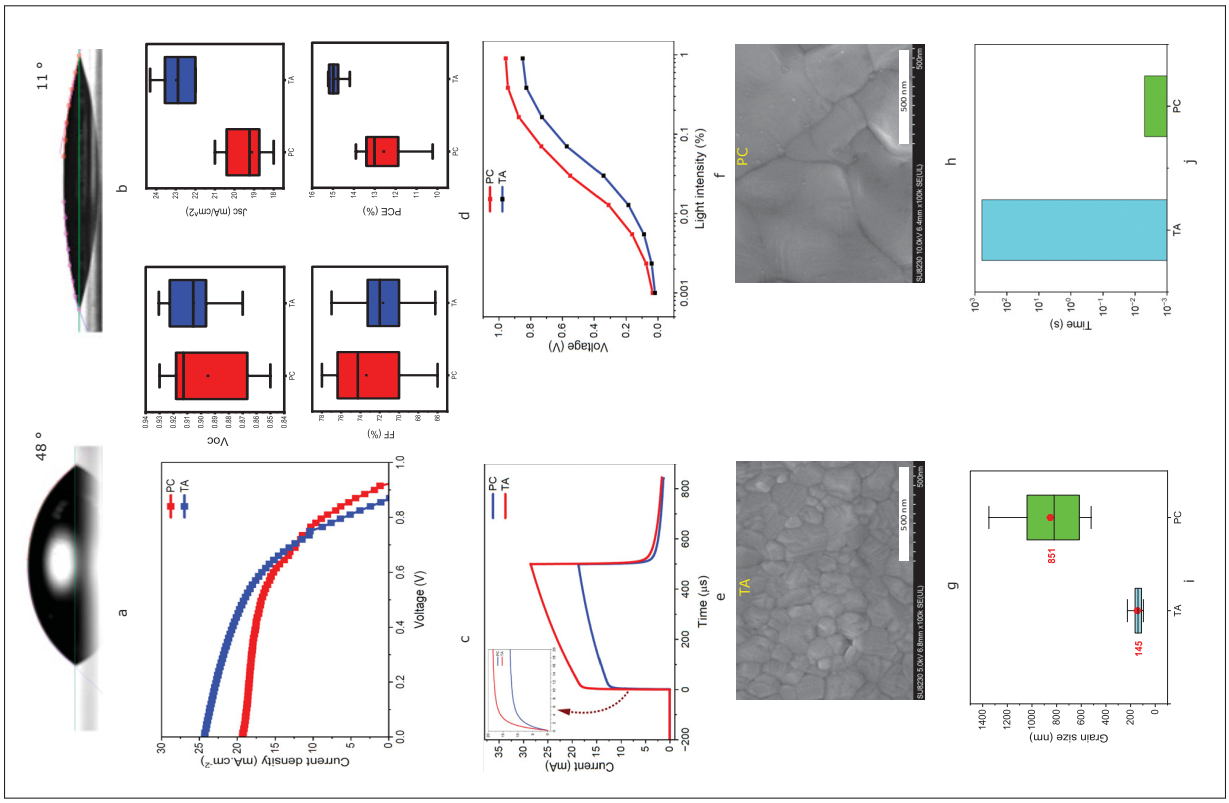


FIGURE 6.4 Contact angle measurement of the ink droplet on the $SnO_2$ coated substrate, (**a**) before plasma treatment and (**b**) after plasma treatment. (**c**) Device performance of champion of TA and PC, (**d**) Statistical distribution of the photovoltaic parameters for photonically and thermally annealed perovskite solar cells. (**e**) Transient photocurrent of the champion devices of TA and PC. (**f**) Open circuit voltage vs. light intensity of TA and PC champion devices. (**g-h**) SEM images of thermally and photonically annealed perovskite films. (**i**) Grain size distribution of thermally and photonically annealed perovskite films. (**j**) Comparison of the processing time for PC and TA

## 6.4 Conclusions

Photonic annealing is an innovative technique applied to photoactive perovskite films to enhance their optoelectronic properties. This method uses light to induce structural and chemical changes in the film, promoting improved crystallinity and defect reduction. The results of the UV-Vis analysis enabled the mapping of the conversion zones of the perovskite films based on two independent parameters : energy density and pulse duration. PL measurements, coupled with SEM characterization, allowed us to define the optimal parameters for the conversion zone and

to study the granularity and microstructure of photonically annealed films. A low radiant energy of 3.52 J.cm$^{-2}$ and a pulse duration of 5000 µs provide the best performance. According to our treatment process, grain size increases with density up to a maximum, then begins to decrease with the presence of structural defects. The champion PCE of the PC (13.95%) is relatively modest compared to that of the TA (15.01%). However, the performance of the PSCs fabricated by TA is on average comparable to those fabricated by PC. The major advantage for PC is the reduction in energy and processing time by 120,000 times compared to TA. These improvements lead to increased photovoltaic performance, making photonic annealing a promising method for producing more efficient and durable perovskite-based solar cells.

**Author Contributions**

Writing–original draft, methodology, resources, conceptualization, formal analysis, M.A.S.; Photonic curing test and review, A.W.; Simulation test and review, L.F.G.; PL test review, J.A.B.-G.; Contact angle test and review, M.H.T.; Supervision, visualization, review and editing, R.I. and S.G.C. All authors have read and agreed to the published version of the manuscript.

**Funding**

The authors would like to acknowledge the financial support received from NSERC for the Discovery grants (RGPIN-2023-05211, RGPIN 2022-03083) as well as the Canada Research Chairs (CRC-2021-00490).

**Data availability**

The data that support the findings of this study are available from the corresponding author upon reasonable request.

**acknowledgments**

The authors would like to express their gratitude to Mohammad Saadati for conducting the SEM measurements and to Mathieu Gratuze for providing assistance with the LaTeX.

**Conflicts of interest**

The authors declare no conflicts of interest.

**Abbreviations**

The following abbreviations are used in this manuscript :

| | |
|---|---|
| TA | Thermal annealing |
| PC | Photonic curing |
| PSC | perovskite solar cell |
| PL | Photoluminsence |
| TPC | Transient photocurrent |

# CONCLUSION ET RECOMMANDATIONS

## Résumé

Ce doctorat a pour objectif d'étudier, caractériser, optimiser et concevoir des couches de $SnO_2$ et de pérovskite en utilisant le recuit photonique. Les travaux s'articulent autour de trois contributions majeures visant à optimiser les performances des cellules solaires à base de pérovskite. La première contribution consiste en une optimisation fine de la température de traitement des films de pérovskite, permettant de libérer les contraintes résiduelles présentes dans ces films. En diminuant ces déformations internes, les propriétés électriques des films de pérovskite se trouvent significativement améliorées, contribuant à une efficacité accrue des dispositifs.

La deuxième contribution porte sur l'amélioration des performances des films de transport d'électrons $SnO_2$ par recuit photonique. Cette technique innovante, évaluée par spectroscopie d'impédance, permet un recuit rapide et précis, compatible même avec des substrats plastiques sensibles à la chaleur. Le recuit photonique apporte ainsi des gains en termes de rapidité de fabrication de performance et de coût, tout en maintenant l'intégrité des matériaux utilisés, ce qui est crucial pour l'industrialisation de ces dispositifs.

Enfin, la troisième contribution majeure de cette thèse a été la fabrication de cellules solaires en pérovskite exclusivement via le recuit photonique dans des conditions ambiantes. Ce procédé permet une cristallisation rapide de la pérovskite, limitant les effets néfastes de l'oxydation et aboutissant à des performances comparables à celles obtenues avec des recuits thermiques conventionnels. Cette approche ouvre des perspectives prometteuses pour une production à grande échelle de cellules solaires pérovskites, notamment par des procédés de fabrication en rouleau à rouleau (R2R), ce qui contribuerait à réduire significativement les coûts de production et à rendre cette technologie plus accessible.

**Discussion et Recommandations**

Les connaissances, le savoir-faire et les résultats acquis au cours de ce projet de doctorat ouvrent de nouvelles perspectives pour la recherche future. Afin d'étudier des aspects non abordés dans cette thèse, je propose plusieurs recommandations qui couvrent les matériaux et les procédés :

1. Étude de la compatibilité avec différents matériaux de transport : Explorer l'effet du recuit photonique sur des matériaux de transport d'électrons (ETL) et de trous (HTL) alternatifs pourrait ouvrir la voie à de nouvelles combinaisons de couches plus efficaces et stables.
2. Analyse de la stabilité à long terme : Une étude approfondie de la stabilité des films de pérovskite recuits par voie photonique dans des conditions de stress thermique et environnemental serait bénéfique pour garantir une durabilité accrue des cellules solaires.
3. Intégration du recuit photonique dans des processus de production en continu : Tester et adapter le recuit photonique dans des procédés de production en rouleau à rouleau (R2R) à grande échelle permettrait de rendre la fabrication de cellules solaires à base de pérovskite plus économique et rapide.
4. Investigation des effets sur l'interface et les défauts : Mener des études microscopiques pour comprendre l'impact du recuit photonique sur les interfaces et les défauts au niveau des grains pourrait offrir des solutions pour améliorer la qualité des films et réduire les pertes énergétiques.
5. Environnement contrôlé : Mener une étude comparative entre le recuit photonique dans un environnement contrôlé et le recuit thermique conventionnel afin d'évaluer les performances des cellules solaires dans des conditions optimales.
6. Finalement, une étude approfondie de l'imagerie et du contrôle in situ du recuit photonique apparaît indispensable pour faire progresser cette technologie. L'utilisation de techniques de diagnostic rapides telles que la spectroscopie transitoire, la caméra infrarouge (IR) ou

la photoluminescence (PL) permettrait de surveiller en temps réel l'évolution des couches minces pendant le recuit. Cela permettrait de détecter des phénomènes critiques comme la cristallisation, la diffusion ionique ou la dégradation thermique. Ces informations sont essentielles pour concevoir un système de recuit photonique auto-ajustable, capable d'adapter ses paramètres (intensité, durée, profil de flash) en fonction de la réponse instantanée du matériau. L'objectif serait alors de coupler intelligemment ce système de recuit dynamique avec les techniques d'impression additive. Une telle intégration ouvrirait la voie à la fabrication de dispositifs à architectures 2.5D multicouches, où chaque couche bénéficierait d'un recuit intermédiaire optimisé. Cela renforcerait à la fois les performances et la fiabilité des dispositifs imprimés, tout en accélérant leur développement dans des applications avancées comme l'IoT, les capteurs flexibles ou les cellules solaires organo-halogénées.

Ces recommandations visent à approfondir la compréhension et à améliorer les performances des cellules solaires à base de pérovskite par recuit photonique, tout en facilitant leur intégration dans des applications pratiques.

## Contributions

Cette thèse de doctorat met en évidence plusieurs contributions :

### Amélioration des performances électriques par relaxation des contraintes résiduelles dans les films de pérovskite

La première contribution de cette thèse porte sur la relaxation des contraintes résiduelles par la température. Elle examine l'impact des déformations résiduelles dans les films de pérovskite sur leurs propriétés électriques, optiques, et leur stabilité. Bien que les films de pérovskite soient prisés pour leurs propriétés optoélectroniques uniques, ils souffrent souvent d'inhomogénéités dues aux déformations résiduelles causées par le post-traitement. Ces déformations influencent

de manière significative les performances et la stabilité des films. Cette recherche offre ainsi des pistes pour optimiser les films de pérovskite en minimisant les déformations résiduelles, ce qui améliore leurs performances et leur durabilité.

**Amélioration des performances des couches $\mathrm{SnO_2}$ par recuit photonique basée sur la spectroscopie d'impédance**

La deuxième contribution est l'utilisation du recuit photonique pour améliorer les performances des films nanocristallins de $\mathrm{SnO_2}$ dans les cellules solaires. Les méthodes de recuit thermique traditionnelles nécessitent des températures élevées et des temps de traitement prolongés, limitant le choix des substrats et l'évolutivité du processus. Le recuit photonique, quant à lui, emploie une lumière pulsée intense pour cristalliser rapidement les films de $\mathrm{SnO_2}$, réduisant ainsi considérablement la durée et l'énergie consommée lors du traitement. Cette étude basée sur la spectroscopie d'impédance montre le potentiel du recuit photonique pour accroître l'efficacité et la stabilité des films de $\mathrm{SnO_2}$, en constituant une alternative prometteuse aux méthodes de recuit thermique classiques.

**Contrôle des propriétés optiques et électriques des films de pérovskite et optimisation des performances des cellules solaires par recuit photonique**

La troisième contribution concerne la fabrication de cellules solaires entièrement recuites par voie photonique dans des conditions ambiantes. Cette technique, évolutive et rapide, a permis d'améliorer les propriétés électriques et d'optimiser la topographie des films, tout en réduisant la consommation d'énergie. Contrairement au recuit thermique traditionnel, le recuit photonique permet une production à grande échelle et à faible coût, ouvrant ainsi la voie à une fabrication économique et durable des cellules solaires.

**Accomplissements académiques**

Au cours de cette thèse de doctorat, les articles suivants ont été publiés dans des revues à comité de lecture :

Articles de revue avec comité de lecture :

1. **Slimani, M. A.**, Cloutier, S. G., & Izquierdo, R. (2024). Recent Advances in the Photonic Curing of the Hole Transport Layer, the Electron Transport Layer, and the Perovskite Layers to Improve the Performance of Perovskite Solar Cells. Nanomaterials, 14(10), 886.
2. **Slimani, M. A.**, Gerlein, L. F., Izquierdo, R., & Cloutier, S. G. (2024). Impact of Residual Strains on the Carrier Mobility and Stability of Perovskite Films. Nanomaterials, 14(15), 1310.
3. **Slimani, M. A.**, Benavides-Guerrero, J. A., Cloutier, S. G., & Izquierdo, R. (2024). Enhancing the performance of nanocrystalline SnO2 for solar cells through photonic curing using impedance spectroscopy analysis. Nanomaterials, 14(18), 1508.
4. **Slimani, M. A.**, Wadhwa, A., Gerlein, L. F., Benavides-Guerrero, J. A., Taherian, M. H., Izquierdo, R., & Cloutier, S. G. (2024). Controlling the optical and electrical properties of perovskite films and enhancing solar cell performance using the photonic curing process. Nanomaterials, 14(23), 1975.
5. Guo, X., Banerjee, D., Asuo, I. M., Fortier, F. X.,**Slimani, M. A.**, & Cloutier, S. G. (2023). Plasmon-enhanced photodetectors fabricated using digital inkjet-printing on chemically nanopatterned silicon wafers. AIP Advances, 13(5).
6. Taherian, M.H., **Slimani, M. A.**, Shah, K., Gerlein, L.F., Wadhwa, A., Benavides-Guerrero, J., Cloutier, S.G., & Bolduc, M. Photonic Sintering of Non-Oxide Ceramics for Printed Electronics : A Comprehensive Mini Review.
   *Submitted to : Journal of Synthesis and Sintering*

## LISTE DE RÉFÉRENCES BIBLIOGRAPHIQUES


Abadias, G., Chason, E., Keckes, J., Sebastiani, M., Thompson, G. B., Barthel, E., Doll, G. L., Murray, C. E., Stoessel, C. H. & Martinu, L. (2018). Stress in thin films and coatings : Current status, challenges, and prospects. *Journal of Vacuum Science & Technology A : Vacuum, Surfaces, and Films*, 36(2), 020801. Type : Journal Article.

Abdelmageed, G., Mackeen, C., Hellier, K., Jewell, L., Seymour, L., Tingwald, M., Bridges, F., Zhang, J. Z. & Carter, S. (2018). Effect of temperature on light induced degradation in methylammonium lead iodide perovskite thin films and solar cells. *Solar Energy Materials and Solar Cells*, 174, 566–571. Type : Journal Article.

Abdulrahim, S. M., Ahmad, Z., Bahadra, J. & Al-Thani, N. J. (2020). Electrochemical impedance spectroscopy analysis of hole transporting material free mesoporous and planar perovskite solar cells. *Nanomaterials*, 10(9), 1635. Type : Journal Article.

Abulikemu, M., Neophytou, M., Barbé, J. M., Tietze, M. L., El Labban, A., Anjum, D. H., Amassian, A., McCulloch, I. & Del Gobbo, S. (2017). Microwave-synthesized tin oxide nanocrystals for low-temperature solution-processed planar junction organo-halide perovskite solar cells. *Journal of Materials Chemistry A*, 5(17), 7759–7763. Type : Journal Article.

Agarwal, U. P. & Atalla, R. H. (2020). Raman spectroscopy. Dans *Surface analysis of paper* (pp. 152–181). CRC Press.

Akbari, M., He, H., Juuti, J., Tentzeris, M. M., Virkki, J. & Ukkonen, L. (2017). 3D printed and photonically cured graphene UHF RFID tags on textile, wood, and cardboard substrates. *International Journal of Antennas and Propagation*, 2017. Type : Journal Article.

Akhavan, V., Schroder, K. & Farnsworth, S. (2022). Photonic Curing. Dans *Inkjet Printing in Industry* (pp. 1051–1064). John Wiley & Sons, Ltd. doi : 10.1002/9783527828074.ch44.

Akhtar, K., Khan, S. A., Khan, S. B. & Asiri, A. M. (2018). *Scanning electron microscopy : Principle and applications in nanomaterials characterization*. Springer.

Albrecht, A., Rivadeneyra, A., Abdellah, A., Lugli, P. & Salmerón, J. F. (2016). Inkjet printing and photonic sintering of silver and copper oxide nanoparticles for ultra-low-cost conductive patterns. *Journal of Materials Chemistry C*, 4(16), 3546–3554. Type : Journal Article.

Ali Akhavan Kazemi, M., Jamali, A. & Sauvage, F. (2021). A holistic study on the effect of annealing temperature and time on CH3NH3PbI3-based perovskite solar cell characteristics. *Frontiers in Energy Research*, 9, 732886. Type : Journal Article.

Aljuaid, F. (2023). *Stability Enhanced Perovskite Thin Films for Solar Energy Applications*. (Thesis).

Almora, O., Zarazua, I., Mas-Marza, E., Mora-Sero, I., Bisquert, J. & Garcia-Belmonte, G. (2015). Capacitive dark currents, hysteresis, and electrode polarization in lead halide perovskite solar cells. *The journal of physical chemistry letters*, 6(9), 1645–1652. Type : Journal Article.

Altay, B. N., Turkani, V. S., Pekarovicova, A., Fleming, P. D., Atashbar, M. Z., Bolduc, M. & Cloutier, S. G. (2021). One-step photonic curing of screen-printed conductive Ni flake electrodes for use in flexible electronics. *Scientific Reports*, 11(1), 3393. Type : Journal Article.

Alvarez, A. O., Arcas, R., Aranda, C. A., Bethencourt, L., Mas-Marzá, E., Saliba, M. & Fabregat-Santiago, F. (2020). Negative capacitance and inverted hysteresis : matching features in perovskite solar cells. *The journal of physical chemistry letters*, 11(19), 8417–8423. Type : Journal Article.

Al-Katrib, M., Perrin, L., Flandin, L. & Planes, E. (2023). Electrodeposition in perovskite solar cells : a critical review, new insights, and promising paths to future industrial applications. *Advanced Materials Technologies*, 8(23), 2300964. Type : Journal Article.

Ankireddy, K., Ghahremani, A. H., Martin, B., Gupta, G. & Druffel, T. (2018). Rapid thermal annealing of CH 3 NH 3 PbI 3 perovskite thin films by intense pulsed light with aid of diiodomethane additive. *Journal of Materials Chemistry A*, 6(20), 9378–9383. Type : Journal Article.

Ardimas, Pakornchote, T., Sukmas, W., Chatraphorn, S., Clark, S. J. & Bovornratanaraks, T. (2023). Phase transformations and vibrational properties of hybrid organic–inorganic perovskite MAPbI3 bulk at high pressure. *Scientific Reports*, 13(1), 16854. Type : Journal Article.

Aukštuolis, A., Girtan, M., Mousdis, G. A., Mallet, R., Socol, M., Rasheed, M. & Stanculescu, A. (2017). Measurement of charge carrier mobility in perovskite nanowire films by photo-CELIV method. *Proceedings of the Romanian Academy-Series A (Mathematics, Physics, Technical Sciences, Information Science)*, 18(1), 34–41.

Aydin, E., De Bastiani, M. & De Wolf, S. (2019). Defect and contact passivation for perovskite solar cells. *Advanced Materials*, 31(25), 1900428. Type : Journal Article.

Baena, J. P. C., Steier, L., Tress, W., Saliba, M., Neutzner, S., Matsui, T., Giordano, F., Jacobsson, T. J., Kandada, A. R. S. & Zakeeruddin, S. M. (2015). Highly efficient planar perovskite solar cells through band alignment engineering. *Energy & Environmental Science*, 8(10), 2928–2934. Type : Journal Article.

Bandara, T., Aththanayake, A., Kumara, G., Samarasekara, P., DeSilva, L. A. & Tennakone, K. (2021). Transparent and conductive F-Doped SnO 2 nanostructured thin films by sequential nebulizer spray pyrolysis. *MRS Advances*, 6, 417–421. Type : Journal Article.

Banerjee, S., Askari, S. S. A. & Das, M. (2023). Effect of rear contact coverage and improvement of efficiency of crystalline p-Si solar cell compared to state of art PERC cell. *IEEE Access*, 11, 34999–35006. Type : Journal Article.

Barbillat, J., Bougeard, D., Buntinx, G., Delhaye, M., Dhamelincourt, P. & Fillaux, F. (1999). Spectrométrie raman. *Techniques de l'ingénieur. Analyse et caractérisation*, 4(P2865), P2865. 1–P2865. 31. Type : Journal Article.

Barbé, J., Tietze, M. L., Neophytou, M., Murali, B., Alarousu, E., Labban, A. E., Abulikemu, M., Yue, W., Mohammed, O. F. & McCulloch, I. (2017). Amorphous tin oxide as a low-temperature-processed electron-transport layer for organic and hybrid perovskite solar cells. *ACS applied materials & interfaces*, 9(13), 11828–11836. Type : Journal Article.

Belayachi, W., Boujmiraz, S., Zouhair, S., Yaşaroğlu, K., Schmerber, G., Rehspringer, J.-L., Fix, T., Slaoui, A., Abd-Lefdil, M. & Dinia, A. (2021). Study of hybrid organic–inorganic halide perovskite solar cells based on MAI[(PbI2)1x(CuI)x] absorber layers and their long-term stability. *Journal of Materials Science : Materials in Electronics*, 32(15), 20684–20697. doi : 10.1007/s10854-021-06582-2.

Benetti, D. (2019). *Engineered Semiconducting Nanomaterials for Photovoltaic Applications*. (Ph.D., Institut National de la Recherche Scientifique (Canada), Canada – Quebec, CA). Repéré à ISBN : 9798379449919.

Berdiyorov, G. R., Kachmar, A., El-Mellouhi, F., Carignano, M. A. & El-Amine Madjet, M. (2016a). Role of cations on the electronic transport and optical properties of lead-iodide perovskites. *The Journal of Physical Chemistry C*, 120(30), 16259–16270. Type : Journal Article.

Berdiyorov, G., Madjet, M., El-Mellouhi, F. & Peeters, F. (2016b). Effect of crystal structure on the electronic transport properties of the organometallic perovskite CH3NH3PbI3. *Solar Energy Materials and Solar Cells*, 148, 60–66. Type : Journal Article.

Bhargava, R., Sharma, P. K., Kumar, S., Pandey, A. C. & Kumar, N. (2010). Consequence of doping mediated strain and the activation energy on the structural and optical properties of ZnO : Cr nanoparticles. *Journal of Solid State Chemistry*, 183(6), 1400–1408. Type : Journal Article.

Bouras, M. E. (2019). *Ingénierie des propriétés diélectriques d'oxydes pérovskites par nanostructuration jusqu'à l'échelle de la monocouche*. (PhD Thesis, Université de Lyon).

Bredar, A. R., Chown, A. L., Burton, A. R. & Farnum, B. H. (2020). Electrochemical impedance spectroscopy of metal oxide electrodes for energy applications. *ACS Applied Energy Materials*, 3(1), 66–98. Type : Journal Article.

Brenner, T. M., Egger, D. A., Kronik, L., Hodes, G. & Cahen, D. (2016). Hybrid organic—inorganic perovskites : low-cost semiconductors with intriguing charge-transport properties. *Nature Reviews Materials*, 1(1), 1–16. Type : Journal Article.

Buchoux, J. (2011). *Nanotubes de carbone comme sondes en microscopie à force atomique : nanomécanique et étude à l'interface air-liquide de fluides complexes*. (Thesis).

Byranvand, M. M. & Saliba, M. (2021). Defect passivation of perovskite films for highly efficient and stable solar cells. *Solar Rrl*, 5(8), 2100295. Type : Journal Article.

Calvo, M. E. (2017). Materials chemistry approaches to the control of the optical features of perovskite solar cells. *Journal of Materials Chemistry A*, 5(39), 20561–20578. Type : Journal Article.

Carnie, M. J., Charbonneau, C., Davies, M. L., O'Regan, B., Worsley, D. A. & Watson, T. M. (2014). Performance enhancement of solution processed perovskite solar cells incorporating functionalized silica nanoparticles. *Journal of Materials Chemistry A*, 2(40), 17077–17084. Type : Journal Article.

Chang, A. Y., Cho, Y., Chen, K., Chen, C., Kinaci, A., Diroll, B. T., Wagner, M. J., Chan, M. K., Lin, H. & Schaller, R. D. (2016). Slow organic-to-inorganic sub-lattice thermalization in methylammonium lead halide perovskites observed by ultrafast photoluminescence. *Advanced Energy Materials*, 6(15), 1600422. Type : Journal Article.

Chang, B.-Y. & Park, S.-M. (2006). Integrated description of electrode/electrolyte interfaces based on equivalent circuits and its verification using impedance measurements. *Analytical chemistry*, 78(4), 1052–1060. Type : Journal Article.

Chao, L., Niu, T., Gao, W., Ran, C., Song, L., Chen, Y. & Huang, W. (2021). Solvent engineering of the precursor solution toward large-area production of perovskite solar cells. *Advanced Materials*, 33(14), 2005410. Type : Journal Article.

Chatterjee, N., Weidling, A. M. & Swisher, S. L. (2022). Photonic Curing : Rapid Thermal Processing of Oxide Thin-film Transistors on Plastic. *2022 Device Research Conference (DRC)*, pp. 1–2. doi : 10.1109/DRC55272.2022.9855807.

Chen, B., Rudd, P. N., Yang, S., Yuan, Y. & Huang, J. (2019). Imperfections and their passivation in halide perovskite solar cells. *Chemical Society Reviews*, 48(14), 3842–3867. Type : Journal Article.

Chen, J., Jia, D., Qiu, J., Zhuang, R., Hua, Y. & Zhang, X. (2022). Multidentate passivation crosslinking perovskite quantum dots for efficient solar cells. *Nano Energy*, 96, 107140. Type : Journal Article.

Cheng, Y. & Ding, L. (2021a). Perovskite/Si tandem solar cells : Fundamentals, advances, challenges, and novel applications. *SusMat*, 1(3), 324–344. Type : Journal Article.

Cheng, Y. & Ding, L. (2021b). Pushing commercialization of perovskite solar cells by improving their intrinsic stability. *Energy & Environmental Science*, 14(6), 3233–3255. Type : Journal Article.

Cheng, Y., So, F. & Tsang, S.-W. (2019). Progress in air-processed perovskite solar cells : from crystallization to photovoltaic performance. *Materials Horizons*, 6(8), 1611–1624. Type : Journal Article.

Cherian, C. T., Zheng, M., Reddy, M., Chowdari, B. & Sow, C. H. (2013). Zn2SnO4 nanowires versus nanoplates : electrochemical performance and morphological evolution during Li-cycling. *ACS applied materials & interfaces*, 5(13), 6054–6060.

Chiang, C.-H., Kan, C.-W. & Wu, C.-G. (2021). Synergistic engineering of conduction band, conductivity, and interface of bilayered electron transport layers with scalable TiO2 and SnO2 nanoparticles for high-efficiency stable perovskite solar cells. *ACS Applied Materials & Interfaces*, 13(20), 23606–23615. Type : Journal Article.

Chien, C. (2013). *The Hall effect and its applications*. Springer Science & Business Media.

Choi, H. H., Paterson, A. F., Fusella, M. A., Panidi, J., Solomeshch, O., Tessler, N., Heeney, M., Cho, K., Anthopoulos, T. D., Rand, B. P. & others. (2020). Hall effect in polycrystalline organic semiconductors : The effect of grain boundaries. *Advanced Functional Materials*, 30(20), 1903617. Publisher : Wiley Online Library.

Cloutier, S. G., Guico, R. S. & Xu, J. M. (2005). Phonon localization in periodic uniaxially nanostructured silicon. *Applied Physics Letters*, 87(22). doi : https://doi.org/10.1063/1.2135881. Publisher : AIP Publishing.

Creager, S. E., Hockett, L. A. & Rowe, G. K. (1992). Consequences of microscopic surface roughness for molecular self-assembly. *Langmuir*, 8(3), 854–861. Publisher : ACS Publications.

Crescentini, M., Syeda, S. F. & Gibiino, G. P. (2021). Hall-effect current sensors : Principles of operation and implementation techniques. *IEEE Sensors Journal*, 22(11), 10137–10151. Type : Journal Article.

Das, S., Yang, B., Gu, G., Joshi, P. C., Ivanov, I. N., Rouleau, C. M., Aytug, T., Geohegan, D. B. & Xiao, K. (2015a). High-performance flexible perovskite solar cells by using a combination of ultrasonic spray-coating and low thermal budget photonic curing. *Acs Photonics*, 2(6), 680–686. Type : Journal Article.

Das, S., Gu, G., Joshi, P. C., Yang, B., Aytug, T., Rouleau, C. M., Geohegan, D. B. & Xiao, K. (2016). Low thermal budget, photonic-cured compact TiO 2 layers for high-efficiency perovskite solar cells. *Journal of Materials Chemistry A*, 4(24), 9685–9690. Type : Journal Article.

Das, S., Cormier, D. & Williams, S. (2015b). Potential for multi-functional additive manufacturing using pulsed photonic sintering. *Procedia Manufacturing*, 1, 366–377. Type : Journal Article.

Davies, C. L., Filip, M. R., Patel, J. B., Crothers, T. W., Verdi, C., Wright, A. D., Milot, R. L., Giustino, F., Johnston, M. B. & Herz, L. M. (2018). Bimolecular recombination in methylammonium lead triiodide perovskite is an inverse absorption process. *Nature communications*, 9(1), 1–9. Type : Journal Article.

de Boode, B., Phillips, C., Lau, Y. C., Adomkevicius, A., McGettrick, J. & Deganello, D. (2022). Glassy carbon manufacture using rapid photonic curing. *Journal of Materials Science*, 57(1), 299–310. doi : 10.1007/s10853-021-06648-w.

Deva Arun Kumar, K., Valanarasu, S., Capelle, A., Nar, S., Karim, W., Stolz, A., Aspe, B. & Semmar, N. (2024). Nanostructured Oxide (SnO2, FTO) Thin Films for Energy Harvesting : A Significant Increase in Thermoelectric Power at Low Temperature. *Micromachines*, 15(2), 188. Publisher : MDPI.

Ding, B., Li, Y., Huang, S.-Y., Chu, Q.-Q., Li, C.-X., Li, C.-J. & Yang, G.-J. (2017). Material nucleation/growth competition tuning towards highly reproducible planar perovskite solar cells with efficiency exceeding 20%. *Journal of Materials Chemistry A*, 5(15), 6840–6848. Type : Journal Article.

Dong, Q., Shi, Y., Wang, K., Li, Y., Wang, S., Zhang, H., Xing, Y., Du, Y., Bai, X. & Ma, T. (2015). Insight into perovskite solar cells based on SnO2 compact electron-selective layer. *The Journal of Physical Chemistry C*, 119(19), 10212–10217. Type : Journal Article.

Dunlap-Shohl, W. A., Zhou, Y., Padture, N. P. & Mitzi, D. B. (2018). Synthetic approaches for halide perovskite thin films. *Chemical reviews*, 119(5), 3193–3295. Type : Journal Article.

Dıaz-Flores, L., Ramırez-Bon, R., Mendoza-Galvan, A., Prokhorov, E. & Gonzalez-Hernandez, J. (2003). Impedance spectroscopy studies on SnO2 films prepared by the sol–gel process. *Journal of Physics and Chemistry of Solids*, 64(7), 1037–1042. Publisher : Elsevier.

Eames, C., Frost, J. M., Barnes, P. R., O'regan, B. C., Walsh, A. & Islam, M. S. (2015). Ionic transport in hybrid lead iodide perovskite solar cells. *Nature communications*, 6(1), 1–8. Type : Journal Article.

Esward, T., Knox, S., Jones, H., Brewer, P., Murphy, C., Wright, L. & Williams, J. (2011). A metrology perspective on the dark injection transient current method for charge mobility determination in organic semiconductors. *Journal of Applied Physics*, 109(9). Type : Journal Article.

Feleki, B., Bex, G., Andriessen, R., Galagan, Y. & Di Giacomo, F. (2017). Rapid and low temperature processing of mesoporous TiO2 for perovskite solar cells on flexible and rigid substrates. *Materials Today Communications*, 13, 232–240. Type : Journal Article.

Fraas, L. M. & O'Neill, M. J. (2023). History of Solar Cell Development. Dans Fraas, L. M. & O'Neill, M. J. (Éds.), *Low-Cost Solar Electric Power* (pp. 1–12). Cham : Springer International Publishing. doi : 10.1007/978-3-031-30812-3_1.

Francisco-López, A., Charles, B., Alonso, M. I., Garriga, M., Campoy-Quiles, M., Weller, M. T. & Goñi, A. R. (2020). Phase diagram of methylammonium/formamidinium lead iodide perovskite solid solutions from temperature-dependent photoluminescence and Raman spectroscopies. *The Journal of Physical Chemistry C*, 124(6), 3448–3458. Type : Journal Article.

Frolova, L. A., Dremova, N. N. & Troshin, P. A. (2015). The chemical origin of the p-type and n-type doping effects in the hybrid methylammonium–lead iodide (MAPbI 3) perovskite solar cells. *Chemical Communications*, 51(80), 14917–14920. Type : Journal Article.

Gable, S. (2022). *Microdispositifs suspendus à base de couches minces épitaxiées d'oxydes ferroélectriques à actionnement optique*. (phdthesis, Université Paris-Saclay). Repéré à https://theses.hal.science/tel-04368881.

Gamal, K., Gamal, M., Okaz, A., Shehata, N. & Kandas, I. (2024). Comprehensive performance analysis of perovskite solar cells based on different crystalline structures of MAPbI3. *Optical and Quantum Electronics*, 56(5), 827. doi : 10.1007/s11082-024-06655-6.

Garlapati, S. K., Marques, G. C., Gebauer, J. S., Dehm, S., Bruns, M., Winterer, M., Tahoori, M. B., Aghassi-Hagmann, J., Hahn, H. & Dasgupta, S. (2018). High performance printed oxide field-effect transistors processed using photonic curing. *Nanotechnology*, 29(23), 235205. doi : 10.1088/1361-6528/aab7a2. Publisher : IOP Publishing.

Gedamu, D., Asuo, I. M., Benetti, D., Basti, M., Ka, I., Cloutier, S. G., Rosei, F. & Nechache, R. (2018). Solvent-antisolvent ambient processed large grain size perovskite thin films for high-performance solar cells. *Scientific reports*, 8(1), 12885. Type : Journal Article.

Ghahremani, A. H., Martin, B., Ankireddy, K. & Druffel, T. (2019). Rapid processing of perovskite solar cells through pulsed photonic annealing : a review. *Journal of Coatings Technology and Research*, 16, 1637–1642. Type : Journal Article.

Ghahremani, A. H., Martin, B., Gupta, A., Bahadur, J., Ankireddy, K. & Druffel, T. (2020). Rapid fabrication of perovskite solar cells through intense pulse light annealing of SnO2 and triple cation perovskite thin films. *Materials & Design*, 185, 108237.

Ghosh, D., Aziz, A., Dawson, J. A., Walker, A. B. & Islam, M. S. (2019). Putting the squeeze on lead iodide perovskites : pressure-induced effects to tune their structural and optoelectronic behavior. *Chemistry of Materials*, 31(11), 4063–4071. Type : Journal Article.

Ghufran Hashmi, S., Martineau, D., Ibrahim Dar, M., T. Myllymäki, T. T., Sarikka, T., Ulla, V., Mohammed Zakeeruddin, S. & Grätzel, M. (2017). High performance carbon-based printed perovskite solar cells with humidity assisted thermal treatment. *Journal of Materials Chemistry A*, 5(24), 12060–12067. doi : 10.1039/C7TA04132B. Publisher : Royal Society of Chemistry.

Gielen, D., Boshell, F., Saygin, D., Bazilian, M. D., Wagner, N. & Gorini, R. (2019). The role of renewable energy in the global energy transformation. *Energy Strategy Reviews*, 24, 38–50. doi : 10.1016/j.esr.2019.01.006.

Gong, J., Cui, Y., Li, F. & Liu, M. (2023). Progress in surface modification of SnO2 electron transport layers for stable perovskite solar cells. *Small Science*, 3(6), 2200108. Type : Journal Article.

Gordillo, G., Torres, O. G., Abella, M. C., Peña, J. C. & Virguez, O. (2020). Improving the stability of MAPbI3 films by using a new synthesis route. *Journal of Materials Research and Technology*, 9(6), 13759–13769. Type : Journal Article.

Grote, C. & Berger, R. F. (2015). Strain tuning of tin–halide and lead–halide perovskites : a first-principles atomic and electronic structure study. *The Journal of Physical Chemistry C*, 119(40), 22832–22837. Type : Journal Article.

Guerrero, A., Garcia-Belmonte, G., Mora-Sero, I., Bisquert, J., Kang, Y. S., Jacobsson, T. J., Correa-Baena, J.-P. & Hagfeldt, A. (2016). Properties of contact and bulk impedances in hybrid lead halide perovskite solar cells including inductive loop elements. *The Journal of Physical Chemistry C*, 120(15), 8023–8032. Type : Journal Article.

Guerrero-Pérez, M. O. & Patience, G. S. (2020). Experimental methods in chemical engineering : Fourier transform infrared spectroscopy—FTIR. *The Canadian Journal of Chemical Engineering*, 98(1), 25–33. Type : Journal Article.

Guo, R., Dahal, B., Thapa, A., Poudel, Y. R., Liu, Y. & Li, W. (2021). Ambient processed (110) preferred MAPbI 3 thin films for highly efficient perovskite solar cells. *Nanoscale Advances*, 3(7), 2056–2064. Type : Journal Article.

Głowienka, D., Miruszewski, T. & Szmytkowski, J. (2018). The domination of ionic conductivity in tetragonal phase of the organometal halide perovskite CH3NH3PbI3-xClx. *Solid State Sciences*, 82, 19–23. Type : Journal Article.

Hadouchi, W. (2017). *Etude de l'utilisation du ZnO comme contact de type n dans des dispositifs photovoltaïques à base de pérovskite hybride*. (Thesis).

Hall, W. (1949). X-ray line broadening in metals. *Proceedings of the Physical Society. Section A*, 62(11), 741. Type : Journal Article.

Hamdi, M., Saleh, M. N. & Poulis, J. A. (2020). Improving the adhesion strength of polymers : effect of surface treatments. *Journal of Adhesion Science and Technology*. Repéré à https://www.tandfonline.com/doi/abs/10.1080/01694243.2020.1732750. Publisher : Taylor & Francis.

Heeger, A. J., MacDiarmid, A. G. & Shirakawa, H. (2000). The Nobel Prize in chemistry, 2000 : conductive polymers. *Stockholm, Sweden : Royal Swedish Academy of Sciences*, 1–16. Type : Journal Article.

Hernández, H. H., Reynoso, A. R., González, J. T., Morán, C. G., Hernández, J. M., Ruiz, A. M., Hernández, J. M. & Cruz, R. O. (2020). Electrochemical impedance spectroscopy (EIS) : A review study of basic aspects of the corrosion mechanism applied to steels. *Electrochemical Impedance Spectroscopy*, 137–144. Type : Journal Article.

Hilt, F., Hovish, M. Q., Rolston, N., Brüning, K., Tassone, C. J. & Dauskardt, R. H. (2018). Rapid route to efficient, scalable, and robust perovskite photovoltaics in air. *Energy & Environmental Science*, 11(8), 2102–2113. Type : Journal Article.

Homola, T., Pospisil, J., Shekargoftar, M., Svoboda, T., Hvojnik, M., Gemeiner, P., Weiter, M. & Dzik, P. (2020). Perovskite solar cells with low-cost TiO2 mesoporous photoanodes prepared by rapid low-temperature (70° C) plasma processing. *ACS Applied Energy Materials*, 3(12), 12009–12018. Type : Journal Article.

Hoque, M. N. F., Islam, N., Zhu, K. & Fan, Z. (2017). Hybrid perovskite phase transition and its ionic, electrical and optical properties. *MRS Advances*, 2(53), 3077–3082. Type : Journal Article.

Hsu, J. W. (2021). *Higher Throughput, Lower Cost Processing of Flexible Perovskite Solar Cells by Photonic Curing*.

Hsu, J. W. & Piper, R. T. (2024). Photonic curing for innovative fabrication of flexible metal oxide optoelectronics. *Journal of Physics D : Applied Physics*, 57(25), 252001. Type : Journal Article.

Hu, M., Zhang, L., She, S., Wu, J., Zhou, X., Li, X., Wang, D., Miao, J., Mi, G. & Chen, H. (2020a). Electron transporting bilayer of SnO2 and TiO2 nanocolloid enables highly efficient planar perovskite solar cells. *Solar RRL*, 4(1), 1900331. Type : Journal Article.

Hu, Q., Chen, W., Yang, W., Li, Y., Zhou, Y., Larson, B. W., Johnson, J. C., Lu, Y.-H., Zhong, W. & Xu, J. (2020b). Improving efficiency and stability of perovskite solar cells enabled by a near-infrared-absorbing moisture barrier. *Joule*, 4(7), 1575–1593. Type : Journal Article.

Hu, X., Zhang, X., Chen, X. & Luo, M. (2020c). Solution route to large area all-TiO2 one-dimensional photonic crystals with high reflectivity and different structural colors. *Nanotechnology*, 31(13), 135209. Type : Journal Article.

Huang, H., Cui, P., Chen, Y., Yan, L., Yue, X., Qu, S., Wang, X., Du, S., Liu, B. & Zhang, Q. (2022). 24.8%-efficient planar perovskite solar cells via ligand-engineered TiO2 deposition. *Joule*, 6(9), 2186–2202. Type : Journal Article.

Hutchinson, J. W. (1996). Stresses and failure modes in thin films and multilayers. *Notes for a Dcamm Course. Technical University of Denmark, Lyngby*, 1, 14. Type : Journal Article.

Hwang, H.-J., Oh, K.-H. & Kim, H.-S. (2016). All-photonic drying and sintering process via flash white light combined with deep-UV and near-infrared irradiation for highly conductive copper nano-ink. *Scientific reports*, 6(1), 19696. Type : Journal Article.

Iqbal, Z., Zu, F., Musiienko, A., Gutierrez-Partida, E., Kobler, H., Gries, T. W., Sannino, G. V., Canil, L., Koch, N., Stolterfoht, M. & others. (2023). Interface modification for energy level alignment and charge extraction in CsPbI3 perovskite solar cells. *ACS Energy Letters*, 8(10), 4304–4314. Publisher : ACS Publications.

Irfan, M., Ünlü, F., Lê, K., Fischer, T., Ullah, H. & Mathur, S. (2022). Electrospun Networks of ZnO-SnO2 Composite Nanowires as Electron Transport Materials for Perovskite Solar Cells. *Journal of Nanomaterials*, 2022, 1–13. Type : Journal Article.

Jassim, S. M., Bakr, N. A. & Mustafa, F. I. (2020). Synthesis and characterization of MAPbI3 thin film and its application in C-Si/perovskite tandem solar cell. *Journal of Materials Science : Materials in Electronics*, 31(19), 16199–16207. Type : Journal Article.

Jena, A. K., Kulkarni, A. & Miyasaka, T. (2019). Halide perovskite photovoltaics : background, status, and future prospects. *Chemical reviews*, 119(5), 3036–3103. Type : Journal Article.

Jeon, T., Jin, H. M., Lee, S. H., Lee, J. M., Park, H. I., Kim, M. K., Lee, K. J., Shin, B. & Kim, S. O. (2016). Laser crystallization of organic–inorganic hybrid perovskite solar cells. *ACS nano*, 10(8), 7907–7914. Type : Journal Article.

Jia, P., Qin, L., Zhao, D., Tang, Y., Song, B., Guo, J., Li, X., Li, L., Cui, Q. & Hu, Y. (2021). The trapped charges at grain boundaries in perovskite solar cells. *Advanced Functional Materials*, 31(49), 2107125. Type : Journal Article.

Jiang, Q., Chu, Z., Wang, P., Yang, X., Liu, H., Wang, Y., Yin, Z., Wu, J., Zhang, X. & You, J. (2017). Planar-structure perovskite solar cells with efficiency beyond 21%. *Advanced materials*, 29(46), 1703852. Type : Journal Article.

Jiang, S., Wang, R., Li, M., Yu, R., Wang, F. & Tan, Z. (2024). Synergistic electrical and light management enables efficient monolithic inorganic perovskite/organic tandem solar cells with over 24% efficiency. *Energy & Environmental Science*, 17(1), 219–226. Publisher : Royal Society of Chemistry.

Jin, B., Cao, J., Yuan, R., Cai, B., Wu, C. & Zheng, X. (2023). Strain relaxation for perovskite lattice reconfiguration. *Advanced Energy and Sustainability Research*, 4(4), 2200143. Type : Journal Article.

Jing, H., Zhu, Y., Peng, R.-W., Li, C.-Y., Xiong, B., Wang, Z., Liu, Y. & Wang, M. (2020). Hybrid organic-inorganic perovskite metamaterial for light trapping and photon-to-electron conversion. *Nanophotonics*, 9(10), 3323–3333. Type : Journal Article.

Jones, R. R., Hooper, D. C., Zhang, L., Wolverson, D. & Valev, V. K. (2019a). Raman techniques : fundamentals and frontiers. *Nanoscale research letters*, 14, 1–34. Type : Journal Article.

Jones, T. W., Osherov, A., Alsari, M., Sponseller, M., Duck, B. C., Jung, Y.-K., Settens, C., Niroui, F., Brenes, R. & Stan, C. V. (2019b). Lattice strain causes non-radiative losses in halide perovskites. *Energy & Environmental Science*, 12(2), 596–606. Type : Journal Article.

Joshua, A., Cheng, G. & Lau, E. (2023). Soft matter analysis via atomic force microscopy (AFM) : A review. *Applied Surface Science Advances*, 17, 100448. Type : Journal Article.

Karim, A., Khan, M. & Hossain, M. (2021). Temperature dependency of excitonic effective mass and charge carrier conduction mechanism in CH3NH3PbI3 - xClx thin films. *Scientific reports*, 11(1), 1–10.

Kauffmann, T. H., Kokanyan, N. & Fontana, M. D. (2019). Use of Stokes and anti-Stokes Raman scattering for new applications. *Journal of Raman Spectroscopy*, 50(3), 418–424. Type : Journal Article.

Kay, A. M., Riley, D. B., Meredith, P., Armin, A. & Sandberg, O. J. (2024). A New Framework for Understanding Recombination-Limited Charge Extraction in Disordered Semiconductors. *The Journal of Physical Chemistry Letters*, 15, 4416–4421. Publisher : ACS Publications.

Ke, W., Fang, G., Liu, Q., Xiong, L., Qin, P., Tao, H., Wang, J., Lei, H., Li, B. & Wan, J. (2015). Low-temperature solution-processed tin oxide as an alternative electron transporting layer for efficient perovskite solar cells. *Journal of the American Chemical Society*, 137(21), 6730–6733. Type : Journal Article.

Keshtmand, R., Zamani-Meymian, M. R., Mohamadkhani, F. & Taghavinia, N. (2021). Smoothing and coverage improvement of SnO2 electron transporting layer by NH4F treatment : Enhanced fill factor and efficiency of perovskite solar cells. *Solar Energy*, 228, 253–262. Publisher : Elsevier.

Kim, H., Seo, J. & Park, N. (2016). Material and device stability in perovskite solar cells. *ChemSusChem*, 9(18), 2528–2540. Type : Journal Article.

Kim, M., Choi, I.-w., Choi, S. J., Song, J. W., Mo, S.-I., An, J.-H., Jo, Y., Ahn, S., Ahn, S. K. & Kim, G.-H. (2021a). Enhanced electrical properties of Li-salts doped mesoporous TiO2 in perovskite solar cells. *Joule*, 5(3), 659–672. Type : Journal Article.

Kim, S. U., Kwon, M. J. & Yu, J.-W. (2022). Recrystallization and grain growth by intense pulsed light with mixed solvent annealing for efficient perovskite solar cells. *Organic Electronics*, 110, 106637. Type : Journal Article.

Kim, Y. C., An, H. J., Kim, D. H., Myoung, J., Heo, Y. J. & Cho, J. H. (2021b). High-performance perovskite-based blue light-emitting diodes with operational stability by using organic ammonium cations as passivating agents. *Advanced Functional Materials*, 31(5), 2005553. Type : Journal Article.

Knapp, E. & Ruhstaller, B. (2012). The role of shallow traps in dynamic characterization of organic semiconductor devices. *Journal of Applied Physics*, 112(2). Type : Journal Article.

Kwang, Z.-w., Chang, C.-W., Hsieh, T.-Y., Wei, T.-C. & Lu, S.-Y. (2018). Solvent-modulated reaction between mesoporous PbI2 film and CH3NH3I for enhancement of photovoltaic performances of perovskite solar cells. *Electrochimica Acta*, 266, 118–129. Type : Journal Article.

Laschuk, N. O., Easton, E. B. & Zenkina, O. V. (2021). Reducing the resistance for the use of electrochemical impedance spectroscopy analysis in materials chemistry. *RSC advances*, 11(45), 27925–27936. Type : Journal Article.

Lavery, B. W., Kumari, S., Konermann, H., Draper, G. L., Spurgeon, J. & Druffel, T. (2016). Intense pulsed light sintering of CH3NH3PbI3 solar cells. *ACS applied materials & interfaces*, 8(13), 8419–8426. Type : Journal Article.

Lee, J., Kim, B. S., Park, J., Lee, J. & Kim, K. (2023). Opportunities and challenges for perovskite solar cells based on vacuum thermal evaporation. *Advanced Materials Technologies*, 8(20), 2200928. Type : Journal Article.

Lee, J.-H., Deng, Z., Bristowe, N. C., Bristowe, P. D. & Cheetham, A. K. (2018). The competition between mechanical stability and charge carrier mobility in MA-based hybrid perovskites : insight from DFT. *Journal of Materials Chemistry C*, 6(45), 12252–12259. Type : Journal Article.

Lee, S.-W., Bae, S., Cho, K., Kim, S., Hwang, J.-K., Lee, W., Lee, S., Hyun, J. Y., Lee, S. & Choi, S. B. (2019). Sputtering of TiO2 for high-efficiency perovskite and 23.1% perovskite/silicon 4-terminal tandem solar cells. *ACS Applied Energy Materials*, 2(9), 6263–6268. Type : Journal Article.

Leguy, A. M., Hu, Y., Campoy-Quiles, M., Alonso, M. I., Weber, O. J., Azarhoosh, P., Van Schilfgaarde, M., Weller, M. T., Bein, T. & Nelson, J. (2015). Reversible hydration of CH3NH3PbI3 in films, single crystals, and solar cells. *Chemistry of Materials*, 27(9), 3397–3407. Type : Journal Article.

Leguy, A. M., Azarhoosh, P., Alonso, M. I., Campoy-Quiles, M., Weber, O. J., Yao, J., Bryant, D., Weller, M. T., Nelson, J. & Walsh, A. (2016). Experimental and theoretical optical properties of methylammonium lead halide perovskites. *Nanoscale*, 8(12), 6317–6327. Type : Journal Article.

Lei, Y., Liu, W., Li, C., Da, S., Zheng, Y., Wu, Y. & Ran, F. (2024). Microstress for metal halide perovskite solar cells : from source to influence and management. *Nanoscale*. Type : Journal Article.

Li, J. V. & Ferrari, G. (2018). *Capacitance spectroscopy of semiconductors*. CRC Press.

Li, L., Zhang, R., Wu, Z., Wang, Y., Hong, J., Rao, H., Pan, Z. & Zhong, X. (2023). Crystallization control of air-processed wide-bandgap perovskite for carbon-based perovskite solar cells with 17.69% efficiency. *Chemical Engineering Journal*, 455, 140566. Type : Journal Article.

Li, N., Yan, J., Ai, Y., Jiang, E., Lin, L., Shou, C., Yan, B., Sheng, J. & Ye, J. (2020). A low-temperature TiO2/SnO2 electron transport layer for high-performance planar perovskite solar cells. *Sci. China Mater*, 63, 207–215. Type : Journal Article.

Li, W. & Ning, Z. (2024). Performance enhancement of perovskite solar cells : surface is the key. *Science China Materials*, 67(1), 375–376. doi : 10.1007/s40843-023-2740-4.

Liang, C., Gu, H., Xia, J., Mei, S., Pang, P., Zhang, N., Guo, J., Guo, R., Shen, Y. & Yang, S. (2022). Recent Progress in Perovskite-Based Reversible Photon–Electricity Conversion Devices. *Advanced Functional Materials*, 32(8), 2108926. Type : Journal Article.

Liang, P., Liao, C., Chueh, C., Zuo, F., Williams, S. T., Xin, X., Lin, J. & Jen, A. K. (2014). Additive enhanced crystallization of solution-processed perovskite for highly efficient planar-heterojunction solar cells. *Advanced materials*, 26(22), 3748–3754. Type : Journal Article.

Liang, Z., Zhang, S., Xu, X., Wang, N., Wang, J., Wang, X., Bi, Z., Xu, G., Yuan, N. & Ding, J. (2015). A large grain size perovskite thin film with a dense structure for planar heterojunction solar cells via spray deposition under ambient conditions. *RSC advances*, 5(74), 60562–60569. Type : Journal Article.

Liao, K., Li, C., Xie, L., Yuan, Y., Wang, S., Cao, Z., Ding, L. & Hao, F. (2020). Hot-casting large-grain perovskite film for efficient solar cells : film formation and device performance. *Nano-Micro Letters*, 12, 1–22. Type : Journal Article.

Ling, P. S. V., Hagfeldt, A. & Sanchez, S. (2021). Flash infrared annealing for perovskite solar cell processing. *JoVE (Journal of Visualized Experiments)*, (168), e61730. Type : Journal Article.

Liu, C., Hu, M., Zhou, X., Wu, J., Zhang, L., Kong, W., Li, X., Zhao, X., Dai, S. & Xu, B. (2018a). Efficiency and stability enhancement of perovskite solar cells by introducing CsPbI3 quantum dots as an interface engineering layer. *NPG Asia materials*, 10(6), 552–561. Type : Journal Article.

Liu, H., Shi, G., Khan, R., Chu, S., Huang, Z., Shi, T., Sun, H., Li, Y., Zhou, H. & Xiao, P. (2024). Large-Area Flexible Perovskite Light-Emitting Diodes Enabled by Inkjet Printing. *Advanced Materials*, 36(8), 2309921. Type : Journal Article.

Liu, S.-C., Yang, Y., Li, Z., Xue, D.-J. & Hu, J.-S. (2020). GeSe thin-film solar cells. *Materials Chemistry Frontiers*, 4(3), 775–787. Type : Journal Article.

Liu, Z., Chang, J., Lin, Z., Zhou, L., Yang, Z., Chen, D., Zhang, C., Liu, S. & Hao, Y. (2018b). High-Performance Planar Perovskite Solar Cells Using Low Temperature, Solution–Combustion-Based Nickel Oxide Hole Transporting Layer with Efficiency Exceeding 20%. *Advanced Energy Materials*, 8(19), 1703432. Type : Journal Article.

Luo, D., Yu, L., Wang, H., Zou, T., Luo, L., Liu, Z. & Lu, Z. (2015). Cubic structure of the mixed halide perovskite CH 3 NH 3 PbI 3 x Cl x via thermal annealing. *RSC Advances*, 5(104), 85480–85485. Type : Journal Article.

Luo, Z., Liu, Y., Zhang, X., Wang, C., Wen, S., Zhang, W., Chen, S. & Zheng, W. (2023). Grain boundary engineering with Cl-terminated Ti2C quantum dots for enhancing perovskite solar cell performance. *ACS Sustainable Chemistry & Engineering*, 11(18), 7072–7082. Type : Journal Article.

Magar, H. S., Hassan, R. Y. & Mulchandani, A. (2021). Electrochemical impedance spectroscopy (EIS) : Principles, construction, and biosensing applications. *Sensors*, 21(19), 6578. Type : Journal Article.

Mahapatra, A., Parikh, N., Kumar, P., Kumar, M., Prochowicz, D., Kalam, A., Tavakoli, M. M. & Yadav, P. (2020). Changes in the electrical characteristics of perovskite solar cells with aging time. *Molecules*, 25(10), 2299. Type : Journal Article.

Makenali, M., Kazeminezhad, I., Ahmadi, V. & Roghabadi, F. A. (2021). Charge transfer balancing of planar perovskite solar cell based on a low cost and facile solution-processed CuO x as an efficient hole transporting layer. *Journal of Materials Science : Materials in Electronics*, 32, 2312–2325. Type : Journal Article.

Martínez-Denegri, G., Colodrero, S., Kramarenko, M. & Martorell, J. (2018). All-nanoparticle SnO2/TiO2 electron-transporting layers processed at low temperature for efficient thin-film perovskite solar cells. *ACS Applied Energy Materials*, 1(10), 5548–5556. Type : Journal Article.

Maskey, B. B., Koirala, G. R., Kim, Y., Park, H., Yadav, P., Park, J., Sun, J. & Cho, G. (2019). Photonic curing for enhancing the performance of roll-to-roll printed electronic devices. Type : Journal Article.

Matacena, I. (2019). Equivalent circuit extraction procedure from Nyquist plots for graphene-silicon solar cells. *2019 15th Conference on Ph.D Research in Microelectronics and Electronics (PRIME)*, pp. 273–276. doi : 10.1109/PRIME.2019.8787771.

Matacena, I., Guerriero, P., Lancellotti, L., Alfano, B., De Maria, A., La Ferrara, V., Mercaldo, L. V., Miglietta, M. L., Polichetti, T. & Rametta, G. (2023). Impedance spectroscopy analysis of perovskite solar cell stability. *Energies*, 16(13), 4951. Type : Journal Article.

Mehdi, H., Matheron, M., Mhamdi, A., Cros, S. & Bouazizi, A. (2021). Effect of the hole transporting layers on the inverted perovskite solar cells. *Journal of Materials Science : Materials in Electronics*, 32(16), 21579–21589. Type : Journal Article.

Meng, Q., Chen, Y., Xiao, Y. Y., Sun, J., Zhang, X., Han, C. B., Gao, H., Zhang, Y. & Yan, H. (2021). Effect of temperature on the performance of perovskite solar cells. *Journal of Materials Science : Materials in Electronics*, 32, 12784–12792. Type : Journal Article.

Middlemiss, L. A., Rennie, A. J., Sayers, R. & West, A. R. (2020). Characterisation of batteries by electrochemical impedance spectroscopy. *Energy Reports*, 6, 232–241. Type : Journal Article.

Min, M., Hossain, R. F., Adhikari, N. & Kaul, A. B. (2020). Inkjet-printed organohalide 2D layered perovskites for high-speed photodetectors on flexible polyimide substrates. *ACS applied materials & interfaces*, 12(9), 10809–10819. Type : Journal Article.

Miyata, A., Mitioglu, A., Plochocka, P., Portugall, O., Wang, J. T.-W., Stranks, S. D., Snaith, H. J. & Nicholas, R. J. (2015). Direct measurement of the exciton binding energy and effective masses for charge carriers in organic–inorganic tri-halide perovskites. *Nature Physics*, 11(7), 582–587. Type : Journal Article.

Mohammad, A. & Mahjabeen, F. (2023). Promises and Challenges of Perovskite Solar Cells : A Comprehensive Review. *BULLET : Jurnal Multidisiplin Ilmu*, 2(5), 1147–1157. Type : Journal Article.

Mohammed, A. & Abdullah, A. (2018). Scanning electron microscopy (SEM) : A review. *Proceedings of the 2018 International Conference on Hydraulics and Pneumatics—HERVEX, Băile Govora, Romania*, 2018, 7–9.

Montaño, B., Diaz, J. J., Koudriavtsev, I., Cosme, I., Korneev, N. & Mansurova, S. (2023). In-depth study of the effect of annealing temperature on the structural, chemical, and optical properties of MAPI thin films prepared by a one-step deposition method. *Journal of Materials Science : Materials in Electronics*, 34(12), 1016. doi : 10.1007/s10854-023-10437-3.

Mote, V., Purushotham, Y. & Dole, B. (2012). Williamson-Hall analysis in estimation of lattice strain in nanometer-sized ZnO particles. *Journal of theoretical and applied physics*, 6(1), 1–8. Type : Journal Article.

Mudgal, T., Bhadrachalam, K., Bischoff, P., Cormier, D., Manley, R. & Hirschman, K. (2017). Communication—CMOS thin-film transistors via Xe flash-lamp crystallization of patterned amorphous Si. *ECS Journal of Solid State Science and Technology*, 6(12), Q179. Type : Journal Article.

Mukhamedshina, D. M. & Beisenkhanov, N. B. (2012). Influence of crystallization on the properties of SnO2 thin films. Dans *Advances in Crystallization Processes*. IntechOpen.

Murali, B., Yengel, E., Peng, W., Chen, Z., Alias, M. S., Alarousu, E., Ooi, B. S., Burlakov, V., Goriely, A. & Eddaoudi, M. (2017). Temperature-induced lattice relaxation of perovskite crystal enhances optoelectronic properties and solar cell performance. *The journal of physical chemistry letters*, 8(1), 137–143. Type : Journal Article.

Namsheer, K. & Rout, C. S. (2021). Conducting polymers : a comprehensive review on recent advances in synthesis, properties and applications. *RSC advances*, 11(10), 5659–5697. Type : Journal Article.

Namvar, A., Dehghany, M., Sohrabpour, S. & Naghdabadi, R. (2016). Thermal residual stresses in silicon thin film solar cells under operational cyclic thermal loading : A finite element analysis. *Solar Energy*, 135, 366–373. Type : Journal Article.

Nandigana, P., Saminathan, B., Sriram, P., Sujatha, D., Subramanian, B. & Panda, S. K. (2024). An ambient process for hole transport layer-free highly stable MAPbI 3 by addition of MACl for efficient perovskite solar cells. *Energy Advances*, 3(2), 442–450. Type : Journal Article.

Nayak, M., Akthar, A. J., Guchhait, A. & Saha, S. K. (2021). A roadmap towards stable perovskite solar cells : prospective on substitution of organic (A) & inorganic (B) cations. *Journal of Materials Science : Materials in Electronics*, 32(14), 18466–18511. doi : 10.1007/s10854-021-06431-2.

Nayak, P. K., Moore, D. T., Wenger, B., Nayak, S., Haghighirad, A. A., Fineberg, A., Noel, N. K., Reid, O. G., Rumbles, G. & Kukura, P. (2016). Mechanism for rapid growth of organic–inorganic halide perovskite crystals. *Nature communications*, 7(1), 13303. Type : Journal Article.

Nijsse, F. J., Mercure, J.-F., Ameli, N., Larosa, F., Kothari, S., Rickman, J., Vercoulen, P. & Pollitt, H. (2023). The momentum of the solar energy transition. *Nature Communications*, 14(1), 6542. Type : Journal Article.

Nishimura, K., Hirotani, D., Kamarudin, M. A., Shen, Q., Toyoda, T., Iikubo, S., Minemoto, T., Yoshino, K. & Hayase, S. (2019). Relationship between lattice strain and efficiency for Sn-perovskite solar cells. *ACS applied materials & interfaces*, 11(34), 31105–31110. Type : Journal Article.

Nishimura, K., Kamarudin, M. A., Hirotani, D., Hamada, K., Shen, Q., Iikubo, S., Minemoto, T., Yoshino, K. & Hayase, S. (2020). Lead-free tin-halide perovskite solar cells with 13% efficiency. *Nano Energy*, 74, 104858. Type : Journal Article.

Nizamuddin, A., Arith, F., Rong, J., Zaim, M., Rahimi, A. S. & Saat, S. (2021). Investigation of copper (I) thiocyanate (CuSCN) as a hole transporting layer for perovskite solar cells application. *Journal of Advanced Research in Fluid Mechanics and Thermal Sciences*, 78(2), 153–159. Type : Journal Article.

NovaCentrix. (2024). The evolution of photonic curing. Repéré à https://pulseforge.com/pulseforge_blog/the-evolution-of-photonic-curing/.

NREL. (2024). Best Research-Cell Efficiency Chart. Repéré à https://www.nrel.gov/pv/cell-efficiency.html.

Orlando, A., Franceschini, F., Muscas, C., Pidkova, S., Bartoli, M., Rovere, M. & Tagliaferro, A. (2021). A comprehensive review on Raman spectroscopy applications. *Chemosensors*, 9(9), 262. Type : Journal Article.

Otoufi, M. K., Ranjbar, M., Kermanpur, A., Taghavinia, N., Minbashi, M., Forouzandeh, M. & Ebadi, F. (2020). Enhanced performance of planar perovskite solar cells using TiO2/SnO2 and TiO2/WO3 bilayer structures : Roles of the interfacial layers. *Solar Energy*, 208, 697–707. Type : Journal Article.

Pan, D., Fan, H., Li, Z., Wang, S., Huang, Y., Jiao, Y. & Yao, H. (2017). Influence of substrate on structural properties and photocatalytic activity of TiO2 films. *Micro & Nano Letters*, 12(2), 82–86. doi : 10.1049/mnl.2016.0550. _eprint : https ://onlinelibrary.wiley.com/doi/pdf/10.1049/mnl.2016.0550.

Pan, H., Shao, H., Zhang, X. L., Shen, Y. & Wang, M. (2021). Interface engineering for high-efficiency perovskite solar cells. *Journal of Applied Physics*, 129(13). Type : Journal Article.

Pandey, A., Dalal, S., Dutta, S. & Dixit, A. (2021). Structural characterization of polycrystalline thin films by X-ray diffraction techniques. *Journal of Materials Science : Materials in Electronics*, 32, 1341–1368. Publisher : Springer.

Park, N.-G. (2013). Organometal perovskite light absorbers toward a 20% efficiency low-cost solid-state mesoscopic solar cell. *The Journal of Physical Chemistry Letters*, 4(15), 2423–2429. Type : Journal Article.

Park, S. Y. & Zhu, K. (2022). Advances in SnO2 for efficient and stable n–i–p perovskite solar cells. *Advanced materials*, 34(27), 2110438. Type : Journal Article.

Pascoe, A. R., Duffy, N. W., Scully, A. D., Huang, F. & Cheng, Y.-B. (2015). Insights into planar CH3NH3PbI3 perovskite solar cells using impedance spectroscopy. *The Journal of Physical Chemistry C*, 119(9), 4444–4453. Type : Journal Article.

Patil, G. E., Kajale, D. D., Gaikwad, V. B. & Jain, G. H. (2012). Preparation and characterization of SnO2 nanoparticles by hydrothermal route. *International Nano Letters*, 2(1), 17. Publisher : Springer.

Patil, S. A., Hwang, H.-J., Yu, M.-H., Shrestha, N. K. & Kim, H.-S. (2017). Photonic sintering of a ZnO nanosheet photoanode using flash white light combined with deep UV irradiation for dye-sensitized solar cells. *RSC advances*, 7(11), 6565–6573. Type : Journal Article.

Patru, R. E., Khassaf, H., Pasuk, I., Botea, M., Trupina, L., Ganea, C.-P., Pintilie, L. & Pintilie, I. (2021). Tetragonal–Cubic Phase Transition and Low-Field Dielectric Properties of CH3NH3PbI3 Crystals. *Materials*, 14(15), 4215. Type : Journal Article.

Peiris, T. N., Benitez, J., Sutherland, L., Sharma, M., Michalska, M., Scully, A. D., Vak, D., Gao, M., Weerasinghe, H. C. & Jasieniak, J. (2022). A stable aqueous SnO2 nanoparticle dispersion for roll-to-Roll fabrication of flexible perovskite solar cells. *Coatings*, 12(12), 1948. Publisher : MDPI.

Peng, J. (2006). *Determination of residual stresses in coating by pseudo-grazing incidence X-Ray diffraction method*. (Thesis).

Perrin, L., Lemercier, T., Planès, E., Berson, S. & Flandin, L. (2021). Perovskite Inverted Solar Cells : Impact of Hole Transport Layer and Anti-Solvent Ejection Time. *2021 IEEE 48th Photovoltaic Specialists Conference (PVSC)*, pp. 1324–1327. doi : 10.1109/PVSC43889.2021.9518490.

Piper, R. T., Daunis, T. B., Xu, W., Schroder, K. A. & Hsu, J. W. (2021). Photonic curing of nickel oxide transport layer and perovskite active layer for flexible perovskite solar cells : a path towards high-throughput manufacturing. *Frontiers in Energy Research*, 9, 640960. Type : Journal Article.

Piper, R. T., Xu, W. & Hsu, J. W. (2022). How Optical and Electrical Properties of ITO Coated Willow Glass Affect Photonic Curing Outcome for Upscaling Perovskite Solar Cell Manufacturing. *IEEE Journal of Photovoltaics*, 12(3), 722–727. Type : Journal Article.

Pramanick, A., Wang, X., Hoffmann, C., Diallo, S., Jørgensen, M. & Wang, X.-L. (2015). Microdomain dynamics in single-crystal BaTi O 3 during paraelectric-ferroelectric phase transition measured with time-of-flight neutron scattering. *Physical Review B*, 92(17), 174103. Type : Journal Article.

Prochowicz, D., Trivedi, S., Parikh, N., Saliba, M., Kalam, A., Mahdi Tavakoli, M. & Yadav, P. (2021). In the Quest of Low-Frequency Impedance Spectra of Efficient Perovskite Solar Cells. *Energy Technology*, 9(7), 2100229. Type : Journal Article.

Qiao, L., Fang, W.-H., Long, R. & Prezhdo, O. V. (2021). Elimination of Charge Recombination Centers in Metal Halide Perovskites by Strain. *Journal of the American Chemical Society*, 143(26), 9982–9990. Type : Journal Article.

Qiu, L., He, S., Yang, J., Deng, J. & Peng, H. (2016). Fiber-shaped perovskite solar cells with high power conversion efficiency. *Small*, 12(18), 2419–2424. Type : Journal Article.

Raman, C. V. (1928). A new radiation. *Indian Journal of physics*, 2, 387–398. Type : Journal Article.

Regalado-Pérez, E., Díaz-Cruz, E. B., Landa-Bautista, J., Mathews, N. & Mathew, X. (2021). Impact of vertical inhomogeneity on the charge extraction in perovskite solar cells : a study by depth-dependent photoluminescence. *ACS Applied Materials & Interfaces*, 13(10), 11833–11844. Type : Journal Article.

Ren, N., Zhu, C., Li, R., Mazumdar, S., Sun, C., Chen, B., Xu, Q., Wang, P., Shi, B. & Huang, Q. (2022). 50° C low-temperature ALD SnO2 driven by H2O2 for efficient perovskite and perovskite/silicon tandem solar cells. *Applied Physics Letters*, 121(3). Type : Journal Article.

Ren, X., Yang, Z., Yang, D., Zhang, X., Cui, D., Liu, Y., Wei, Q., Fan, H. & Liu, S. F. (2016). Modulating crystal grain size and optoelectronic properties of perovskite films for solar cells by reaction temperature. *Nanoscale*, 8(6), 3816–3822. Type : Journal Article.

Ren, Z., Wang, N., Wei, P., Cui, M., Li, X. & Qin, C. (2020). Ultraviolet-ozone modification on TiO2 surface to promote both efficiency and stability of low-temperature planar perovskite solar cells. *Chemical Engineering Journal*, 393, 124731. Type : Journal Article.

Robinson, I. & Harder, R. (2009). Coherent X-ray diffraction imaging of strain at the nanoscale. *Nature materials*, 8(4), 291–298. Type : Journal Article.

Rodriguez, M. A., Babuska, T. F., Curry, J., Griego, J. J., Dugger, M. T., Larson, S. R. & Mings, A. (2024). Characterization of MoS2 films via simultaneous grazing incidence X-ray diffraction and grazing incidence X-ray fluorescence (GIXRD/GIXRF). *Powder Diffraction*, 1–9. Type : Journal Article.

Rolston, N., Bush, K. A., Printz, A. D., Gold-Parker, A., Ding, Y., Toney, M. F., McGehee, M. D. & Dauskardt, R. H. (2018). Engineering stress in perovskite solar cells to improve stability. *Advanced Energy Materials*, 8(29), 1802139. Type : Journal Article.

Rong, Y., Hou, X., Hu, Y., Mei, A., Liu, L., Wang, P. & Han, H. (2017). Synergy of ammonium chloride and moisture on perovskite crystallization for efficient printable mesoscopic solar cells. *Nature communications*, 8(1), 1–8. Type : Journal Article.

Rong, Y., Hu, Y., Mei, A., Tan, H., Saidaminov, M. I., Seok, S. I., McGehee, M. D., Sargent, E. H. & Han, H. (2018). Challenges for commercializing perovskite solar cells. *Science*, 361(6408), eaat8235. Type : Journal Article.

Saffari, M., Mohebpour, M. A., Soleimani, H. R. & Tagani, M. B. (2017). DFT analysis and FDTD simulation of CH3NH3PbI3 xClx mixed halide perovskite solar cells : role of halide mixing and light trapping technique. *Journal of Physics D : Applied Physics*, 50(41), 415501.

Sajid, S., Elseman, A. M., Huang, H., Ji, J., Dou, S., Jiang, H., Liu, X., Wei, D., Cui, P. & Li, M. (2018). Breakthroughs in NiOx-HTMs towards stable, low-cost and efficient perovskite solar cells. *Nano Energy*, 51, 408–424. Type : Journal Article.

Salado, M., Contreras-Bernal, L., Caliò, L., Todinova, A., López-Santos, C., Ahmad, S., Borras, A., Idígoras, J. & Anta, J. A. (2017). Impact of moisture on efficiency-determining electronic processes in perovskite solar cells. *Journal of Materials Chemistry A*, 5(22), 10917–10927. Type : Journal Article.

Salek Esfahani, S. (2022). Photoelectrochemistry of lead halide perovskite. Type : Journal Article.

Sanchez, S., Hua, X., Phung, N., Steiner, U. & Abate, A. (2018). Flash infrared annealing for antisolvent-free highly efficient perovskite solar cells. *Advanced Energy Materials*, 8(12), 1702915. Type : Journal Article.

Saraf, R. (2020). Polymer-Integrated Organolead Halide Perovskite for Solar Cells and Self-Powered Electronic Devices. Type : Journal.

Sarda, N., Vidhan, A., Basak, S., Hazra, P., Behera, T., Ghosh, S., Choudhary, R. J., Chowdhury, A. & Sarkar, S. K. (2023). Photonically Cured Solution-Processed SnO2 Thin Films for High-Efficiency and Stable Perovskite Solar Cells and Minimodules. *ACS Applied Energy Materials*, 6(7), 3996–4006. Type : Journal Article.

Schileo, G. & Grancini, G. (2021). Lead or no lead ? Availability, toxicity, sustainability and environmental impact of lead-free perovskite solar cells. *Journal of materials chemistry C*, 9(1), 67–76. Type : Journal Article.

Schroder, K. A. (2011). Mechanisms of photonic curing™ : Processing high temperature films on low temperature substrates. *Nanotechnology*, 2, 220–223. Type : Journal Article.

Schube, J., Fellmeth, T., Maier, F., Keding, R., Clement, F. & Glunz, S. W. (2018). Applicability of photonic sintering and autoclaving as alternative contact formation methods for silicon solar cells with passivating contacts. *AIP Conference Proceedings*, 1999.

Schwartz, J. J., Jakob, D. S. & Centrone, A. (2022). A guide to nanoscale IR spectroscopy : resonance enhanced transduction in contact and tapping mode AFM-IR. *Chemical Society Reviews*, 51(13), 5248–5267. Type : Journal Article.

Secor, E. B., Ahn, B. Y., Gao, T. Z., Lewis, J. A. & Hersam, M. C. (2015). Rapid and versatile photonic annealing of graphene inks for flexible printed electronics. *Advanced Materials*, 27(42), 6683–6688. Type : Journal Article.

Segovia, R., Qu, G., Peng, M., Sun, X., Shi, H. & Gao, B. (2018). Evolution of Photoluminescence, Raman, and Structure of CH 3 NH 3 PbI 3 Perovskite Microwires Under Humidity Exposure. *Nanoscale research letters*, 13(1), 1–8. Type : Journal Article.

Semerci, A., Buyruk, A., Emin, S., Hooijer, R., Kovacheva, D., Mayer, P., Reus, M. A., Blätte, D., Günther, M. & Hartmann, N. F. (2023). A Novel Multi-Functional Thiophene-Based Organic Cation as Passivation, Crystalline Orientation, and Organic Spacer Agent for Low-Dimensional 3D/1D Perovskite Solar Cells. *Advanced Optical Materials*, 11(16), 2300267. Type : Journal Article.

Sen, S. & Islam, R. (2022). Investigation of Charge Carrier Transport of Bulk Heterojunction Organic Solar Cell Using Photo-CELIV Electrical Simulation. *Proceedings of the National Academy of Sciences, India Section A : Physical Sciences*, 92(4), 713–717. Publisher : Springer.

Seo, S., Shin, S., Kim, E., Jeong, S., Park, N.-G. & Shin, H. (2021). Amorphous TiO2 coatings stabilize perovskite solar cells. *ACS Energy Letters*, 6(9), 3332–3341. Type : Journal Article.

Serafini, P., Boix, P. P., Barea, E. M., Edvinson, T., Sánchez, S. & Mora-Seró, I. (2022). Photonic Processing of MAPbI3 Films by Flash Annealing and Rapid Growth for High-Performance Perovskite Solar Cells. *Solar RRL*, 6(12), 2200641. doi : 10.1002/solr.202200641. _-eprint : https ://onlinelibrary.wiley.com/doi/pdf/10.1002/solr.202200641.

Shan, D., Tong, G., Cao, Y., Tang, M., Xu, J., Yu, L. & Chen, K. (2019). The effect of decomposed PbI2 on microscopic mechanisms of scattering in CH3NH3PbI3 films. *Nanoscale Research Letters*, 14(1), 1–6. Type : Journal Article.

Shao, J.-Y., Li, D., Shi, J., Ma, C., Wang, Y., Liu, X., Jiang, X., Hao, M., Zhang, L. & Liu, C. (2023). Recent progress in perovskite solar cells : material science. *Science China Chemistry*, 66(1), 10–64. Type : Journal Article.

Sharif, R., Khalid, A., Ahmad, S. W., Rehman, A., Qutab, H. G., Akhtar, H. H., Mahmood, K., Afzal, S. & Saleem, F. (2023). A comprehensive review of the current progresses and material advances in perovskite solar cells. *Nanoscale Advances*, 5(15), 3803–3833. Type : Journal Article.

Shi, S., Li, J., Bu, T., Yang, S., Xiao, J., Peng, Y., Li, W., Zhong, J., Ku, Z. & Cheng, Y.-B. (2019). Room-temperature synthesized SnO 2 electron transport layers for efficient perovskite solar cells. *RSC advances*, 9(18), 9946–9950. Type : Journal Article.

Shibuya, H., Inoue, S. & Ihara, M. (2009). Evaluation of dye-sensitized solar cells using forward bias applied impedance spectroscopy under dark. *ECS Transactions*, 16(50), 93. Type : Journal Article.

Shih, C. F., Zhang, T., Li, J. & Bai, C. (2018). Powering the Future with Liquid Sunshine. *Joule*, 2(10), 1925–1949. doi : 10.1016/j.joule.2018.08.016.

Shohan, S., Harm, J., Hasan, M., Starly, B. & Shirwaiker, R. (2021). Non-destructive quality monitoring of 3D printed tissue scaffolds via dielectric impedance spectroscopy and supervised machine learning. *Procedia Manufacturing*, 53, 636–643. Type : Journal Article.

Shrivastav, N., Madan, J. & Pandey, R. (2024). Optimizing tandem solar cells efficiency through current matching technique in lead-free perovskite/c-Si and lead-free perovskite/CIGS absorbers. *Indian Journal of Physics*, 1–9. Type : Journal Article.

Sinclair, D. C. (1995). Characterisation of electro-materials using ac impedance spectroscopy. *Boletín de la Sociedad Española de Cerámica y Vidrio*, 34(2), 55–65. Type : Journal Article.

Singh, R. K., Jain, N., Singh, J. & Kumar, R. (2017). Stability behavior of chemically synthesized organic electrolyte salts and methylammonium lead halide perovskite light harvester. *Adv Mater Lett*, 8(6), 707–711. Type : Journal Article.

Slimani, M. A. (2019). *Cellules solaires pérovskites imprimées et optimisation des couches pérovskites pour les cellules tandems*. (Thesis).

Slimani, M. A., Benavides-Guerrero, J. A., Cloutier, S. G. & Izquierdo, R. (2024a). Enhancing the Performance of Nanocrystalline SnO2 for Solar Cells through Photonic Curing Using Impedance Spectroscopy Analysis. *Nanomaterials*, 14(18), 1508. doi : 10.3390/nano14181508. Number : 18 Publisher : Multidisciplinary Digital Publishing Institute.

Slimani, M. A., Cloutier, S. G. & Izquierdo, R. (2024b). Recent Advances in the Photonic Curing of the Hole Transport Layer, the Electron Transport Layer, and the Perovskite Layers to Improve the Performance of Perovskite Solar Cells. *Nanomaterials*, 14(10), 886. Type : Journal Article.

Song, H. (2010). *Analyse expérimentale et numérique de la distribution des contraintes résiduelles induites par choc-laser dans les alliages d'aluminium*. (Thesis).

Song, L. (2022). Perovskite solar cells toward industrialization : Screen printed perovskite films. *Materials Reports : Energy*, 2, 100171.

Song, S., Kang, G., Pyeon, L., Lim, C., Lee, G.-Y., Park, T. & Choi, J. (2017). Systematically optimized bilayered electron transport layer for highly efficient planar perovskite solar cells (n = 21.1%). *ACS Energy Letters*, 2(12), 2667–2673.

Spalla, M. (2019). *Stabilité intrinsèque des cellules solaires pérovskites : impact de la formulation de la couche active et des couches de transport de charges*. (Thesis).

Steele, J. A., Jin, H., Dovgaliuk, I., Berger, R. F., Braeckevelt, T., Yuan, H., Martin, C., Solano, E., Lejaeghere, K. & Rogge, S. M. (2019). Thermal unequilibrium of strained black CsPbI3 thin films. *Science*, 365(6454), 679–684. Type : Journal Article.

Stephen, M., Genevičius, K., Juška, G., Arlauskas, K. & Hiorns, R. C. (2017). Charge transport and its characterization using photo-CELIV in bulk heterojunction solar cells. *Polymer International*, 66(1), 13–25. Type : Journal Article.

Subbiah, A. S., Halder, A., Ghosh, S., Mahuli, N., Hodes, G. & Sarkar, S. K. (2014). Inorganic hole conducting layers for perovskite-based solar cells. *The journal of physical chemistry letters*, 5(10), 1748–1753. Type : Journal Article.

Sum, T. C. & Mathews, N. (2014). Advancements in perovskite solar cells : photophysics behind the photovoltaics. *Energy & Environmental Science*, 7(8), 2518–2534. Type : Journal Article.

Sun, K., Guo, R., Liang, Y., Heger, J. E., Liu, S., Yin, S., Reus, M. A., Spanier, L. V., Deschler, F. & Bernstorff, S. (2023a). Morphological insights into the degradation of perovskite solar cells under light and humidity. *ACS Applied Materials & Interfaces*, 15(25), 30342–30349. Type : Journal Article.

Sun, X., Li, L., Shen, S. & Wang, F. (2023b). TiO2/SnO2 Bilayer Electron Transport Layer for High Efficiency Perovskite Solar Cells. *Nanomaterials*, 13(2), 249. Type : Journal Article.

Sun, Y., Chen, W., Wu, Y., He, Z., Zhang, S. & Chen, S. (2019). A low-temperature-annealed and UV-ozone-enhanced combustion derived nickel oxide hole injection layer for flexible quantum dot light-emitting diodes. *Nanoscale*, 11(3), 1021–1028. Type : Journal Article.

Suo, Z., Xiao, Z., Li, S., Liu, J., Xin, Y., Meng, L., Liang, H., Kan, B., Yao, Z., Li, C. & others. (2023). Efficient and stable inverted structure organic solar cells utilizing surface-modified SnO2 as the electron transport layer. *Nano Energy*, 118, 109032. Publisher : Elsevier.

Sánchez, S., Vallés-Pelarda, M., Alberola-Borràs, J.-A., Vidal, R., Jerónimo-Rendón, J. J., Saliba, M., Boix, P. P. & Mora-Seró, I. (2019). Flash infrared annealing as a cost-effective and low environmental impact processing method for planar perovskite solar cells. *Materials Today*, 31, 39–46. Type : Journal Article.

Sánchez, S., Jerónimo-Rendon, J., Saliba, M. & Hagfeldt, A. (2020). Highly efficient and rapid manufactured perovskite solar cells via Flash InfraRed Annealing. *Materials Today*, 35, 9–15. Type : Journal Article.

Tavakoli, M. M., Yadav, P., Tavakoli, R. & Kong, J. (2018). Surface engineering of TiO2 ETL for highly efficient and hysteresis-less planar perovskite solar cell (21.4%) with enhanced open-circuit voltage and stability. *Advanced Energy Materials*, 8(23), 1800794. Type : Journal Article.

Tennyson, E. M., Doherty, T. A. & Stranks, S. D. (2019). Heterogeneity at multiple length scales in halide perovskite semiconductors. *Nature Reviews Materials*, 4(9), 573–587. Repéré à https://idp.nature.com/authorize/casa?redirect_uri=https://www.nature.com/articles/s41578-019-0125-0&casa_token=SsRbwYXp8fIAAAAA:65juYVrlqvqoFICYkQ3qa0wFfXxp1406ZShI3DpaFB7ji7BuaE5G12u5GQSRohrlCmTX4JSPyG40nWyh. Publisher : Nature Publishing Group UK London.

Tkachenko, Y. & Niedzielski, P. (2022). FTIR as a method for qualitative assessment of solid samples in geochemical research : a review. *Molecules*, 27(24), 8846. Type : Journal Article.

Todinova, A., Contreras-Bernal, L., Salado, M., Ahmad, S., Morillo, N., Idígoras, J. & Anta, J. A. (2017). Towards a universal approach for the analysis of impedance spectra of perovskite solar cells : equivalent circuits and empirical analysis. *ChemElectroChem*, 4(11), 2891–2901. Type : Journal Article.

Touzani, L. (2023). LES ENERGIES RENOUVENABLES AU MAROC : ENERGIE SOLAIRE. *La Revue D'économie et D'environnement*, 3(1), 28–44. Repéré à https://revuecoenvi.org/index.php/laree/article/view/24. Number : 1.

Troughton, J., Charbonneau, C., Carnie, M. J., Davies, M. L., Worsley, D. A. & Watson, T. M. (2015). Rapid processing of perovskite solar cells in under 2.5 seconds. *Journal of Materials Chemistry A*, 3(17), 9123–9127.

Troughton, J., Carnie, M. J., Davies, M. L., Charbonneau, C., Jewell, E. H., Worsley, D. A. & Watson, T. M. (2016). Photonic flash-annealing of lead halide perovskite solar cells in 1 ms. *Journal of Materials Chemistry A*, 4(9), 3471–3476. Type : Journal Article.

Tu, Y., Wu, J., Xu, G., Yang, X., Cai, R., Gong, Q., Zhu, R. & Huang, W. (2021). Perovskite Solar Cells for Space Applications : Progress and Challenges. *Advanced Materials*, 33(21), 2006545. doi : 10.1002/adma.202006545. _eprint : https ://onlinelibrary.wiley.com/doi/pdf/10.1002/adma.202006545.

Umeda, K., McArthur, S. J. & Kodera, N. (2023). Spatiotemporal resolution in high-speed atomic force microscopy for studying biological macromolecules in action. *Microscopy*, 72(2), 151–161. Type : Journal Article.

Vaenas, N., Konios, D., Stergiopoulos, T. & Kymakis, E. (2015). Slow photocharging and reduced hysteresis in low-temperature processed planar perovskite solar cells. *RSC advances*, 5(130), 107771–107776. Type : Journal Article.

Wang, C., Xiao, C., Yu, Y., Zhao, D., Awni, R. A., Grice, C. R., Ghimire, K., Constantinou, I., Liao, W. & Cimaroli, A. J. (2017a). Understanding and eliminating hysteresis for highly efficient planar perovskite solar cells. *Advanced Energy Materials*, 7(17), 1700414. Type : Journal Article.

Wang, D.-L., Cui, H.-J., Hou, G.-J., Zhu, Z.-G., Yan, Q.-B. & Su, G. (2016). Highly efficient light management for perovskite solar cells. *Scientific Reports*, 6(1), 18922. doi : 10.1038/srep18922. Publisher : Nature Publishing Group.

Wang, H.-Q., Wang, S., Chen, L., Yin, Z., Mei, S., Zhong, Y., Yao, Y., Li, N., Wang, J. & Song, W. (2021a). Understanding degradation mechanisms of perovskite solar cells due to electrochemical metallization effect. *Solar Energy Materials and Solar Cells*, 230, 111278. Type : Journal Article.

Wang, H., Zhu, C., Liu, L., Ma, S., Liu, P., Wu, J., Shi, C., Du, Q., Hao, Y. & Xiang, S. (2019). Interfacial residual stress relaxation in perovskite solar cells with improved stability. *Advanced Materials*, 31(48), 1904408. Type : Journal Article.

Wang, Q., Shao, Y., Xie, H., Lyu, L., Liu, X., Gao, Y. & Huang, J. (2014). Qualifying composition dependent p and n self-doping in CH3NH3PbI3. *Applied Physics Letters*, 105(16), 163508. Type : Journal Article.

Wang, S. (2024). *Stabilizing metastable lead-free double perovskite by morphological and molecular level dimensional reduction*. (Text.PhDThesis, Ludwig-Maximilians-Universität München). Repéré à https://edoc.ub.uni-muenchen.de/34201/.

Wang, S., Hu, J., Wang, A., Cui, Y., Chen, B., Niu, X. & Hao, F. (2022a). Facile lattice tensile strain compensation in mixed-cation halide perovskite solar cells. *Journal of Energy Chemistry*, 66, 422–428. Type : Journal Article.

Wang, T., Hou, S., Zhang, H., Yang, Y., Xu, W., Ao, T., Kang, M., Pan, G. & Mao, Y. (2021b). Highly controllable synthesis of MAPbI3 perovskite nanocrystals with long carrier lifetimes and narrow band gap for application in photodetectors. *Journal of Alloys and Compounds*, 872, 159589. Type : Journal Article.

Wang, X., Feng, Y., Sun, K., Chai, N., Mai, B., Li, S., Chen, X., Zhao, W. & Zhang, Q. (2024). Ultrafast Laser-Induced Excellent Thermoelectric Performance of PEDOT : PSS Films. *Energy & Environmental Materials*, 7(3), e12650. Type : Journal Article.

Wang, Y., Su, N., Liu, J., Lin, Y., Wang, J., Guo, X., Zhang, Y., Qin, Z., Liu, J., Zhang, C. & others. (2022b). Enhanced visible-light photocatalytic properties of SnO2 quantum dots by niobium modification. *Results in Physics*, 37, 105515. Publisher : Elsevier.

Wang, Y., Duan, L., Zhang, M., Hameiri, Z., Liu, X., Bai, Y. & Hao, X. (2022c). PTAA as efficient hole transport materials in perovskite solar cells : a review. *Solar RRL*, 6(8), 2200234. Type : Journal Article.

Wang, Y., Mahmoudi, T., Rho, W.-Y., Yang, H.-Y., Seo, S., Bhat, K. S., Ahmad, R. & Hahn, Y.-B. (2017b). Ambient-air-solution-processed efficient and highly stable perovskite solar cells based on CH3NH3PbI3 xClx-NiO composite with Al2O3/NiO interfacial engineering. *Nano Energy*, 40, 408–417. Type : Journal Article.

Weber, D. (1978). CH3NH3PbX3, ein Pb (II)-system mit kubischer perowskitstruktur/CH3NH3PbX3, a Pb (II)-system with cubic perovskite structure. *Zeitschrift für Naturforschung B*, 33(12), 1443–1445. Type : Journal Article.

Wehrenfennig, C., Eperon, G. E., Johnston, M. B., Snaith, H. J. & Herz, L. M. (2014). High charge carrier mobilities and lifetimes in organolead trihalide perovskites. *Advanced materials*, 26(10), 1584–1589. Type : Journal Article.

Wei, Z., Zhao, Y., Jiang, J., Yan, W., Feng, Y. & Ma, J. (2020). Research progress on hybrid organic–inorganic perovskites for photo-applications. *Chinese Chemical Letters*, 31(12), 3055–3064. Type : Journal Article.

Wijesinghe, U., Tetlow, W. D., Maiello, P., Fleck, N., O'Dowd, G., Beattie, N. S., Longo, G. & Hutter, O. S. (2024). Crystalline Antimony Selenide Thin Films for Optoelectronics through Photonic Curing. *Chemistry of Materials*. Type : Journal Article.

Wolff, C. M., Zu, F., Paulke, A., Toro, L. P., Koch, N. & Neher, D. (2017). Reduced interface-mediated recombination for high open-circuit voltages in CH3NH3PbI3 solar cells. *Advanced materials*, 29(28), 1700159. Type : Journal Article.

Word, E. (2024). Fostering Effective Energy Transition 2024. Repéré à https://www.weforum.org/publications/fostering-effective-energy-transition-2024/.

Wozny, S., Yang, M., Nardes, A. M., Mercado, C. C., Ferrere, S., Reese, M. O., Zhou, W. & Zhu, K. (2015). Controlled humidity study on the formation of higher efficiency formamidinium lead triiodide-based solar cells. *Chemistry of Materials*, 27(13), 4814–4820. Type : Journal Article.

Wu, J., Liu, S.-C., Li, Z., Wang, S., Xue, D.-J., Lin, Y. & Hu, J.-S. (2021). Strain in perovskite solar cells : origins, impacts and regulation. *National science review*, 8(8), nwab047. Type : Journal Article.

Wu, W. (2017). Inorganic nanomaterials for printed electronics : a review. *Nanoscale*, 9(22), 7342–7372. doi : 10.1039/C7NR01604B. Publisher : Royal Society of Chemistry.

Xie, H., Yin, X., Chen, P., Liu, J., Yang, C., Que, W. & Wang, G. (2019). Solvothermal synthesis of highly crystalline SnO2 nanoparticles for flexible perovskite solar cells application. *Materials Letters*, 234, 311–314. Type : Journal Article.

Xie, Z., Feng, K., Xiong, Y., Chen, X., Liang, Y., Abid, K. & Xu, L. (2021). A High Seebeck Voltage Thermoelectric Module with P-type and N-type MAPbI3 Perovskite Single Crystals. *Advanced Electronic Materials*, 7(3), 2001003. Type : Journal Article.

Xiong, L., Guo, Y., Wen, J., Liu, H., Yang, G., Qin, P. & Fang, G. (2018). Review on the application of SnO2 in perovskite solar cells. *Advanced Functional Materials*, 28(35), 1802757. Type : Journal Article.

Xiong, S., Hou, Z., Zou, S., Lu, X., Yang, J., Hao, T., Zhou, Z., Xu, J., Zeng, Y. & Xiao, W. (2021). Direct observation on p-to n-type transformation of perovskite surface region during defect passivation driving high photovoltaic efficiency. *Joule*, 5(2), 467–480. Type : Journal Article.

Xu, L., Yuan, S., Zeng, H. & Song, J. (2019). A comprehensive review of doping in perovskite nanocrystals/quantum dots : evolution of structure, electronics, optics, and light-emitting diodes. *Materials Today Nano*, 6, 100036. Type : Journal Article.

Xu, W., Hart, L. J., Moss, B., Caprioglio, P., Macdonald, T. J., Furlan, F., Panidi, J., Oliver, R. D., Pacalaj, R. A. & Heeney, M. (2023a). Impact of Interface Energetic Alignment and Mobile Ions on Charge Carrier Accumulation and Extraction in p-i-n Perovskite Solar Cells. *Advanced Energy Materials*, 13(36), 2301102. Type : Journal Article.

Xu, W., Daunis, T. B., Piper, R. T. & Hsu, J. W. (2020a). Effects of photonic curing processing conditions on MAPbI3 film properties and solar cell performance. *ACS Applied Energy Materials*, 3(9), 8636–8645. Type : Journal Article.

Xu, W., Piper, R. T., Daunis, T. B., Schroder, K. A. & Hsu, J. W. (2020b). Photonic Curing Enabling High-Speed Processing for Perovskite Solar Cells. *2020 47th IEEE Photovoltaic Specialists Conference (PVSC)*, pp. 0079–0081.

Xu, W., Piper, R. T., Zheng, Y., Malko, A. V. & Hsu, J. W. (2022). Elucidating Diiodomethane-Induced Improvement in Photonically Cured MAPbI3 Solar Cells. *ACS Applied Energy Materials*, 5(6), 7328–7334. Type : Journal Article.

Xu, W., Bonner, J. C., Piper, R. T. & Hsu, J. W. (2023b). Effects of Residual DMSO Adduct on Photonically Cured MAPbI3 Solar Cells. *The Journal of Physical Chemistry C*, 127(30), 14933–14939. Type : Journal Article.

Xu, Y., Xia, R., Gao, J., Wang, S., Zhu, J., Xiong, W., Yuan, N. & Ding, J. (2023c). A Facile Approach for the Encapsulation of Perovskite Solar Cells. *Energies*, 16(2), 598. Publisher : MDPI.

Xue, T., Chen, D., Li, T., Chou, X., Wang, X., Tang, Z., Zhang, F., Huang, J., Guo, K. & Takaloo, A. V. (2023). Boosting the Performance of Perovskite Solar Cells through Systematic Investigation of the Annealing Effect of E-Beam Evaporated TiO2. *Micromachines*, 14(6), 1095. Type : Journal Article.

Yamada, T., Yamada, Y. & Kanemitsu, Y. (2020). Photon recycling in perovskite CH3NH3PbX3 (X= I, Br, Cl) bulk single crystals and polycrystalline films. *Journal of Luminescence*, 220, 116987. Type : Journal Article.

Yang, J., Meissner, M., Yamaguchi, T., Zhang, X., Ueba, T., Cheng, L., Ideta, S., Tanaka, K., Zeng, X. & Ueno, N. (2018). Band dispersion and hole effective mass of methylammonium lead iodide perovskite. *Solar RRL*, 2(10), 1800132. Type : Journal Article.

Yang, Y., Yang, L. & Feng, S. (2020). Interfacial engineering and film-forming mechanism of perovskite films revealed by synchrotron-based GIXRD at SSRF for high-performance solar cells. *Materials Today Advances*, 6, 100068. Type : Journal Article.

Yang, Z., Lai, J., Zhu, R., Tan, J., Luo, Y. & Ye, S. (2022). Electronic Disorder Dominates the Charge-Carrier Dynamics in Two-Dimensional/Three-Dimensional Organic–Inorganic Perovskite Heterostructure. *The Journal of Physical Chemistry C*, 126(30), 12689–12695. Type : Journal Article.

Yarali, E., Koutsiaki, C., Faber, H., Tetzner, K., Yengel, E., Patsalas, P., Kalfagiannis, N., Koutsogeorgis, D. C. & Anthopoulos, T. D. (2020). Recent progress in photonic processing of metal-oxide transistors. *Advanced Functional Materials*, 30(20), 1906022. Type : Journal Article.

Yi, H., Wang, D., Mahmud, M. A., Haque, F., Upama, M. B., Xu, C., Duan, L. & Uddin, A. (2018). Bilayer SnO2 as electron transport layer for highly efficient perovskite solar cells. *ACS Applied Energy Materials*, 1(11), 6027–6039. Type : Journal Article.

Yin, W.-J., Shi, T. & Yan, Y. (2014). Unusual defect physics in CH3NH3PbI3 perovskite solar cell absorber. *Applied Physics Letters*, 104(6), 063903. Type : Journal Article.

Yoo, J., Jung, U., Jung, B., Shen, W. & Park, J. (2021). Improved Photoresponse Characteristics of a ZnO-Based UV Photodetector by the Formation of an Amorphous SnO2 Shell Layer. *Sensors*, 21(18), 6124. Type : Journal Article.

You, P., Li, G., Tang, G., Cao, J. & Yan, F. (2020). Ultrafast laser-annealing of perovskite films for efficient perovskite solar cells. *Energy & Environmental Science*, 13(4), 1187–1196. Type : Journal Article.

Zaitsev, S. V., Vaschilin, V. S., Kolesnik, V. V., Limarenko, M. V., Prokhorenkov, D. S. & Evtushenko, E. I. (2019). Effect of the Temperature of Photonic Annealing on the Structural and Optical Properties of ZnO Films Synthesized by Dual Magnetron-Assisted Sputtering. *Semiconductors*, 53(2), 255–259. doi : 10.1134/S106378261902026X.

Zak, A. K., Majid, W. A., Abrishami, M. E. & Yousefi, R. (2011). X-ray analysis of ZnO nanoparticles by Williamson–Hall and size–strain plot methods. *Solid State Sciences*, 13(1), 251–256. Type : Journal Article.

Zarazua, I., Bisquert, J. & Garcia-Belmonte, G. (2016a). Light-induced space-charge accumulation zone as photovoltaic mechanism in perovskite solar cells. *The journal of physical chemistry letters*, 7(3), 525–528. Type : Journal Article.

Zarazua, I., Han, G., Boix, P. P., Mhaisalkar, S., Fabregat-Santiago, F., Mora-Seró, I., Bisquert, J. & Garcia-Belmonte, G. (2016b). Surface recombination and collection efficiency in perovskite solar cells from impedance analysis. *The journal of physical chemistry letters*, 7(24), 5105–5113. Type : Journal Article.

Zhang, L., Zuo, C. & Ding, L. (2021). Efficient MAPbI3 solar cells made via drop-coating at room temperature. *Journal of Semiconductors*, 42(7), 072201. doi : 10.1088/1674-4926/42/7/072201. Publisher : Chinese Institute of Electronics.

Zhang, L., Li, H., Zhang, K., Li, W., Zuo, C., Odunmbaku, G. O., Chen, J., Chen, C., Zhang, L., Li, R. & others. (2023). Major strategies for improving the performance of perovskite solar cells. *iEnergy*, 2(3), 172–199. Publisher : TUP.

Zhang, X., Zhang, Y., Wang, Y., Wang, Q., Liu, Z., Geng, R., Wang, H., Jiang, W. & Ding, W. (2022). Improving the performance of perovskite solar cells via TiO2 electron transport layer prepared by direct current pulsed magnetron sputtering. *Journal of Alloys and Compounds*, 929, 167278. Type : Journal Article.

Zhang, X., Yao, J., Ali, M., Wei, J., Wang, H., Yeo, L. Y., Friend, J. R. & MacFarlane, D. R. (2014). UV/ozone-assisted low temperature preparation of mesoporous TiO 2 with tunable phase composition and enhanced solar light photocatalytic activity. *Journal of Materials Chemistry A*, 2(44), 18791–18795. Type : Journal Article.

Zhao, J., Deng, Y., Wei, H., Zheng, X., Yu, Z., Shao, Y., Shield, J. E. & Huang, J. (2017). Strained hybrid perovskite thin films and their impact on the intrinsic stability of perovskite solar cells. *Science advances*, 3(11), eaao5616. Type : Journal Article.

Zhao, X., Liu, G., Sui, Y., Xu, M. & Tong, L. (2021). Denoising method for Raman spectra with low signal-to-noise ratio based on feature extraction. *Spectrochimica Acta Part A : Molecular and Biomolecular Spectroscopy*, 250, 119374. Type : Journal Article.

Zhao, Y., Xiang, H., Ran, R., Zhou, W., Wang, W. & Shao, Z. (2023). Beyond two-dimension : One-and zero-dimensional halide perovskites as new-generation passivators for high-performance perovskite solar cells. *Journal of Energy Chemistry*. Publisher : Elsevier.

Zheng, X., Chen, B., Dai, J., Fang, Y., Bai, Y., Lin, Y., Wei, H., Zeng, X. C. & Huang, J. (2017). Defect passivation in hybrid perovskite solar cells using quaternary ammonium halide anions and cations. *Nature Energy*, 2(7), 1–9. Type : Journal Article.

Zhou, J.-S. (2020). Structural distortions in rare-earth transition-metal oxide perovskites under high pressure. *Physical Review B*, 101(22), 224104. Type : Journal Article.

Zhou, Y., Fernando, K., Wan, J., Liu, F., Shrestha, S., Tisdale, J., Sheehan, C. J., Jones, A. C., Tretiak, S. & Tsai, H. (2021). Millimeter-Size All-inorganic Perovskite Crystalline Thin Film Grown by Chemical Vapor Deposition. *Advanced Functional Materials*, 31(23), 2101058. Type : Journal Article.

Zhu, C., Niu, X., Fu, Y., Li, N., Hu, C., Chen, Y., He, X., Na, G., Liu, P., Zai, H., Ge, Y., Lu, Y., Ke, X., Bai, Y., Yang, S., Chen, P., Li, Y., Sui, M., Zhang, L., Zhou, H. & Chen, Q. (2019). Strain engineering in perovskite solar cells and its impacts on carrier dynamics. *Nature Communications*, 10(1), 815. doi : 10.1038/s41467-019-08507-4. Type : Journal Article.

Zhu, M., Liu, W., Ke, W., Clark, S., Secor, E. B., Song, T.-B., Kanatzidis, M. G., Li, X. & Hersam, M. C. (2017). Millisecond-pulsed photonically-annealed tin oxide electron transport layers for efficient perovskite solar cells. *Journal of Materials Chemistry A*, 5(46), 24110–24115. Type : Journal Article.

Zhu, Y., Zhang, Y., Hu, M., Wan, L., Huang, W., Chu, J., Hao, Y., Cheng, Y.-B., Simonov, A. N. & Lu, J. (2024). Scalable Slot-Die Coating of Passivation Layers for Improved Performance of Perovskite Solar Cell Modules. *Small Methods*, n/a(n/a), 2401244. doi : 10.1002/smtd.202401244. _eprint : https ://onlinelibrary.wiley.com/doi/pdf/10.1002/smtd.202401244.

Zhu, Z., Bai, Y., Liu, X., Chueh, C., Yang, S. & Jen, A. K. (2016). Enhanced efficiency and stability of inverted perovskite solar cells using highly crystalline SnO2 nanocrystals as the robust electron-transporting layer. *Advanced Materials*, 28(30), 6478–6484. Type : Journal Article.